

Review

Passivating contacts for high-efficiency silicon-based solar cells: From single-junction to tandem architecture



Jiakai Zhou^{a,b,c,d}, Qian Huang^{a,b,c,d,*}, Yi Ding^{a,b,c,d}, Guofu Hou^{a,b,c,d,*}, Ying Zhao^{a,b,c,d}

^a Institute of Photoelectronic Thin Film Devices and Technology of Nankai University, Tianjin 300350, China

^b Key Laboratory of Photoelectronic Thin Film Devices and Technology of Tianjin, Tianjin 300350, China

^c Collaborative Innovation Center of Chemical Science and Engineering (Tianjin), Tianjin 300072, China

^d Renewable Energy Conversion and Storage Center of Nankai University, Tianjin 300071, China

ARTICLE INFO

Keywords:

Crystalline silicon solar cell
Passivation contacts
Tandem
Energy conversion efficiency

ABSTRACT

The electricity market from renewable energies is strongly driven by the pursuit of high energy conversion efficiency, which at present represents the most effective pathway to achieve substantial cost reductions. Silicon (Si) have been dominating the photovoltaic industry for decades, while the conversion efficiencies of Si single-junction solar cells are practically limited to around 27%, and intrinsically constrained to 29.4%. To tackle this long-term bottleneck, it is necessary to develop novel technologies and transfer them into industrial production. This paper commences with a review concentrating on two critical concepts enabling high-efficiency Si-based solar cells: passivating contacts and tandem technologies. Since the gradual evolution from full area Al back surface field cells to passivated emitter and rear contact cells, passivating contacts are considered as an essential concept to circumvent the recombination losses caused by the contacts. The theoretical background of the three prominent technologies for passivating contacts and their application prospects to solar cells are described in detail. The fundamental limit of single junction Si solar cells is attainable with the introduction of passivating contacts. To obtain conversion efficiencies greater than 30%, upgrading Si with a high-bandgap tandem partner is a promising approach to improve the utilization of the solar spectrum, having the potential to produce efficiency surpassing the single junction Shockley–Queisser limit. Si is proven to be an ideal bottom cells material in tandem architectures due to its appropriate bandgap for the lower sub-cell and the advantage of compatibility with existing production lines, the technologies for crystalline Si as bottom-cell are already quite mature with a gigawatt scale. The two widely considered ideal options for the top-cell, i.e., III/V and perovskites, are summarized, respectively. Building on these two concepts, a clear technology route is provided to maximize energy conversion efficiency by integration of passivating contacts into Si based tandem solar cells. According to this discussion, guidelines for further developments of Si photovoltaics emerge clearly, proving that Si will continue to maintain its irreplaceable position in photovoltaics in the long term.

1. Introduction

Solar energy is considered as an ideal alternative to traditional resources with its rapid development owing to promising properties of renewability and sustainability [1]. Photovoltaic technology is an important utilization approach, which can directly convert solar energy into electricity [2,3]. Recently, balance-of-system costs (BOS) such as installation, cabling, construction, connecting, inverter and mounting structure, account for most of the cost of photovoltaics. Since most of the

above costs are area-dependent, the key to reducing the levelized cost of electricity (LCOE) lies in improving conversion efficiencies [4–6].

Crystallize silicon (c-Si)-based solar cells have acquired enormous success in advancing the photovoltaic industry worldwide owing to their characteristics of low fabrication costs and high reliability [7]. While c-Si, currently holds 95% of the photovoltaic market share and is thought to remain viable for a long time. At present, the efficiencies of typical module are around 17.5%, and the efficiency record of commercial product is 22.2% [8,9]. For research cell, the efficiency record

* Corresponding authors at: Institute of Photoelectronic Thin Film Devices and Technology of Nankai University, Tianjin 300350, China.

E-mail addresses: carolinehq@nankai.edu.cn (Q. Huang), gfhou@nankai.edu.cn (G. Hou).

has just been broken by Kaneka in 2017, with certified result of 26.6% [10,11]. Given that the theoretical limit for the c-Si solar cells is 29.4% (defined by considering Auger recombination and intrinsic losses), only marginal improvements in performance are still possible [12–14].

In recent years, the innovations of the cell structure allow the incremental improvements on the cell efficiencies in the industry production. Fig. 1 depicts the evolution of the average cell conversion efficiency at Hanwha Q-Cells in recent years. Overall, these results indicate that the industry remains on an efficiency improvement path of 0.5–0.6%_{abs} per year.

Since it was reported in about a decade ago, aluminum back surface field (Al-BSF) cell has been attracting much interest, which almost exclusively dominates the market of Si solar cells [16]. A typical p-type Al-BSF cell features a phosphorus-doped n⁺ emitter and an aluminum (Al) doped p⁺ BSF, which is formed by a firing process after screen-printing Al paste [17,18]. However, its efficiency stagnated at nearly 20% by 2012, which was constrained by the high carrier recombination velocity at Si rear surface originated from the full-area Al rear contact [19]. Interestingly, this efficiency stagnation of the Al-BSF cell has prompted scientists to develop new techniques to circumvent the existing limitations.

A passivation dielectric layer is designed to insert between the Si rear side and Al contacts to solve the problem of rear surface recombination, forming the so-called PERC (passivated emitter and rear cell) technology, which has superior performance compared to the Al-BSF cell. The reasonable explanations for the performance increase include the improvement of passivation performance and, at the same time, this inserted layer acts as an efficient reflection layer [20]. The manufacturing process of PERC devices is similar to that of the Al-BSF cell, except for with additional rear-surface passivation (often aluminum oxide, AlO_x) and localized Al BSF contacts (typically defined by laser ablation of the AlO_x layer), the fabrication process steps of Al-BSF cell and PERC are shown in Fig. 2. The rear surface recombination is strongly suppressed by the introduction of the passivation layer, thus increasing the device voltage. On this account, PERC devices possess the potential for higher efficiency and benefit from being manufactured on monocrystalline silicon wafers with higher bulk lifetimes. Besides, an ingenious design of PERC devices lies in the concept of “selective emitter”. Specifically, the emitter of the electrode is divided into two parts: heavy doping is carried out below the front metal grid to achieve good ohmic contact, while light doping is conducted in the non-electrode region [22,23]. Similarly, the basic limitation of this cell

structure is also the highly recombinative metal-semiconductor contacts, which are expected to be made small enough to reduce recombination losses. Metals will induce large densities of electronic states in the vicinity of interface within the bandgap of Si when directly in contact with c-Si, which result in nonnegligible recombination losses and attenuate the performance of devices [24]. Additionally, the heavily doping can induce numerous problems, such as the Auger recombination, the narrowing of bandgap and free carrier adsorption of c-Si [25]. Based on the research and development (R&D) roadmap, the efficiency bottleneck of Al-BSF and PERC in industrial production is approximately 20% and 24%, respectively [15]. Therefore, new technologies must be implemented to maintain the efficiency growth path of 0.6%_{abs} per year.

In this article, two key concepts to ensure high-efficiency Si-based solar cells will be discussed: the first, passivating contacts, for the next generation of single-junction Si solar cells, and the second, tandem architecture, for medium-to-long-term implementation in multi-junction cells. We identify the applications of passivating contacts for high-efficiency Si-based solar cells: from single-junction to tandem architecture.

Featuring the ability of lowering the recombination loss at the metal contacts, passivating contacts have been spotlighted as a crucial research issue to improve the core competitiveness of Si-based solar cells [26]. The basic principles and implementations of passivating contacts will be introduced in detail. The advent of this technology has facilitated single junction Si solar cells to approach the theoretical limit, with efficiencies close to 27% already achieved. The theoretical limit of 29.4%, which is calculated by considering unavoidable spectral losses and Auger recombination, can be broken by introducing a partner cell. Such multi-junction concepts and the integration of passivating contacts into tandem architecture will also be discussed.

It will be shown that the introduction of these technologies breathes new life into conventional Si-based solar cells, ensuring the yearly efficiency improvement can be maintained.

2. Passivating contacts

2.1. Passivating contact concept

The essential function of the electrical contacts is to extract photo-generated carriers, which originate from the absorption of photons with energies above the bandgap by the absorber material. Contact area is a region between the highly recombination active metal interface and the bulk absorber layer. The defects in the bulk absorber region have been minimized, but the absorber surface still has a very high density of defects and carrier recombination rate (J_0), and the metal does not provide chemical passivation of these defects [27]. The contact can therefore be defined as the region between the highly recombination active metal interface and the bulk absorber. Specifically, the definition of metal contacts is not limited to the sense stricto of metal-semiconductor interface, the induced or diffused regions inside of the Si wafer are also included. In general, the contacts refer to the structure responsible for the extraction of photo-generated carriers.

The essence of passivation is to reduce the surface recombination rate in two fundamental pathways: 1. Reduce the recombination rates of electrons and holes on the device surface, which entails reducing the chances of electrons and holes being trapped on the device surface, reducing the density of defect states on the surface, etc. This is typically achieved by depositing an insulating dielectric film on the wafer surface with unsaturated hanging bonds that can be combined with the wafer surface, or by introducing chemical atoms and molecules to saturate the hanging bonds on the device surface, most typically hydrogen and hydrogen atoms which have excellent surface passivation effects, often referred to as chemical passivation in this category; 2. Since the recombination process requires the presence of both electrons and holes, the recombination rate can be reduced by changing the ratio of surface carriers (the total number is constant under steady-state conditions), i.e.

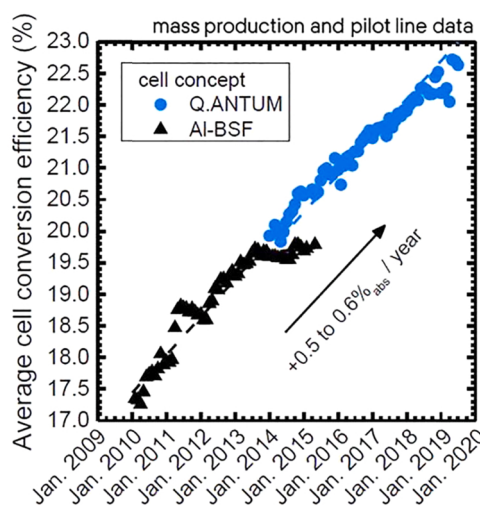


Fig. 1. Change of the average cell conversion efficiency at Hanwha Q-Cells in recent years. The cell concept of Q.ANTUM refers to the passivated emitter and rear contact cell (PERC) trademark [15].

Reproduced with permission. Copyright 2020, AIP Publishing Group.

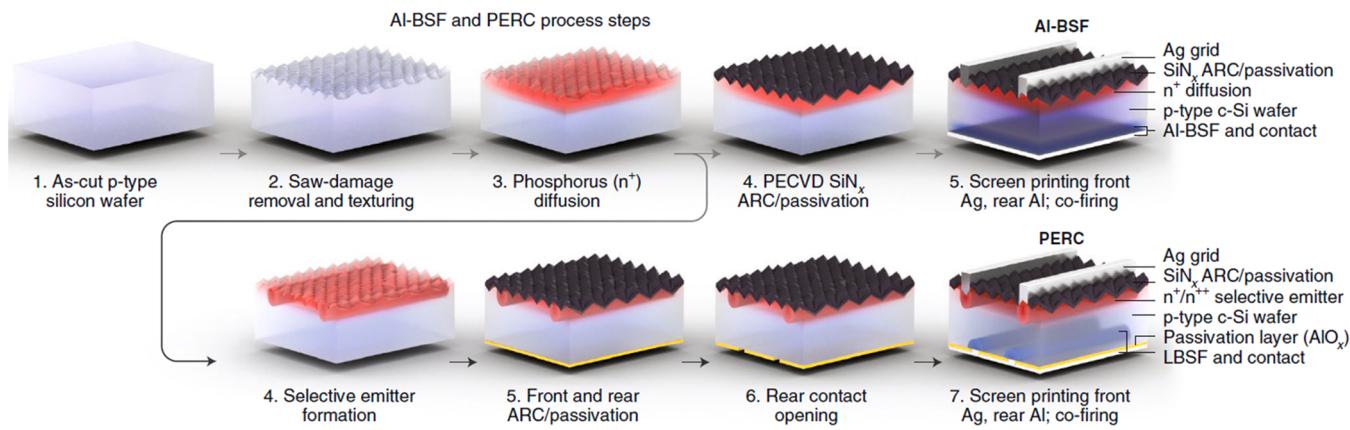


Fig. 2. Fabrication process steps of Al-BSF cell and PERC [21].

Reproduced with permission. Copyright 2019, Nature Publishing Group.

by reducing the number of one specific carrier on the surface. This can be achieved by introducing a fixed electric field on the surface of the device or by doping the surface at a high concentration to reduce the concentration of one specific carrier. The fixed electric field, which usually consists of a fixed charge at the interface between the dielectric film and the Si, creates a charge-rich region on the surface of the Si, which has the effect of repelling one type of the carriers, called field effect passivation.

For an exquisitely designed contact, surface passivation and low majority carrier resistive loss (ρ_c) are two pivotal criteria [28]. Here, the majority carriers refer to carriers wanted to be collected by contact, while the minority carriers are the opposite. For instance, at the hole collecting contact, the majority carriers and the minority carriers represent holes and electrons, respectively, and vice versa. Since the c-Si surface of all Si solar cells has a high defect density, the external attachment of metals will not reduce the surface state and the transport of carriers at the contact is affected, and the applicable solution of this issue is passivation. For solar cells fabricated with high-quality c-Si materials, bulk recombination is mainly restricted by intrinsic Auger recombination and radiation recombination, and the effect of passivation at the contact becomes more pronounced on the conversion efficiency. The main purpose of passivation is to minimize the carrier recombination, which allows Si solar cells to achieve the highest possible quasi-Fermi level splitting, thus giving Si solar cells the potential to obtain higher open-circuit voltages and conversion efficiencies [29,30].

Low power losses can be achieved by unblocked transport of the majority carriers when extracting current from Si solar cells, which requires an extremely low resistance for the majority carriers at the contacts. The voltage drop across the contact will be caused by the resistance for the majority carriers as the solar cell works, which will manifest through the gradient of the conduction and valence bands at the contact, thus affecting the transport of the majority carriers [31]. Therefore, the low resistance for the majority carriers at the contacts is vital for Si solar cells to obtain high fill factor (FF) and high conversion efficiency. The passivation contacts enable full-area contact without patterning steps on the one hand, and on the other hand, the carriers are 1-D transported, ensuring high FF. Bifacial is also one of the advantages of passivation contacts, which can make the module have better power generation effect.

The carrier selectivity of contact, or the ability to admit carriers of one conductive type while blocking carriers of another conductive type, arises from asymmetries in the conductivity of electrons and holes at the contact [32]. Carrier conductivity is dependent on carrier concentration and mobility, and carrier concentration and mobility are independently variable. In general, the carrier concentration is prone to tune, although the mobility can be adjusted to vary by several orders of magnitude. For

example, regions with different electron and hole concentrations can be produced in the same semiconductor material by doping, and the variation of the work function (Φ_m) and forbidden band width can also be tuned by creating a heterojunction structure to modulate the carrier concentration. Of course, no matter which way of adjustment is adopted, the spatial variation of carrier concentration is the key to carrier-selective contact, and the ability to select one conductive type of carrier to pass through while blocking another conductive type of carrier can further reduce the recombination loss.

An increasingly crucial strategy to boost the conversion efficiencies of solar cells is to reduce the recombination at the regions of metal contacts. The concepts of PERC and passivated emitter and rear locally diffused (PERL) are two typical examples, which solve this problem by patterning the back contact and directly reducing the contact area [33]. However, additional patterning steps are typically required to create point contact-like architecture mentioned above. Besides, there exists an inevitable trade-off between open circuit voltage (V_{OC}) and FF when the lateral conduction of carriers relies on Si or transparent conductive oxide (TCO) instead of the metal. That is to say, there exists a tradeoff between the J_0 and the contact conductivity. To fundamentally solve the problem of recombination losses at the metal contacts (represented by J_0), revisiting the collecting mechanisms of holes and electrons at different contacts is advisable. The contact acts like a carrier-selective semi-permeable membrane, i.e. it collects and transports one type of carrier and blocks another [34]. Besides, it is desirable that the contacts can simultaneously act as a passivation to ensure that the photo-generated carriers are collected before they recombine, and this can be quantified by the minority carrier lifetime, τ_{eff} . Combining these two features, such contacts can therefore be defined as carrier-selective

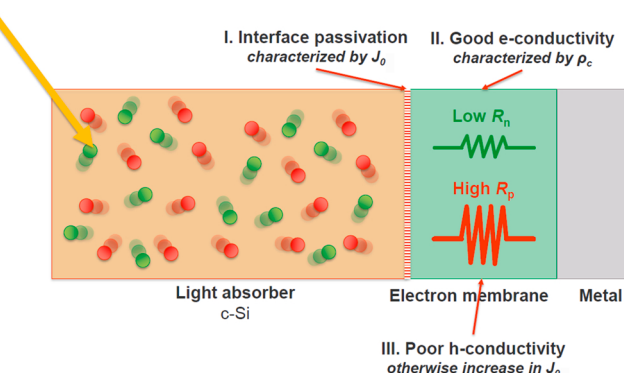


Fig. 3. Schematic representation of the role of passivation contact as an intermediate layer between light absorber and metal contact.

passivating contacts, the schematic representation of the role of passivation contact is shown in Fig. 3 [35,36].

A theoretically feasible way to achieve carrier selectivity is to apply conductive layers directly to the Si wafer with asymmetrical Φ_m relative to the c-Si conduction and valence band edges. According to the theory of Schottky-Mott, by this method, the Φ_m of the introduced metal can modify the surface potential of the underlying Si wafer, with electrons (holes) accumulating at the low (high) Φ_m interface, displacing minority carriers and reducing the J_0 [37–39]. With the introduction of an appropriate contact metal, the Schottky barrier (Φ_b) which impedes the transfer of charge at the contact interface can be reduced to sufficiently small to form a contact with low resistance by thermionic emission (Fig. 4b, in contrast to Fig. 4a). The metal Φ_m can only slightly condition the concentration of carriers at the semiconductor surface. A significant Schottky barrier is commonly formed at the semiconductor surface due to the existence of interface defects regardless of the Φ_m , which is defined as Fermi level pinning (FLP). The effect of FLP, empirically demonstrated plots of barrier height versus metal Φ_m , show a strong pinning effect that typically results in the depletion of charge carriers from the contacted Si sub-surface, as shown in Fig. 4c [40–42]. To circumvent the deteriorations induced by FLP, the Φ_m of the contact material is expected to take extreme values to lower the Φ_b , or the width of the depletion region, W , has to be narrowed, ensuring the tunneling of charge carriers through the Schottky barrier can occur (shown in Fig. 4d) [43,44]. Fig. 4f illustrates the efficacy of the approach of heavy doping, and it describes the variation of the ρ_c values with the surface doping concentration (the p- and n-type doping concentrations are denoted by N_A and N_D , respectively). However, heavy doping also causes

some severe problems simultaneously, it will result in severe Auger-limited recombination of $J_0 > \sim 200 \text{ fA cm}^{-2}$ at directly metallized contacts, far exceeding the most advanced non-metallized passivated surfaces [45–47]. Fig. 4g depicts this phenomenon, and it plots J_0 versus the sheet resistance of heavily doped region. As the doping increases, the sheet resistance decreases and the J_0 plateaus as the Auger recombination contribution come to the fore, which demonstrates the poor applicability of directly metallized contacts with heavily doping. Moreover, applying a suitable interlayer to ‘de-pin’ the Fermi level is also an alternative path to contact formation, that is, the concept of passivating contact.

Passivating contacts avoid direct contact of the metal with Si wafer, thereby ensuring the transfer of the majority carriers. In ideal case (the passivating contacts are formed perfectly), the internal or implied voltage (V_{int}), defined by the separation of the quasi-Fermi levels ($E_{F,n} - E_{F,p}$) in the absorber, is restricted by the intrinsic recombination losses and the external voltage (V_{ext}) measured at the metal electrodes corresponding to the internal voltage.

Based on the above analysis, the following three prerequisites for the passivation contact system can be derived: (1). The recombination near the contact needs to be limited to a low enough level to ensure a high V_{int} ; (2). For open-circuit conditions, the majority Fermi energy in the contact region needs to be immobile ($V_{ext,oc} = V_{int,oc}$). (3). A small voltage drop of the majority carrier at maximum power point is desirable, which guarantees efficient transport of the majority carrier [32].

An Ohmic contact is formed by introducing a highly doped region in direct contact with a suitable metal layer, which satisfies the requirement (2) and (3). However, this is contradiction to requirement (1) due

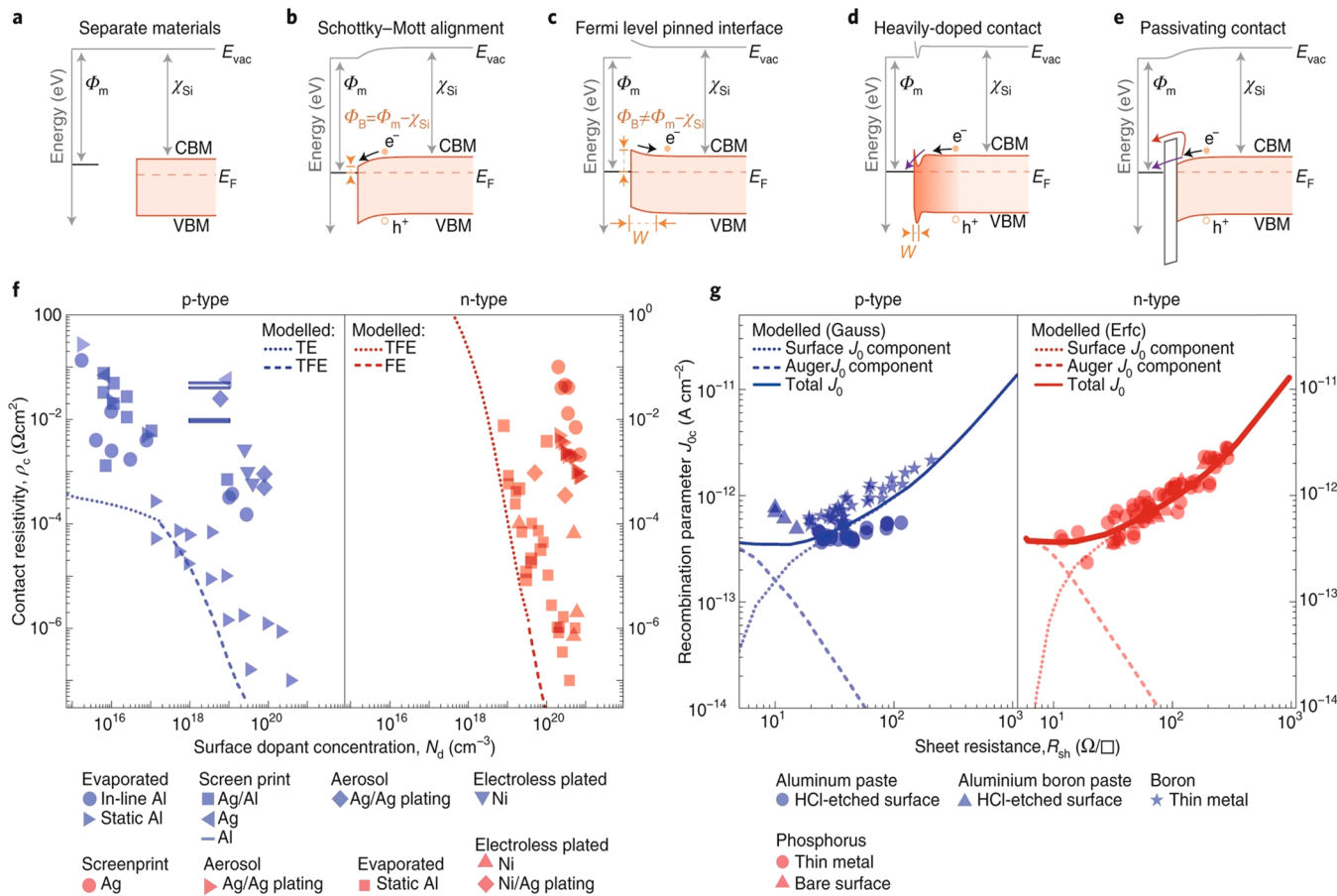


Fig. 4. Schematic idealized equilibrium band diagrams for (a) separate materials, (b) the Schottky-Mott alignment, and (c) Fermi level pinned interface. (d) heavy doping and (e) applying a passivating interlayer are two optional approaches to improve the selectivity of contacts. (f) and (g) reveal the efficacy of heavy doping in terms of resistive ρ_c and J_0 , respectively [21].

Reproduced with permission. Copyright 2019, Nature Publishing Group.

to the problem of Auger recombination that come with it. Highly doped regions in the Si absorber need to be avoided and the surface needs to be passivated to meet requirement (1). An ideal passivating contact needs to have both characteristics: good selectivity and low recombination current. In addition, transparency and manufacturability are also issues that need to be addressed before passivation contacts can be commercialized. Different types for passivating contacts will be introduced in the following sections.

2.2. Doped a-Si:H / intrinsic a-Si:H stacked films

The renowned representative of passivating contacts is the silicon heterojunction (SHJ), which has long been extremely competitive in the photovoltaics market. The fabrication process steps of double-side contacted SHJ solar cell, as well as the schematic diagrams of IBC SHJ and bifacial SHJ solar cells are illustrated in Fig. 5. The high efficiency of this technological approach comes from the high V_{OC} obtained by intrinsic amorphous silicon ((i) a-Si:H) passivation. However, the formation of energy band steps between a-Si:H and adjacent layers (c-Si and the transparent conductive (TCO) layer), as well as the asymmetry between the conductive and valence band steps, affect the transport of photovoltaic carriers and the final performance [50,51]. The typical fabrication sequence of solar cells mainly includes cleaning and texturing by chemical-related treatments, intrinsic / doped a-Si:H preparation using plasma-enhanced chemical vapor deposition (PECVD), sputtering process for deposition of TCO and metallization by screen printing. Typical SHJ device poses a symmetrical architecture, with a thin (i) a-Si:H layer sandwiched between the c-Si wafer and the doped a-Si:H layers [52]. SHJ combined with IBC technology has the advantage of the reduction in the parasitic absorption of the front TCO and a-Si:H layers. However, its complicity in actual preparation limits its application in industry. Relative to the original PERC technology, SHJ process is more concise in the industrial production category, ensuring lower operational expenditures (OPEX). In addition, the sub-200 °C manufacturing process, high bifaciality coefficient, thinner wafer compatibility, low temperature coefficient and high conversion efficiency give it the potential to realize lower LCOE [53].

The SHJ architecture has continued to evolve for decades, until recently when it has returned to the spotlight owing to the emerge of efficiency record of 26.7%. Due to this, the production of SHJ solar cells

is expected to capture more market share in the near future, as illustrated in Fig. 6a. The advantages of SHJ technology are gradually highlighted in the mainstream products. Compared to others, it notably brings efficiency gains while maintaining low production costs [54–56]. Fig. 6b depicts the research progress of SHJ solar cells in terms of conversion efficiency and FF . Thanks to the integration of novel technologies (e.g. IBC, tandem), the conversion efficiency continues to acquire breakthroughs, already exceeding the best result of homojunction PERC cell.

As proved by many research institutes and companies, the superiority for the SHJ solar cells can be concluded as follows: (1). Streamlined structure: complete devices are prepared without complex processes, such as partly doping or oxidation. (2). Low-temperature process: the process is relatively simple and cost effective due to the circumvention of complex process. The high energy consumption caused by the high temperature has also been alleviated. (3). One-step implementation of surface passivation and heterojunction: the utilization of ultra-thin (i) a-Si:H layer at the interface can suppress the surface recombination significantly. (4). Symmetrical structure: this convenient for double-sided design is conducive to improving the effective light-receiving area and increasing energy yield. (5). Stability: it is attractive that the light-induced degradation (S-W) effect common to a-Si based solar cells is not present in the SHJ cell. (6). Superior high-temperature property: the SHJ cell surpasses the conventional PERC cell in terms of temperature dependence.

The most striking feature of SHJ structure is the superior surface passivation of c-Si absorber. Therefore, at least for open-circuit conditions, the efficiency of SHJ solar cells is more sensitive to the intrinsic recombination instead of junction recombination. Consequently, M. Taguchi et al. achieved a very high V_{OC} of about 750 mV [57]. Hence, boosting J_{SC} and FF are particularly needed to further improve device performance. In addition, it is also crucial to implement an appropriate engineering of the SHJ.

A diagram showing the standard energy band of SHJ solar cells at open-circuit conditions is sketched in Fig. 7. The distinctive feature is the emergence of an inversion layer within the absorption region close to emitter, while an electronic barrier is also formed by the c-Si energy band bending and the conduction band ladder between absorption layer and a-Si:H [58,59]. QFL_n and QFL_p represent quasi-Fermi levels of electrons and holes, respectively. iV_{OC} indicates the implied open circuit

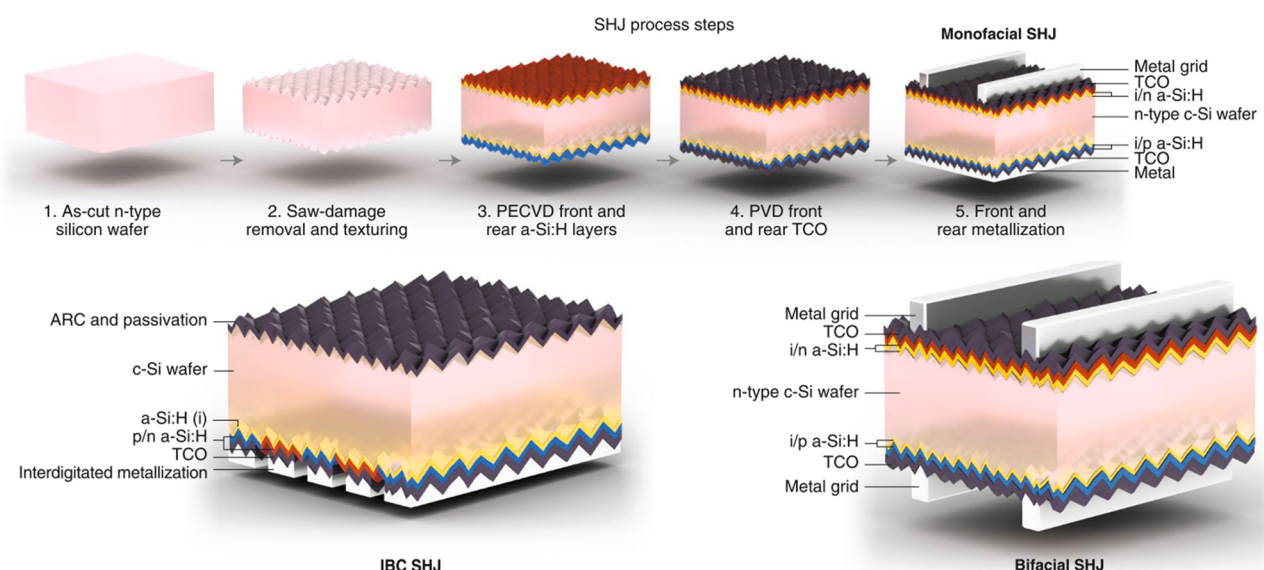


Fig. 5. Fabrication process steps of double-side contacted SHJ solar cell, as well as the schematic diagrams of IBC (interdigitated back contact) SHJ and bifacial SHJ solar cells [21].

Reproduced with permission. Copyright 2019, Nature Publishing Group.

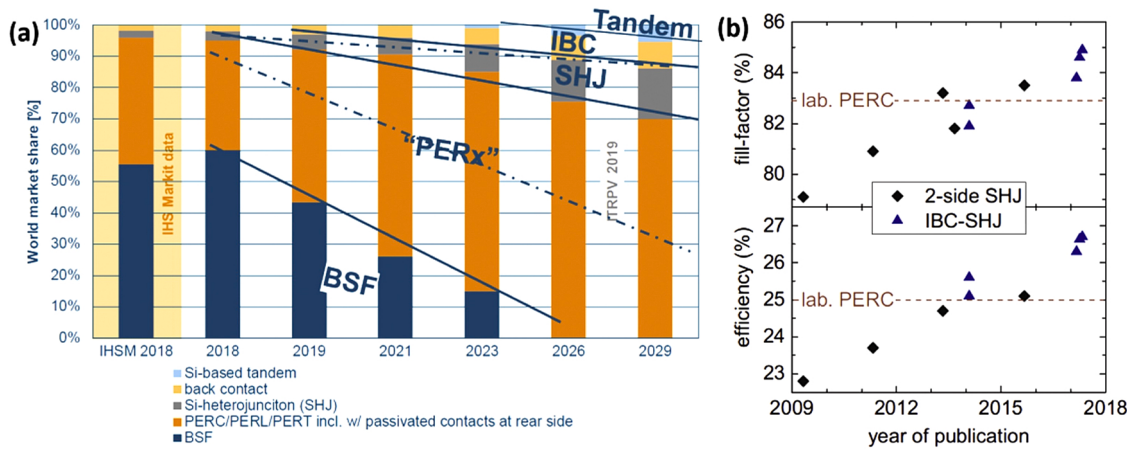


Fig. 6. (a) Projected market share of c-Si solar cells as presented at International Technology Roadmap for Photovoltaic (ITRPV) 2019 [48]. (b) The evolution of conversion efficiency and FF for SHJ solar cells in recent years [49].
Reproduced with permission. Copyright 2018, Elsevier.

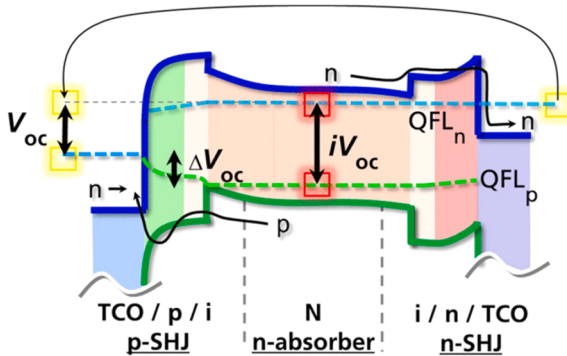


Fig. 7. Energy band of a SHJ solar cell at open-circuit conditions [30].
Reproduced with permission. Copyright 2014, IEEE.

voltage, which is the theoretical maximum V_{oc} that can be obtained with a given structure. The presence of the TCO layer allows more light to be coupled into the absorber region, while ensuring low-loss carrier transport between the doped a-Si and the metal electrode. As for non-doped a-Si layer, its thickness is generally less than 10 nm, which can form passivation on the surface of c-Si.

The function of the nominal undoped a-Si (with a typical thickness of 5–10 nm) is to provide chemical passivation of the absorber surface and to decouple c-Si surface recombination from the abundance of defects in the subsequent layers (essential requirement for passivating contacts). Important requirements for chemical c-Si surface passivation are a properly cleaned c-Si surface, an atomically sharp a-Si / c-Si interface, and an (i) a-Si featuring an extremely low defect density and sufficiently high hydrogen content [60–62]. The characteristic of high bandgap and low mobility for a-Si make itself electrically opaque, which is essential to screen the doped a-Si (TCO and metal) defects from the c-Si surface. Therefore, the (i) a-Si buffer layer is an indispensable part that turns a non-passivating and carrier-selective contact into a passivating and carrier-selective contact [63–67].

The function of the subsequently deposited doped Si films (typically around 10 nm) is to control the concentration of different types of carriers in the contact regions. The doped layer has the effect of so-called “field-effect” passivation, which has a repulsive effect on one type of carrier and is likewise an effective means of minimize recombination. The synergistic effect of chemical and “field-effect” passivation determines the excellent V_{oc} and FF of cells.

To enhance the built-in potential, sufficient n-type or p-type doping and potentially alloying are usually applied to regulate the Φ_m of the a-Si

[68,69]. Specifically, the inserted doped a-Si differs from the c-Si in its Φ_m , which induces homojunction on the surface of c-Si [70,71]. Besides, sufficient selective conductivity is also required at the interface of TCO / doped a-Si, thus leading carriers flow to electrodes. Since the majority of TCOs have a Φ_m near the intermediate gap of a-Si, the requirements for doping a-Si are significantly higher than those for junction formation with absorbers. It has been proved that higher a-Si doping and thickness are often required to cover the large Φ_m mismatch [72–75]. Approaches to further optimize the properties of SHJ solar cells will be listed in next Section III.

2.3. Dopant-free and carrier-selective heterocontacts with high / low work-function films

With the recent rapid development, the theoretical conversion efficiency of dopant-free asymmetric heterocontacts (DASH) solar cells has reached 28%, which has a great development potential and has attracted much attention [76]. For the limitations of traditional c-Si solar cell industry, such as high cost of production equipment, flammable and explosive raw materials, the market expectation for low-cost, green and pollution-free solar cells is increasing, which greatly increases the necessity of research and development of novel solar cells with DASH structure. The selectivity of the passivation contact for different types of carriers can be achieved via doping, represented by the SHJ solar cells, which use a combination of intrinsic and doped a-Si:H to achieve both full-surface passivation and carrier-selective transport. However, this carrier-selective passivation contact requires relatively expensive PECVD equipment, uses flammable and explosive silane (SiH_4) as well as highly toxic borane (B_2H_6) and phosphine (PH_3) raw materials, and the relatively small forbidden band width of the Si film results in a large parasitic light absorption that degrades solar cell performance. In addition, the electron and hole selectivity of the passivating contact can also be achieved via matching the Φ_m of the contact material with the c-Si conductive and valence bands. At present, electron-selective contact materials mainly include LiF_x , MgF_x , MgO_x , TiO_2 and ZnO , and alkaline earth metals Mg and Ca with very low Φ_m . And the hole-selective contact materials are mostly transition metal oxides (TMOs), represented by MoO_x , WO_x , V_2O_x , and NiO_x [77,78]. As shown in Fig. 8, the use of Si-based thin films as electron and hole transport layers greatly limits the range of band gaps and Φ_m , constraining the optical and electrical aspects of contact design. This problem is circumvented by materials such as metal oxides, which enrich the choice of materials and broaden the design space. A DASH solar cell is formed when a heterojunction with a TMO is applied on both sides of the c-Si to achieve selective contact for electrons and holes [79]. TMOs-based DASH devices have several

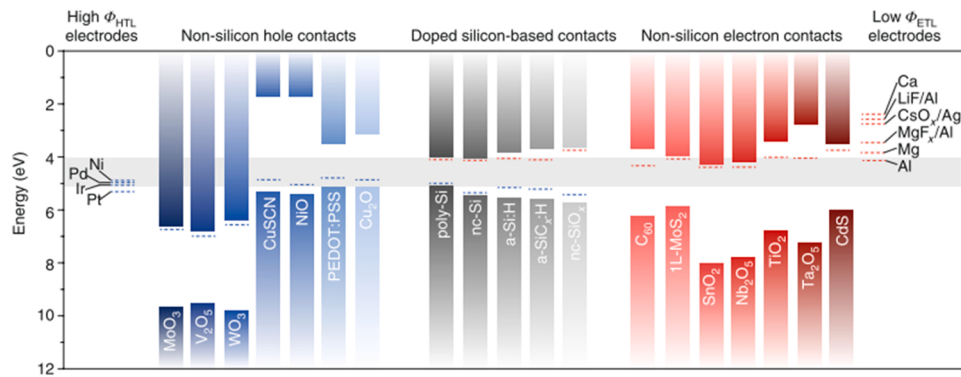


Fig. 8. Conduction and valence band positions of different materials for passivating contacts. And the dashed lines represent positions of indicative Fermi levels [21]. Reproduced with permission. Copyright 2019, Nature Publishing Group.

advantages, such as large forbidden band width of TMOs, small parasitic light absorption, and favorable for improving short-circuit current density. Moreover, most TMOs can be prepared by low-cost techniques (thermal evaporation or solution method), which avoids the use of flammable, explosive and toxic gases and is safer [80–83].

In conventional solar cells, the built-in electric field is considered to be the internal force that separates the photocarriers to form an electric current, whereas it is now believed that a clear PN junction is non-essential and that the driving force to form an electric current can be a quasi-Fermi level gradient. Illumination causes the equilibrium Fermi level to split to form a quasi-Fermi level, and gradient of the latter provides the driving force for the photovoltaic carriers to move. The asymmetric conductivity of the carrier provides the driving force for the separated photocarriers to move in different directions [84,85]. If the solar cell is abstracted into three parts: the absorber, the passivation, and the contact, the carrier transport process is shown in Fig. 9. The working mechanisms of TMO / c-Si heterocontacts have been intensively discussed for a long time. Gerling et al. concluded that the energy level difference between the high Φ_m of TMO and the n-Si Fermi level provides the driving force to achieve the Fermi level equilibrium, and that the n-Si induced energy band bending is responsible for carrier selectivity [86]. The difference in energy level between the TMO Φ_m and n-Si Fermi level (about 1.2 eV) cannot satisfy the need for Fermi level equilibrium, so there should be a dipole with negative charge at the interface between TMO and n-Si, which causes the band shift and complicates the carrier transport. Battaglia et al. suggest that MoO_x exhibits more metal-like behavior with high Φ_m , not only the energy band of c-Si surface bends, but also the energy band of MoO_x bends to a certain extent [43,87,88].

The electron and hole selectivity of the TMO-based passivating contact can be arranged via matching the TMO Φ_m with the c-Si conduction and valence bands. As shown in Fig. 10, the large Φ_m difference

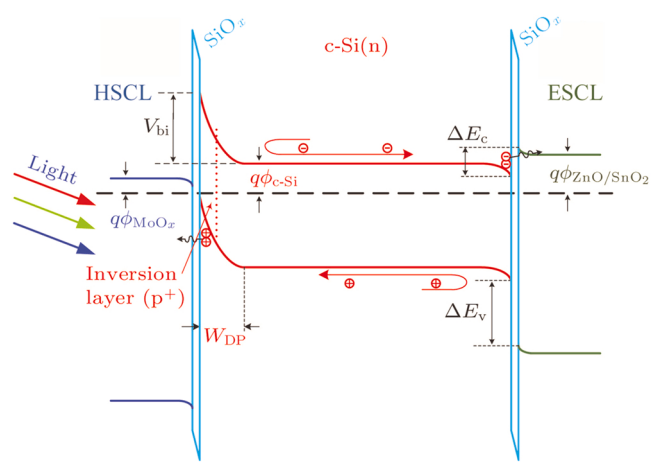


Fig. 10. Energy band structure diagram of TMO-based solar cells [89]. Reproduced with permission.

between MoO_x and c-Si results in the energy band bending of the surface of the latter and the repulsion to electrons by the induced transmutation barrier; the holes can accumulate in the potential well close to the interface and reach the conduction band of MoO_x through interband tunneling or defect-assisted tunneling to achieve selective transport of the holes. For the ZnO (SnO₂) / c-Si interface, the band order difference ΔE_c is negligible, which can facilitate electron transport, while the valence band order difference ΔE_v is large, which can adequately block the holes, thus enabling selective transport of electrons [77]. Battaglia et al. compared the energy band arrangement of MoO_x with that of p-type a-Si:H [87]. The similar characteristics of both types of contacts

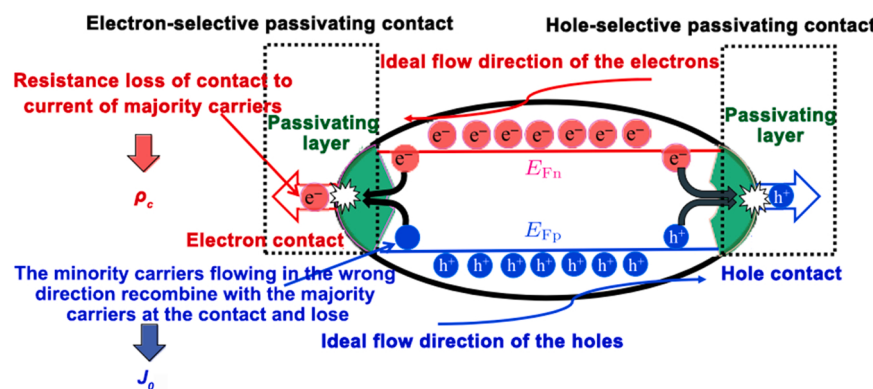


Fig. 9. Passivating contact solar cell structure and carrier transport mode.

are the formation of an inverse layer, the n-Si band bending, and the difference in band steps between the n-Si and a-Si:H conduction bands, which blocks the electrons. The hole extraction processes in the case of MoO_x and (p) a-Si:H are highly similar, i.e., the holes first cross the barrier formed by the difference in the order of the n-Si and a-Si:H valence bands, and then pass through the band-tailed state of a-Si:H or the oxygen vacancy defect of MoO_x to reach the front electrode [43,90]. Vijayan et al. and Messmer et al. respectively simulated and analyzed the transport path of holes at the interface of TMO and Si, and agreed that there were two possibilities, namely direct interband tunneling (B2B) and defect assisted tunneling (TAT) [37,91]. The specific transport mechanism mainly depended on the value of TMO electronic affinity. If the electronic affinity of TMO is large enough (high ϕ_m) that the TMO conduction band is underneath the valence band of c-Si, B2B is dominant way. Conversely, when the electronic affinity is insufficient (low ϕ_m), TAT by means of a body defect in the TMO is required. According to the above results, it can be concluded that increasing the ϕ_m (electronic affinity) of the TMO is pivotal to improve the device performance.

The lattice mismatch between TMO and c-Si inevitably results in a high defect density and consequently in a high carrier recombination at the contact interface, which can be reduced by inserting an ultra-thin dielectric interlayer between the c-Si surface and the contact metal. The ultra-thin dielectric layers have three functions simultaneously, including separating metal from the Si wafer, passivating the Si surface, and serving as a contact to the solar cell. Currently, ultra-thin SiO_2 , Al_2O_3 , and a-Si:H dielectrics are desirable candidates which commonly used as passivating layers. Thicker layers lead to a better passivation effect and high ρ_c , while a poor passivation effect and low ρ_c are the characteristics of thinner layers. Hence, a trade-off between the two is needed to find the optimal thickness of the passivation layer [92,93].

2.4. Doped poly-Si / ultra-thin SiO_x stacked films

In PERC series solar cells, the metal electrode is still in direct contact with the Si substrate, and the metal-semiconductor contact interface produces band bending due to a mismatch in ϕ_m and plentiful minority carrier recombination centers, which negatively affects the device performance. Introducing a thin film to separate the metal from the Si has therefore been proposed for a long time in order to reduce recombination [97]. Fig. 11 shows the various solar cell structures that have been proposed throughout history for passivating contacts. The earliest proposals for passivated metal electrodes were made in the semiconductor industry, and similar structures have been proposed for field effect transistors. Later, some scholars proposed the preparation of SiO_2 layers beneath metal electrodes in solar cells, but it was never realised due to the difficulty of the process [98]. In 2013, the Fraunhofer research center in Germany chemically prepared an ultra-thin layer of Si oxide ($\sim 1.5 \text{ nm}$) on the back of the cell, and then deposited a layer of doped poly-Si [99]. This technology is called tunneling oxide passivation contact (TOPCon) technology. Due to a difference in the ϕ_m between the (n⁺) poly-Si and the absorber layer, the former forms an accumulation layer on the surface of the latter. The accumulation layer or the energy band bending creates a barrier that prevents the hole from reaching the tunneling oxide, whereas electrons can easily reach it. Compared with electrons, the ultra-thin oxide layer also provides a higher barrier for the hole to prevent its tunneling, so the layer is carrier selective. The band diagram and structural schematic of the tunneling oxide passivation contact structure are presented in Fig. 12. The Fraunhofer institute used n-type (float zone) FZ wafers with a normal pyramidal texturing and boron diffusion on the front side [96]. And a stacked layer structure composed of plasma-assisted atomic layer deposition (ALD) aluminium oxide and PECVD silicon nitride has effects of passivation and anti-reflection. On the back side, the TOPCon technology described above (based on a nitric acid thermal oxidation chemistry process) was

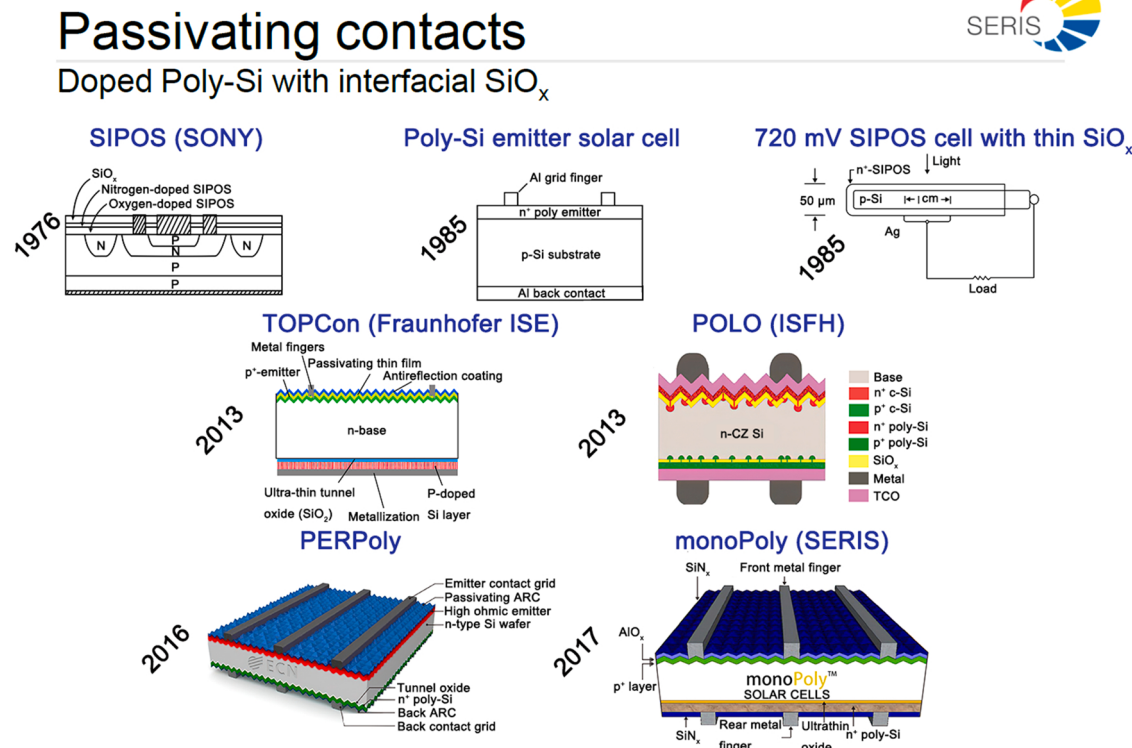


Fig. 11. Several different passivating contacts and techniques [94]. Reproduced with permission.

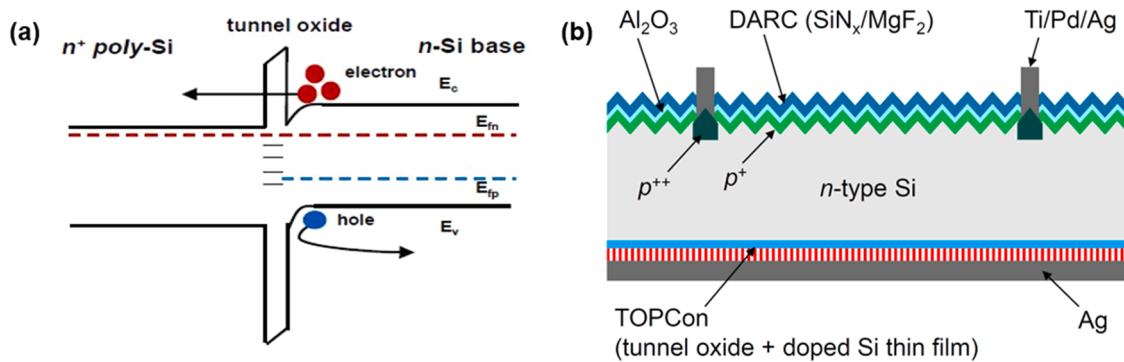


Fig. 12. TOPCon solar cell: (a) energy band diagram [95]; (b) schematic cross-section of the n-type Si solar cell [96]. Reproduced with permission. Copyright 2017, Elsevier.

applied, n⁺-doped poly-Si was deposited by PECVD, followed by high temperature (700–900 °C) annealing and hydrogen passivation to optimize the morphology and bandgap of the Si layer. Finally, the metallization of electrodes was achieved using an electron beam evaporated Ti / Pd / Ag tandem and thermally evaporated Ag. The final device conversion efficiency reached 25.1% [99]. Subsequently, they used an optimal thickness, low resistivity wafer and changed the front surface anti-reflection layer (SiN_x / MgF₂) to further reduce the optical loss, allowing them to further increase the cell efficiency to 25.7% [96]. The finally formed TOPCon structure is characterized by a fully passivated back contact and one-dimensional carrier transport. The most critical technology of TOPCon is how to prepare an excellent ultra-thin oxide layer. Researchers have explored a number of methods, such as ultraviolet (UV) ozone oxidation, plasma-assisted oxidation (N₂ and O₂ mixed atmosphere), wet chemical oxidation (thermal oxidation of nitric acid, thermal oxidation of hydrochloric acid), high-temperature thermal oxidation (rapid thermal oxidation of Ar and O₂ mixed atmosphere, ultra-high vacuum thermal oxidation), high-temperature neutral oxygen atom plasma oxidation, field-induced anodic oxidation, etc. [100–102].

Although the solar cells using TOPCon technology are still in the research and development stage, some progress has been made in the application of this technology. In the laboratory, Yamamoto et al. combined the technology of SHJ on the front surface with the technology of TOPCon on the back, resulting in a solar cell with a new structure (SHJ + TOPCon) with a conversion efficiency close to 25% [103]. Based on the excellent properties of the IBC architecture, Reichel et al. combined the IBC structure with TOPCon technology by ion implantation to produce a new type of solar cell (IBC+TOPCon) with a V_{OC} of 682 mV and a pseudo-FF (pFF) of 82.2% [104].

Tao et al. prepared TOPCon cell with a large area (239 cm²) n-Czochralski (CZ) Si as the substrate with a conversion efficiency of 21.2% [95,105]. They explained that the recombination of emitter on the front surface affected the performance of solar cell, so it had a promising application prospect in industrial production. With the continuous maturity of TOPCon's ultra-thin oxide layer preparation technology, TOPCon solar cell has not only been widely used in the laboratory, but also has a large market industrialization space. The industrial application prospect of TOPCon solar cell lies in the diversity of TOPCon technology. Industrial technologies such as PN junction, metal electrode and anti-reflection layer of c-Si solar cell have been mature, providing a choice for the industrial production of highly efficient c-Si solar cell.

Peibst et al. at the Institut fur Solarenergieforschung Hameln (ISFH) in Germany have been working on P-type monocrystalline Si solar cells that combine polycrystalline Si and oxidation to form a fully passivated contact, called a POLO structure, with an ultra-thin oxide layer separating the dopant layer on both the front and rear surfaces, not only separating the back field, but also the emission area on the front surface [106]. But the agency considered that their oxide layer had many

cavities that formed a conductive channel between the dopant layer and the substrate. Both POLO and TOPCon solar cells adopt poly-Si and oxide layer structure design, and their corresponding oxide layer growth methods are similar. The differences are as follows: (1). The former uses low pressure chemical vapor deposition (LPCVD) method to deposit intrinsic poly-Si, and then uses ion implantation to form (n⁺ / p⁺) poly-Si, while the latter uses PECVD method to deposit (n⁺) poly-Si. (2). The former needs to grow oxide layers on both sides and grow (n⁺ / p⁺) poly-Si respectively; The latter only needs to grow an oxide layer on the back and deposit (n⁺) poly-Si. (3). The former will form (n⁺ / p⁺) c-Si after ion implantation, while the latter will not form (p⁺ / n⁺) c-Si without the use of this doping technology [96,106]. Compared with traditional heterojunction, the advantages of poly-Si / c-Si are mainly reflected in: lower saturation current density, smaller contact resistance, and higher carrier selectivity [107,108].

In 2016, ECN proposed the PERPoly cell, which is basically the same structure as the TOPCon, except that a passivated and anti-reflection film is used on the back surface, and the electrodes on the back surface also use a gridded structure, which makes it possible to achieve the best use of double-sided photovoltaic power generation, with a corresponding increase in conversion efficiency as the back surface also has a passivation film [109]. The MonoPoly concept was proposed by SERIS in 2017, and there is no significant difference from a structural point of view, only some details have been changed, such as the polished back surface and the AlO_x / SiN_x composite structure for the front surface passivation film [110]. Therefore, solar cells combining poly-Si based contacts have fully integrated with various new technologies by now, and the domestic industry is still accustomed to calling it TOPCon structure.

TOPCon structure works through the synergy of ultra-thin interfacial oxide layer and heavily-doped poly-Si layer. Specifically, the basic manufacturing process consists of the following four processes: preparation of interfacial oxide layer; growth of a-Si or poly-Si layer, methods include PEVCD, low-pressure CVD (LPCVD), atmospheric pressure CVD (APCVD), sputtering, evaporation, or liquid Si; crystallization process by annealing in high temperature environment; hydrogenation to replenish atomic hydrogen [111–125].

As an important part of the TOPCon structure, the oxide layer can passivate the hanging bonds on the surface of the c-Si, thus reducing the interface trapped charge density (D_{it}), which is considered as an important indicator of the quality of the oxide layer, which usually results from the high-energy atom bombardment during subsequent deposition processes. During the preparation of doped poly-Si / ultra-thin SiO_x junctions, different materials need to be prepared and interface defects will arise between the different materials, too many defects will directly affect the performance of the cell, so an ideal D_{it} is essential. Research of Zeng et al. has proved that with the increase of D_{it} , V_{OC} decreases slowly at first, and after reaching the critical point of 10¹¹ cm⁻²/eV, it decreases rapidly, which is mainly due to the increase of

recombination center in junction region, and the probability that the majority carriers are captured in the process of tunneling increases greatly [126]. When the thickness of SiO_x is greater than 1 nm, the influence of D_{it} can be restrained to a certain extent. However, as D_{it} increases to $10^{13} \text{ cm}^{-2}/\text{eV}$, this effect is almost eliminated, mainly due to the fact that there are so many interfacial defects that it is essentially the same as without SiO_x , with the majority carriers essentially captured in their entirety and the J_0 reaching a constant value. In view of the fact that the D_{it} will increase due to incomplete ultra-clean space, incomplete cleaning, insufficient oxidation and other reasons, and its negative effect can be suppressed by increasing the thickness of the SiO_x . It is already known that doped poly-Si / ultra-thin SiO_x junctions can achieve extremely low D_{it} (close to $10^9 \text{ cm}^{-2}/\text{eV}$) comparable to doped a-Si:H / intrinsic a-Si:H stacked films [127]. Specifically, the interfacial oxide layer is generally required to be thin to 1–3 nm, which can block the minority carriers and thus reduce recombination [114,126].

In addition, the role of poly-Si layer is also vital, which typically refers to a heavily-doped poly-Si layer, and it can also be alloyed with carbon or oxygen to optimize material properties. Its Φ_m controls carrier selectivity via induced band bending in the area near the surface of c-Si, and adequate electrical conductivity is also an essential feature. During the high temperature annealing process, the doped atoms in the poly-Si layer pass through the oxide layer into the c-Si, forming a doped region, which can effectively reduce the minority carrier concentration, the resulting field passivation effect and the chemical passivation effect of the oxide layer together ensure the excellent passivation quality of the TOPCon structure. However, it is worth noting that too large doping level will increase Auger recombination [126,128]. Therefore, it is essential to control the diffusion of dopant into the c-Si to reach the minimum. Fortunately, the oxide layer can act as an effective diffusion barrier, especially against phosphorus. The high temperature annealing process can change the properties of oxide layer by forming pinholes in the oxide or refactoring structure of the atomic bonds at the Si / SiO_x interface. The formation of pinhole does not necessarily degrade the passivation effect, but may also reduce the contact resistivity. A literature has highlighted that a proper pinhole density (10^8 to 10^9 cm^{-2}) ensures extremely low J_0 and ρ_c [129,130]. Whether the main transport mechanism of carriers in contact is tunneling or transport through pinholes depends on the nature of the sample itself [131]. Currently, the mechanism of carrier transport is still unclear and needs to be further explored.

Hydrogenation is an important means to improve the surface

passivation effect, and atomic hydrogen presumably passivates electrically active defects at the c-Si / SiO_x interface and within the poly-Si layer [132,133]. Commonly used sources of hydrogen include hydrogen plasma and H-containing dielectrics (e.g., SiN_x , Al_2O_3) and even TCOs, while a forming gas annealing (molecular hydrogen) does not bring much improvement to the passivation effect [134,135]. It was reported that high temperature annealing in an atmosphere containing water vapor can be an efficient and simple means of hydrogen replenishment [136,137]. Besides, J_0 can be effectively reduced by the synergistic action of AlO_x and SiN_x to form stacks compared to any single layer [138,139].

3. Passivating contacts for single-junction solar cells

3.1. a-Si / c-Si heterojunction solar cells

3.1.1. Research status and progress

In the 1990 s, company Sanyo Corp. entered the field of amorphous Si heterojunction solar cells, initially via forming p-type amorphous Si onto n-type c-Si and achieving a conversion efficiency of 12.3%. The V_{OC} and FF of this structure were lower than those of conventional cells, owing to plasma damage to the wafer surface and the excessive defects in the p-type Si film. Recently, Si solar cells based on amorphous Si heterojunction were widely reported, and obviously, as indicated in Table 1, the conversion efficiency was growing at an explosive rate. In 1994, SHJ solar cell conversion efficiency of company Sanyo Corp. reached 21.0% with the adoption of a double-side “HIT” (heterojunction with intrinsic thin layer), and since then it optimized all aspects and in 2011 announced a laboratory conversion efficiency of 23.7% for a 100.7 cm^2 SHJ solar cell [140,141]. Until 2013, Panasonic Corp. announced that the FF of their cells reached 0.832, outperforming the PERC cell in laboratory level, but the efficiencies were undesirable due to the relatively low J_{SC} [57]. Until 2015, Adachi et al. optimized the problem of J_{SC} and broke the conversion efficiency bottleneck of 25% [142]. The parasitic absorption issue significantly limits the J_{SC} of two-side contacted SHJ solar cells, which attributes to the excessive absorption coefficient of a-Si:H in visible band. Later in 2017, Yoshikawa et al. of Kaneka Corp. applied IBC-SHJ technology to achieve a conversion efficiency of 26.3%, breaking the world record held by Panasonic [143]. In the same year, this conversion efficiency was increased again to 26.6%, which is the optimal result achieved so far for an amorphous Si heterojunction-based cell [10].

Table 1
Summary of representative Si SHJ solar cells.

Organization	Device configuration	V_{OC} (V)	J_{SC} (mA/cm^2)	FF	Efficiency (%)	Area (cm^2)	Year
Sanyo	SHJ	0.644	39.4	0.790	21.0	1.0	1994[140]
Sanyo	SHJ	0.745	39.4	0.809	23.7	100.7	2011[141]
Panasonic	SHJ	0.750	39.5	0.832	24.7	101.8	2013[57]
Kaneka	SHJ	0.738	40.8	0.835	25.1	151.9	2015[142]
Panasonic	SHJ + IBC	0.740	41.8	0.827	25.6	143.7	2014[50]
Kaneka	SHJ + IBC	0.744	42.3	0.838	26.3	180.4	2017[143]
Kaneka	SHJ + IBC	0.740	42.5	0.846	26.6	151.9	2017[10]
SERIS	SHJ	0.702	38.2	0.786	21.1	1.0	2012[144]
EPFL	SHJ	0.728	39.2	0.786	22.4	4.0	2014[145]
SIMIT	SHJ	0.741	38.3	0.813	23.1	156.0	2016[146]
Silevo	SHJ	0.739	38.9	0.805	23.1	156.0	2015[147]
ASU	SHJ	0.739	40.4	0.780	23.4	4.0	2015[148]
Hanergy	SHJ	0.721	35.8	0.782	21.7	152.3	2015[149]
CIC	SHJ	0.733	37.3	0.818	22.3	243.0	2012[150]
AUO	SHJ	0.730	38.5	0.834	23.4	238.9	2015[151]
HZB	SHJ + IBC	0.673	39.7	0.757	20.2	1.0	2012[152]
LG	SHJ + IBC	0.716	37.5	0.764	20.5	221.0	2013[153]
CEA-INES	SHJ + IBC	0.711	40.1	0.721	20.6	18.1	2016[154]
EPFL	SHJ + IBC	0.726	40.9	0.740	22.0	9.0	2015[155]
IMEC	SHJ + IBC	0.729	41.6	0.753	22.9	3.97	2016[156]
Sharp	SHJ + IBC	0.736	41.7	0.819	25.1	3.72	2014[157]

In terms of electrical performance, high-efficiency SHJ solar cells need to meet three basic requirements: 1) c-Si surface passivation. An important feature is the prominent passivation performance of the c-Si absorber region, in addition to the chemical passivation of the c-Si absorber region provided by the intrinsic amorphous Si buffer layer, i.e. (i) a-Si:H, and the field effect passivation provided by the doped amorphous Si thin film layers, i.e. (p) a-Si:H and (n) a-Si:H [158]. Chemical passivation refers to the saturation of dangling bonds on c-Si surface by H atoms when (i) a-Si:H is formed while field-effect passivation refers to the repulsion effect for a specific type of carrier by the internal potentials, so that electrons are repelled when holes pass through (p) a-Si:H or holes are repelled when electrons pass through (n) a-Si:H, i.e. selective contact is formed for holes and electrons [159]. The two heterojunctions formed by the amorphous Si film layer and the c-Si absorber region also lead to a high quasi-Fermi energy level splitting, enabling a relatively high V_{OC} for SHJ solar cells [160]. The next step can be taken by improving the light management to obtain a higher J_{SC} and reducing the recombination loss at the maximum power point (MPP). 2) c-Si energy band bending. In order to form selective contacts for electrons and holes, (n) a-Si:H and (p) a-Si:H must provide low (4.1 eV near the c-Si conduction band) and high (5.3 eV near the valence band of c-Si) Φ_m respectively, resulting in strong band bending and a high built-in potential in the c-Si absorption region [161]. Neglecting effects such as Fermi level pinning, (p) a-Si:H and c-Si possess different Φ_m causing band bending and forming a barrier to electron diffusion at the hole contact [162]. If the doping concentration of a-Si:H is very low, some band bending will disappear in (p) a-Si:H [163]. 3) Formation of a continuous majority carrier quasi-Fermi energy level QFL at the hole and electron contact [160]. (p) a-Si:H must be sufficiently doped to ensure that the QFL splitting provided by the c-Si absorption region can be maintained in the doped region of (p) a-Si:H and even n-type TCO to obtain a high selectivity for carrier collection. The formation of a continuous majority carrier QFL instead of a QFL gradient (due to the recombination of the majority carrier) ensures that the operating region is not in the high injection level range, i.e., the actual majority carrier concentration does not exceed the equilibrium majority carrier concentration. Diffused homojunction Si solar cells are heavily doped, which will not cause this problem. However, the doping efficiency of a-Si:H and the concentration of equilibrium majority carriers are very low in SHJ solar cells. In addition, the Φ_m mismatch between TCO and doped a-Si:H will lead to carrier depletion. In order to maintain a high actual majority carrier concentration, SHJ solar cells tend to work at a high injection level, indicating that V_{OC} is lost in SHJ solar cells [30]. Thus, doped amorphous Si films and TCO layers are closely related to the final performance.

Heterojunction engineering, especially on the light-receiving side, is critical, and optimizing the thickness and doping concentration of emitter is complicated. Increasing the thickness of emitter will cause the decrease of J_{SC} , and the heavy doping can cause the depassivation of absorber surface, which seriously affects the V_{OC} of devices. In addition, the doping efficiency of Si-based alloy films is usually unsatisfactory due to their amorphous structure [62,69,164].

For p-type a-Si:H emitter, the selection of doping concentration is crucial, which is attributed to the following aspects: 1) The (p) a-Si:H emitter is required to be sufficiently doped so as to produce a high internal potential to drive out the electrons at the (p) a-Si:H / c-Si interface. In general, the activation energy becomes smaller as the doping concentration increases, with a guaranteed activation energy of less than 0.4 eV for amorphous structures and somewhat less for microcrystals (~ 0.3 eV) [165,166]; 2) Sufficient band bending in the c-Si needs to be created to allow the minority carriers tunneling to occur, whereas a low doped emitter will block this process, resulting in a low FF [167,168]; 3) TCO is usually deposited on the emitter to improve the collection of carriers. However, a Schottky can be formed at the interface of TCO / (p) a-Si:H if the TCO Φ_m is lower than that of (p) a-Si:H emitter (the Φ_m of commonly used ITO is 4.7 eV) [169–172]. The Schottky barrier formed

by the Φ_m mismatch has a significant effect on final performance, mainly because the Schottky barrier is in the opposite direction of the p-n junction below [170–172]. The Schottky barrier directly affects the collection of holes and the FF, and also causes the injection of electrons from the TCO into the emitter and recombines with the holes, resulting in the depletion of holes in the emitter or even inversion [173,174]. The total defect recombination in the TCO / (p) a-Si:H / (i) a-Si:H stack includes the interface recombination and the dominant recombination within the (p) a-Si:H. The defect recombination results in the loss of the internal voltage of the MPP in the small injection range, which leads to the loss of FF [175,176]. Therefore, the emitter must be sufficiently doped to maintain flat band conditions in the emitter [177]. The effective screening length represents the characteristic length required to screen the Schottky barrier height, and the effective screening length confirms the lower limiting value of emitter thickness. The degree of Φ_m mismatch is positively correlated with the required effective screening length, while the doping concentration of (p) a-Si:H is opposite [178]. The effective screening length and the TCO / (p) a-Si:H Schottky barrier results in a mutual compromise between the J_{SC} and FF [179–181]. In addition, the growth of doping layer also affects the buffer layer underneath, which in turn affects the passivation performance of the (i) a-Si:H / c-Si interface, and a too thin buffer layer cannot mitigate the damage to the passivation quality [182,183]. Therefore, a compromise is essential between c-Si passivation performance and (p) a-Si:H doping concentration for SHJ devices, and between V_{OC} and FF which vary with doping.

The TCO should produce the minimum contact resistance required for effective carrier transport, and the TCO (and its deposition technique) should not degrade the passivation performance of the underlying thin film layer and not affect the carrier recombination in the c-Si absorber layer [185]. In fact, the key to satisfying these two requirements is the energy band alignment between the TCO and the amorphous Si and c-Si layers [186]. Besides, the conductivity of the TCO must be sufficiently high to minimize carrier recombination and transport losses, allowing the SHJ solar cell to achieve high FF. In terms of the surface passivation, the presence of highly doped TCO has no detrimental effect on the passivation of (i) a-Si:H / (n) a-Si:H stacks, but the opposite effect on (i) a-Si:H / (p) a-Si:H stacks, so the contact of highly doped TCO with the latter stacks should be avoided in the front contact [187]. When the TCO Φ_m is lower than that of the (p) a-Si:H, the contact between the two results in depletion or even inversion. When the doping concentration of (p) a-Si:H is insufficient and the mismatch between TCO and (p) a-Si:H is severe, not only the interface but also the whole a-Si:H layer will be depleted or even inverted. The depletion and inversion affect the extraction of carrier, which in turn reduces the FF. The depletion and inversion also result in the deteriorations in the energy band bending of the (p) a-Si:H / (n) c-Si junction and the built-in potential, which causes a decrease in carrier selectivity at the contact of the SHJ solar cell and a decrease in V_{OC} , as shown in Fig. 13, where the arrows indicate the aggravation in the Φ_m mismatch. Therefore,

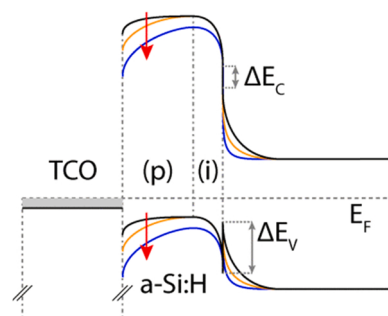


Fig. 13. The evolution trend of band alignment with change of TCO Φ_m [184]. Reproduced with permission. Copyright 2013, IEEE.

reducing the ϕ_m mismatch and increasing the doping concentration of the (p) a-Si:H layer can improve the contact performance [188]. If the ϕ_m of TCO is higher compared to (p) a-Si:H, it will cause accumulation of holes. This accumulation can be regarded as increasing the doping concentration, which is also beneficial to improve the contact performance [189].

Bivour et al. simulated the SHJ device properties based on Sentaurus TCAD software [72]. The n-type TCO was treated as a conductive layer with an interfacial ϕ_m . (p) a-Si:H emitter activation energies of 200 meV and 300 meV correspond to ϕ_m of 5.4 eV and 5.3 eV, respectively, i.e., the higher the doping concentration, the lower the activation energy and the higher the corresponding ϕ_m . Fig. 14 shows the interaction between the TCO ϕ_m , emitter doping concentration and thickness and final performance. It can be seen that optimal solar cell results are obtained for high ϕ_m , which can be attributed to a positive ϕ_m mismatch at the TCO / (p) a-Si:H interface ($\phi_m_{TCO} > \phi_m_{(p)a\text{-Si:H}}$) resulting in the formation of hole accumulation in the emitter. In the case of negative ϕ_m mismatch ($\phi_m_{TCO} < \phi_m_{(p)a\text{-Si:H}}$), the inverse Schottky barrier causes hole depletion, which reduces the device performance. This figure also shows that thicker emitters with highly doped can tolerate the negative ϕ_m mismatch, and the V_{OC} and FF of SHJ solar cells are better.

There exist defects near the TCO / a-Si interface, and interestingly, they are generally considered favorable for transport [37]. Besides, these defects can reduce the screening length and hence barrier width in the doped a-Si [190]. For sufficient doping, partly crystalline materials are considered more advantageous than amorphous Si due to their more desirable doping efficiency [30,190–194]. This is particularly true for (p) a-Si, which is less efficiently doped than (n) a-Si [195].

J_{SC} and FF are two obvious constraints on the efficiencies of SHJ solar cells. In order to improve the blue response, the thickness of the front side a-Si can be reduced directly on the one hand, and on the other hand by using alloying or growing partly crystalline Si films to reduce the absorption coefficient. [69,196–198]. The improvement in the infrared response depends on the trade-off between conductivity and transparency of the TCOs, and it is less pronounced when high mobility TCOs are available [199–202].

One of the characteristics of SHJ devices is an amorphous Si / c-Si interface with high passivation quality, which requires a high degree of

cleanliness and a suitable pyramidal shape on the wafer surface. Therefore, SHJ solar cells require more stringent requirements for the wafer cleaning steps. The RCA cleaning process is generally used for wafer cleaning of SHJ devices. However, the chemical consumption and the total cost of this method is extremely high. In response to the challenges faced by the RCA cleaning process in the large-scale production of SHJ solar cells, ozone (O_3)-based wafer cleaning processes and mass production equipment have been emphasized [203]. Ozone-based cleaning is a process that eliminates the use of ammonia, nitric acid, and hydrogen peroxide solutions, and does not discharge any nitrogenous wastewater, but is highly effective in removing organic (e.g., additive residues) and metallic (e.g., potassium, sodium, and transition metal ions) impurities, and in controlling the microstructure of the pyramidal textures. As a result, the ozone cleaning process has been widely promoted in the global scale production of SHJ solar cells since 2015 [204].

The growth of high quality intrinsic / doped hydrogenated amorphous Si films and obtaining high quality hydrogenated amorphous Si / c-Si interfaces are also crucial. Hydrogenated amorphous Si thin films are usually prepared by CVD, which contains two mainstream methods: PECVD and hot wire CVD (HWCVD) according to different equipment. Compared with PECVD, HWCVD has a narrower application range, but it has achieved success in SHJ devices. The latest mass production technology in Sanyo Company of Japan adopts the latter. HWCVD hydrogenated amorphous Si has a more pronounced interface with c-Si, and the transition layer thickness at the interface is about 1/3 that of PECVD. The slope of the signal change from HWCVD hydrogenated amorphous Si to c-Si is greater, corresponding to a steeper hydrogenated amorphous Si / c-Si interface (shown in Fig. 15). Matsumura et al. studied the passivation effect of (i) a-Si:H deposited by HWCVD and PECVD on Si surfaces and prepared SiN_x / (ii) a-Si:H / c-Si / (iii) a-Si:H / SiN_x double-sided passivation samples, in which SiN_x was grown by HWCVD and (i) a-Si:H was prepared via HWCVD or PECVD [205–207]. The minority carrier lifetimes of the tested samples were 10 ms (HWCVD) and 3 ms (PECVD), respectively, indicating that the HWCVD-grown (i) a-Si:H has better passivation results.

In recent years, advances in TCO thin films on SHJ solar cells have been dominated by improvements in deposition methods and TCO

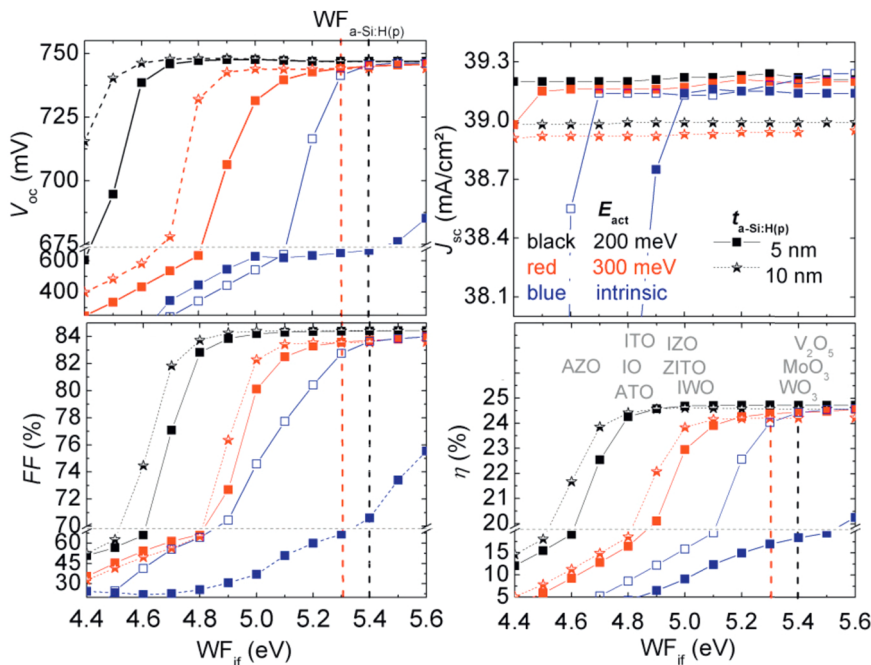


Fig. 14. V_{OC} , FF , J_{SC} and the conversion efficiency with the change of ϕ_m for different (p) a-Si:H doping and (p) a-Si:H thicknesses [72]. Reproduced with permission. Copyright 2013, Elsevier.

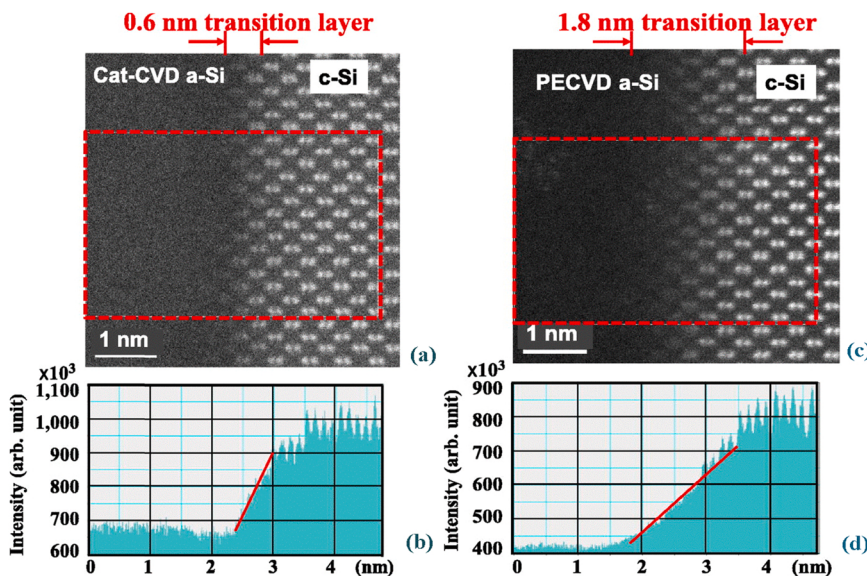


Fig. 15. High resolution STEM image for amorphous Si on c-Si: (a) hydrogenated amorphous Si deposited by HWCVD, (c) hydrogenated amorphous Si deposited by PECVD. (b) and (d) correspond to the signal intensity distribution of closely spaced Si atoms in the red rectangular regions in (a) and (c), respectively. The lower signal intensity plateau corresponds to the region of hydrogenated amorphous Si, and the higher signal intensity plateau corresponds to the region of c-Si [205].

Reproduced with permission. Copyright 2015, AIP Publishing Group.

materials. Since the high V_{OC} of SHJ devices is related to the ideal passivation effect, this requires that the subsequent TCO deposition process must not destroy the initial passivation of a-Si:H films. Obviously, TCO deposition technology with low ion bombardment damage is essential to achieve high FF and high V_{OC} . Considering the demanding requirements of many optoelectronic devices for TCO thin films and their preparation techniques, Sumitomo Corp. has developed a low-temperature, low-damage TCO thin film deposition device - reactive plasma deposition (RPD) or ion platin [208–210]. Compared with the conventional magnetron sputtering deposition technology, the plasma energy distribution of RPD technology is relatively concentrated and the dissociation rate is higher, with the energy distribution of effective particles in the range of 20–30 eV and almost no high-energy particles (> 50 eV) [211–215].

3.2. Technical challenges and future development directions

For SHJ solar cells, reducing the frontal shading loss, reducing the ohmic loss of the grid line, improving the contact between the electrode and TCO, and low-cost electrode preparation are the research directions for metallization. Choosing low resistance silver paste, reducing the width of the grid line and the optimization of grid line aspect ratio are conventional methods applied to improve the electrode properties [216]. The recent emergence of the technology of busbar-free and copper metallization are effective attempts to break through the bottleneck of screen printing technology and improve the probability of carrier collection. It has always been the industrial goal to reduce the consumption of silver paste at low temperature and use other metals instead of silver in the electrodes. The conductivity of copper is second only to that of silver, but its price is only 1/100 of that of silver, so copper paste attracts more attention [217,218]. However, due to its relatively poor printability and higher volume resistivity, copper paste has not been widely used in solar cells. Another method is to realize metallization of SHJ solar cell by copper electroplating technology. Electroplated copper electrode has obvious advantages over screen printing low-temperature silver paste in conductivity, electrode aspect ratio and grid line design. However, the metallization process of copper electroplating is more complicated, and the treatment and discharge of copper electroplating solution will also bring some environmental problems.

Despite the obvious advantages summarized above, the current market share of SHJ solar cells is still small and needs to further improve core competencies [219–221]. New technologies such as back junction

and carrier selective passivation contact are expected to push the conversion efficiency to ~25%. The IBC-SHJ structure combines the advantages of both heterojunction and back contact structures to ensure a superior passivation performance and thus a high V_{OC} , while the removal of the frontal metal grid line allows the solar cell to absorb more photons and increase the J_{SC} , thus maximizing the conversion efficiency. The IBC-SHJ device has achieved the record (26.6%) of single-junction c-Si solar cells, which may be the basis for future mass production with conversion efficiencies of 25–27% or more.

In the future, the SHJ device industry will continue to evolve and more research will focus on reducing the cost of SHJ solar cells, optimizing the performance of related materials, simplifying the manufacturing process and mass reproducible production, rather than simply pursuing higher efficiency. The SHJ solar cells can be further improved by optimizing the constituent materials, the manufacturing process and the component structure, for example, by using a-SiO_x:H, μc-SiO_x:H, a-SiC_x:H materials with variable band gaps to replace the emitter layer and passivation layer; optimization of the interface passivation technique, thinning process of the absorbing layer, doping diffusion technique and the electrode boundary contact.

For the development of SHJ solar cells, from a cost perspective, the wafer texturing process is well established in production and the cost of PECVD equipment for a-Si thin film deposition is still relatively high. In addition, the TCO double-sided integrated deposition combines the advantages of RPD and PVD to reduce the consumption of raw materials and shorten the process time, which is the future direction of process cost reduction. Therefore, researchers should focus their research on SHJ solar cells in the following areas: developing low resistance low temperature pastes, optimizing the deposition process, improving the properties of the passivation layer, and searching for alternative materials with high light transmission and good electrical conductivity for the emitter layer. It is also necessary to streamline the process flow and try out new component structures to further reduce the cost of large-area fabrication.

3.3. Dopant-free asymmetric heterocontact solar cells

3.3.1. Research status and progress

An excellent strategy for realization of passivating contact is the introduction of dopant-free materials to substitute the doped Si. In terms of hole selective contact, a large amount of materials have been studied, such as TAPC, Spiro-OMeTAD, and PEDOT:PSS, and PEDOT:PSS is most widely used among them [222–227]. However, homogeneous

deposition of PEDOT:PSS on a textured c-Si substrate is extremely difficult and can cause serious interface problems. Another problem with the PEDOT:PSS layer is its severe parasitic absorption. A severe problem of parasitic light absorption in the PEDOT:PSS exists when deposited on the front side, therefore, putting it on the back side to form the so-called “BackPEDOT” structure is a reasonable solution. [226].

Alkali and alkaline earth metal salt, such as LiF_x , MgF_x , Mg and Ca, can serve as electron-selective contact materials to enhance electron extraction. Low ϕ_m will be acquired when these materials are integrated underneath metal electrodes, which promotes the collection of electrons. Usually, achieving low-resistance contact between metals and lightly doped n-type c-Si is an intractable problem, which is caused by the high Schottky barrier for electrons due to the Fermi-level pinning effect. In 2016, some scholars successfully designed and realized a DASH structure using the stack of alkali metal fluorides and intrinsic a-Si:H, and the final efficiency reached 19.42% [76]. Magnesium fluoride (MgF_2) is the conventional choice for anti-reflection coating materials due to its ideal transparency and low refractive index [228,229].

Due to its low price, non-toxic and abundant reserves, TMO materials have gained widespread attention, which generally present large band gaps, ϕ_m and conductivities with a wide range of variations. Table 2 summarizes c-Si solar cells containing TMO carrier selective contacts in recent years, and shows a dramatic increase in efficiency. MoO_x , V_2O_x , and WO_x are common TMO candidates for hole-selective contacts, which present an n-type nature and possess high ϕ_m (~ 6.0 eV). The Fermi levels can be aligned and induce energy band bending on the c-Si surface when TMO materials are connected with c-Si, which bring similar results to those of the p-type a-Si:H layer. In terms of band alignment, an obvious conduction band offset is generated on the Si surface, causing an inversion layer of hole accumulation, which ensures an ideal built-in potential [76]. The most studied hole-selective contact material is MoO_x . In 2015, Geissbühler et al. used MoO_x instead of (p⁺) a-Si:H emitters in conventional SHJ devices and obtained a final efficiency of 22.5%, which is the highest efficiency available for TMO-based hole-selective contact solar cells [230]. Many researchers have compared the effects of different hole-selective contacts TMO materials

(MoO_x , V_2O_x , WO_x) on the SHJ devices, and concluded that the performance of V_2O_x is superior to others. Wu et al. designed and implemented a multifunctional V_2O_x / Au / V_2O_x hole-selective contact with an IBC structure, and the device efficiency was 19.02% [82]. The higher FF is ensured by the near perfect match between the energy band of NiO and Si. It is shown that as the doping concentration of NiO decreases, the degradation caused by surface traps increases significantly, and the recombination increases caused by the reduced surface electric field in c-Si. Menchini et al. experimentally characterized the photovoltaic properties of NiO_x as hole-selective contact layer by sputtering, reducing the filtering effect caused by a-Si:H emitter [250]. However, due to the low conductivity of NiO_x , a high conductivity TCO is still required to complete the heterostructure to optimize the series resistance [251–253]. The simulation results have shown that improving the conversion efficiency requires optimization of the NiO_x deposition process and the insertion of an optimized buffer layer between the NiO_x and c-Si interfaces to improve the passivation quality. In 2018, Bullock et al. adopted TiO_x / LiF_x composite structure to improve the efficiency to 20.7% based on the previous research [38,237]. The ideal passivation effect of TiO_2 was due to Si-O-Ti bonds that passivated the dangling bonds [254]. Although the energy band structure of ZnO is very similar to that of TiO_2 , ZnO cannot form similar bonds and cannot passivate. Finally, the V_{OC} of the solar cell with TiO_2 was 643 mV and the FF was 72.4%, while the V_{OC} of the solar cell with ZnO was 637 mV and the FF was 75.2%, which did not show any significant difference between the two. Interestingly, silver-doped aluminium-rich zinc oxide (ZnO:Al:Ag) exhibited a remarkable passivation effect on n-Si in study of Khan et al. ($iV_{OC} = 688.1$ mV) [255]. The passivation is formed by the chemical aspect of SiO_x , and by the field-effect passivation due to the induced charge [256]. There exists problem of lattice mismatch between TMO and c-Si, the c-Si surface is therefore poorly passivated, resulting in a large amount of defect states at the TMO / c-Si interface and poor property of the directly formed device [43]. The most common passivation materials used are a-Si:H and SiO_x . The highest efficiency of the current MoO_x hole-selective contact-based solar cell is achieved by using an intrinsic a-Si:H layer on both c-Si surfaces, realizing a conversion

Table 2
Summary of c-Si solar cells containing TMO carrier selective contact.

Organization	Device architecture	V_{OC} (V)	J_{SC} (mA/cm ²)	FF	Efficiency (%)	Area (cm ²)	Year
UCB	MoO_x / (n) c-Si / (n) a-Si:H	0.580	37.8	0.650	14.3	0.25	2014[43]
IMT	MoO_x / (i) a-Si:H / c-Si / (i) a-Si:H / (n) a-Si:H	0.725	38.6	0.804	22.5	3.93	2015[230]
ANU	p ⁺ -Si / (p) c-Si / MoO_x	0.616	37.0	0.720	16.4	4.00	2015[231]
ANU	p ⁺ -Si / (n) c-Si / TiO_2	0.639	39.2	0.791	19.8	4.00	2015[232]
UCB	MoO_x / (i) a-Si:H / c-Si / (i) a-Si:H / LiF_x	0.716	37.1	0.732	19.4	4.00	2016[38]
UCB	MoO_x / (i) a-Si:H / (n) c-Si / (i) a-Si:H / (n) a-Si:H	0.711	39.4	0.672	18.8	4.00	2014[233]
UPC	V_2O_x / c-Si / (n) a-Si:H	0.606	34.4	0.753	15.7	4.00	2016[86]
UPC	MoO_x / c-Si / (n) a-Si:H	0.581	34.1	0.688	13.6	4.00	2016[86]
UPC	WO_x / c-Si / (n) a-Si:H	0.577	33.3	0.650	12.5	4.00	2016[86]
ANU	p ⁺ -Si / (n) c-Si / SiO_2 / TiO_2	0.650	39.5	0.800	20.5	4.00	2016[234]
SYSU	V_2O_x / Au / V_2O_x	0.651	38.7	0.755	19.0	4.00	2017[82]
ANU	p ⁺ -Si / (n) c-Si / MgO_x	0.628	39.5	0.806	20.0	4.00	2017[235]
NKU	MoO_x / (i) a-Si:H / c-Si / (i) a-Si:H / BZO	0.599	38.1	0.727	16.6	1.00	2017[236]
UCB	MoO_x / (i) a-Si:H / c-Si / (i) a-Si:H / TiO_x / LiF	0.706	38.4	0.762	20.7	4.00	2018[237]
UCAS	MoO_x / (i) a-Si:H / c-Si / (i) a-Si:H / SiO_x / TiO_2	0.696	38.6	0.753	20.2	1.00	2019[238]
ANU	PEDOT:PSS / c-Si / TiO_x / LiF	0.626	31.9	0.756	15.1	1.00	2019[239]
SYSU	p ⁺ -Si / (i) a-Si:H / (n) c-Si / ZnO / LiF_x	0.727	37.6	0.780	21.3	4.00	2020[240]
SYSU	CrO_x / Ag / CrO_x / (p) c-Si / n ⁺ -Si	0.638	39.8	0.801	20.3	4.00	2018[241]
UCAS	MoO_x / CrO_x / (p) c-Si / n ⁺ -Si	0.603	36.5	0.721	15.9	9.73	2020[242]
IIT	NiO_x / (n) c-Si / LiF_x	0.580	36.9	0.711	15.2	1.44	2019[243]
EPFL	MoO_x / (i) a-Si:H / (n) c-Si / (i) a-Si:H / ZnO / LiF_x	0.706	39.2	0.773	21.4	4.00	2020[244]
SIEMIS	p ⁺ -Si / (n) c-Si / (i) a-Si:H / TiO_xN_y	0.698	39.5	0.808	22.3	4.00	2020[245]
SYSU	MgF_x / (i) a-Si:H / (n) c-Si / (i) a-Si:H / MoO_x	0.718	41.5	0.742	22.1	4.00	2020[246]
EPFL	MoO_x / (i) a-Si:H / (n) c-Si / (i) a-Si:H / (n ⁺) a-Si:H	0.734	39.1	0.818	23.5	3.97	2020 [247]
AIST	TiO_x / (n) c-Si / (i) a-Si:H / (n ⁺) a-Si:H	0.677	40.5	0.768	21.1	4.00	2020 [248]
CAS	n ⁺ -Si / (p) c-Si / SiO_x / MoO_x / V_2O_x	0.627	38.5	0.828	20.0	9.73	2020 [249]

efficiency of 23.5% [236]. Many researchers have found that although both thermal evaporation and solution methods for the preparation of MoO_x naturally form SiO_x and provide a certain degree of chemical passivation, but the poor denseness of SiO_x makes it difficult to obtain excellent passivation results [86,255,257]. A separate process is therefore required to achieve a dense SiO_x passivation layer. Ozone treatment, thermal nitric acid method and hydrogen peroxide oxidation of SiO_x passivation layers have given excellent results in TOPCon devices, which also applies to DASH architecture.

Most of the TMO-based DASH cells have a front-junction double-sided contact structure, as shown in Fig. 16, which means that the hole-selective contact is on the incident side of the light, and the electrodes for collecting carriers are located on both sides. This conventional structure achieves a conversion efficiency of up to 22.5%, which is the highest of all TMO-based solar cells so far [230]. As depicted in Fig. 17, to make better use of light, referring to the IBC structure inspired by SunPower, Um et al., Wu et al. and Masmitjà et al. placed both the selective contact for electron and hole on the back side to achieve an all-back-contact structure with efficiencies of 15.4%, 19.02% and 19.1%, respectively [81–83].

There are many techniques for the preparation of TMO, such as thermal evaporation and electron beam evaporation, which are widely used due to the low cost of low particle bombardment in the preparation process, and ALD technique, which allows precise control of film composition and thickness, has also been paid attention to [43,78,258]. Oxygen vacancies in TMO materials are critical to the regulation of electrical properties and ultimately affect device performance [259]. In response to the problem that the evaporation technique cannot control the oxygen vacancies in TMO on a large scale, Greiner et al. used reactive magnetron sputtering to prepare WO_x , which can easily regulate the electrical conductivity, Φ_m and parasitic light absorption of the film [259]. Boccard et al. used magnetron sputtering to prepare MoO_x on c-Si, changing the hole selection ability of MoO_x by adjusting the oxygen content [260]. The sputtering method is more damaging to the wafer, a-Si was therefore added as a passivation layer between MoO_x and c-Si. Although the minority carrier lifetime decreases sharply after sputtering, most of it can be recovered by subsequent annealing. The feasibility of obtaining the MoO_x layer by magnetron sputtering instead of thermal evaporation for solar cell applications has been demonstrated. Magnetron sputtering is also expected to modulate and improve the photovoltaic properties of the material through doping, but the particle bombardment during sputtering is severe and an effective control scheme needs to be proposed. The solution method is also a commonly used method for the preparation of thin films [257,261,262]. MoO_x prepared by the solution method has a bronze structure and contains hydrogen, denoted as H- MoO_x . The greatest advantage of this type of solution method is that the oxygen vacancies of the material can be easily changed by subsequent low-temperature annealing, which allows

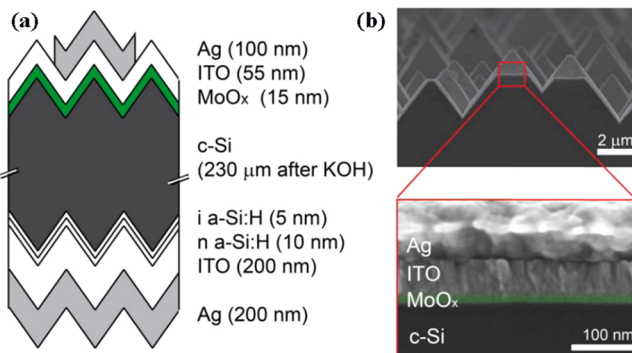


Fig. 16. (a) Structure of a MoO_x -based DASH solar cell. (b) the sectional view measured by scanning electron microscopy (SEM) [43]. Reproduced with permission. Copyright 2014, ACS.

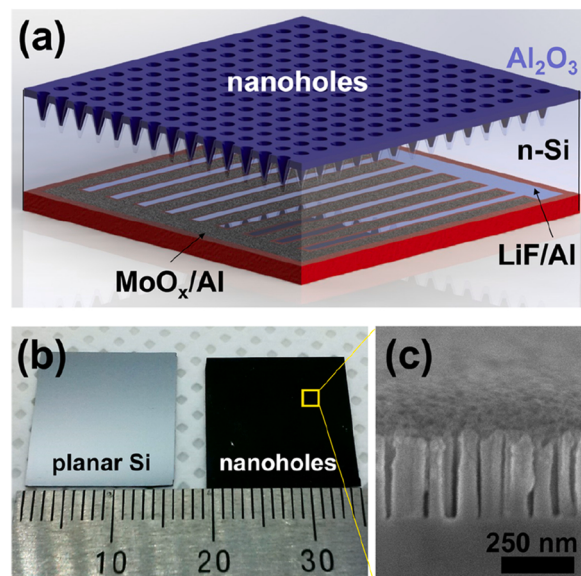


Fig. 17. (a) Schematic of Si nanohole all-back-contact solar cell. (b) optical images of planar and nanohole devices. (c) the sectional view of Si nanoholes [81].

Reproduced with permission. Copyright 2016, ACS.

the Φ_m to be adjusted, and is therefore widely used in organic solar cells [261]. Tong et al. attempted to use H- MoO_x prepared by a similar solution method as a hole-selective contact and found that SiO_x formed naturally during the preparation process, with some passivation effect, as shown in Fig. 18 [257]. Finally, H- MoO_x prepared by the solution method and MoO_x prepared by thermal evaporation formed heterojunctions with c-Si, respectively, with comparable contact resistance and passivation effect. Another potential advantage is that the migration of the hydrogen contained in H- MoO_x to the H- MoO_x / c-Si interface may be further enhanced by a suitable subsequent treatment scheme to improve the passivation property [263,264].

3.4. Technical challenges and future development directions

The research on DASH devices has made rapid progress recently, but there are still some problems that need to be further investigated. (1). Hole-selective contact: TMO / Ag / TMO multifunctional emitters have high conductivity and high transmittance, but the presence of Ag films leads to reduced long-wave transmittance, so an IBC structure is needed [265]. Silver nanowires (AgNWs) are able to improve the conductivity and transmittance over a wide spectral range, but their Φ_m and energy band position are not well matched to c-Si [266]. Therefore, the use of MoO_x / AgNWs / MoO_x multilayers with hole-selective contacts is expected to improve solar cell performance by combining high Φ_m , high conductivity and high transmittance. (2). Interfacial passivation layers: The commonly used a-Si:H passivation layer has parasitic absorption and requires relatively expensive PECVD equipment; natural oxide passivation does not meet the requirements. SiO_x passivation layers have been used in TOPCon solar cells with gratifying results. Thermal oxidation, concentrated nitric acid oxidation and field induction can be used to produce ultra-thin, dense SiO_x passivation layers, and a suitable SiO_x interfacial layer can reduce hanging bonds on the c-Si substrate surface and effectively prevent photogenerated carriers from recombination near the surface [100,101,122]. The possibility of preparing novel SiO_xNy passivation layers by plasma technology can be further explored. (3). BackDASH device architecture: conventional solar cells using MoO_x / c-Si heterojunctions as optical incidence planes need to consider both the optical and electrical properties of MoO_x [38,79]. With the well-designed structure of the BackDASH concept, MoO_x is

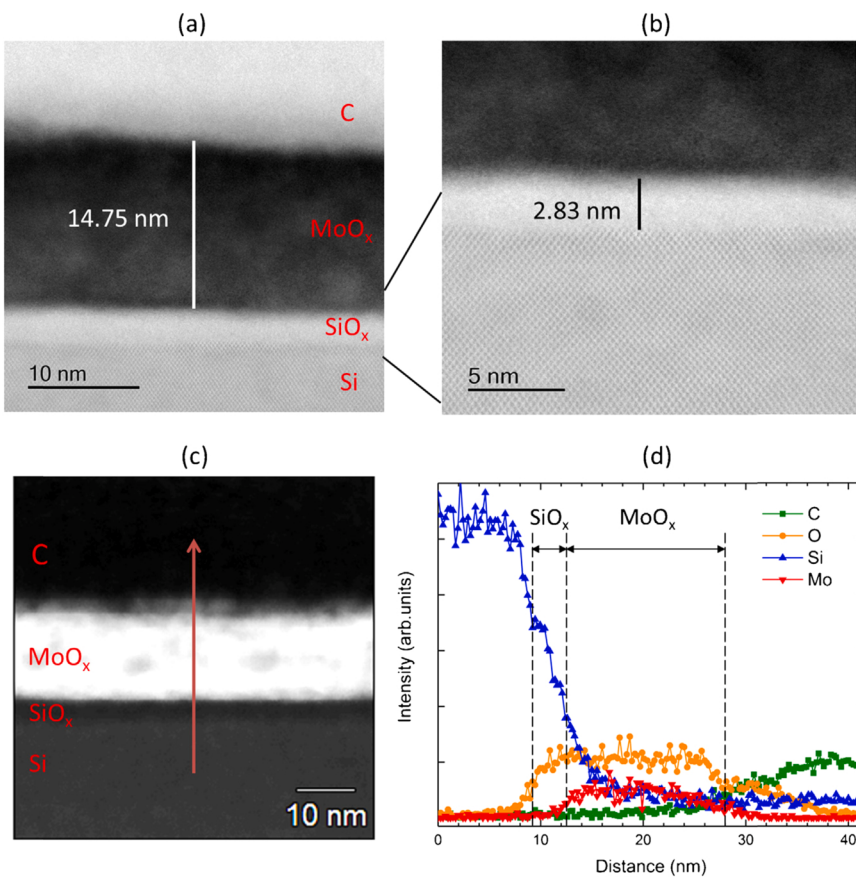


Fig. 18. (a) 10 nm scale sectional view of an as-deposited MoO_x film on Si measured by scanning transmission electron microscopy (STEM). (b) the image of the MoO_x and c-Si interface. (c) cross-sectional STEM image for the region of the (energy dispersive X-ray spectroscopy) EDS line scan. (d) compositional distribution of each element measured using the EDS line scan showing a thin SiO_x layer formed between the MoO_x and the c-Si [257]. Reproduced with permission. Copyright 2017, Elsevier.

placed at the back side, so that it is not necessary to consider its optical performance, but to consider how to regulate its electrical characteristics such as ϕ_m and conductivity. In addition, this solar cell uses ZnO as the plane of light incident, especially the LPCVD-grown ZnO:B has a textured structure with a characteristic size of several tens of nanometers, while the c-Si pyramidal textured surface has a characteristic size of several microns, so the front surface can form a nano / micron composite trapped structure, which is expected to further reduce the reflectivity of the front surface, obtaining ultra-low reflectance over a wide spectral range. (4) Carrier separation mechanism and transport processes: The photogenerated carrier separation mechanism in TMO / c-Si cells is not well understood, and although some models have been proposed, they are only shown to be closely related to the material properties. Clarification of the corresponding mechanism will guide the optimization of the device structure and the improvement of the solar cell performance. (5). Yet, tunnel contacts that rely to a large extent on a sufficiently high fixed charge density for their carrier selectivity have only been marginally investigated so far and may deserve further attention. (6). When further exploring TMOs in the context of passivating contacts, relevant experience in other fields can be referred to, such as microelectronics and organic electronics, where the electrical properties of TMOs have already been investigated. It is likely that this class of materials will attract more attention in research when more examples of promising oxides can be identified and optimized. An example of such a material is hafnium oxide (HfO_x), for which the c-Si passivation quality has recently attracted attention. In addition, tantalum oxide (TaO_x) has recently appeared as a candidate electron-selective passivating material, while hole-selective contact properties have been demonstrated for nitrogen-doped copper oxide ($\text{CuO}_x:\text{N}$). However, these novel materials have not been integrated into an actual passivating contact structure so far, implying that their potential is still being evaluated. (7). Up to now, the efficiencies of DASH devices combining IBC structure have not

exceeded those of the both-sides contacted ones, although the low-temperature deposition and metal patterning techniques, together with the simplicity of the devices themselves, still suggest the great potential of all-back-contact c-Si solar cells using TMO-based passivating contacts.

3.5. Poly-Si / SiO_x passivating contacts solar cells

3.5.1. Research status and progress

The ISFH has given a theoretically detailed analysis of the theoretical efficiency limits of solar cells with different structures based on the concept of carrier selectivity [267]. Fig. 19 shows the limit efficiency calculations for solar cells composed of different electron / hole-selective materials in combination. The solar cells with electron selective material $\text{SiO}_x / (\text{n}^+)$ poly-Si in combination with hole selective material $\text{SiO}_x / (\text{p}^+)$ poly-Si can reach a selectivity of 13.8–14.2, which is higher than the HIT, thus have an even higher efficiency limit (28.2%–28.7%), higher than the 27.5% limit efficiency of HIT, and also much higher than PERC (24.5%), and closest to the theoretical limit efficiency (29.43%). In recent years, passivation contact technology has advanced by leaps and bounds, presenting a range of material combinations. Seen from Fig. 20, poly Si-based contacts combine both excellent ρ_c and J_0 , ensuring that solar cells based on it have the highest conversion efficiency available [268]. Compared with other common contact materials, poly Si is the best candidate in terms of comprehensive performance. While the characteristics of different passivating contact techniques have been well understood, the most significant problem for industrialization is optimizing the strong performer of poly Si-based contacts by improving existing materials or exploring new materials. Table 3 lists some representative achievements reported for solar cells featuring TOPCon architecture. As can be seen, compared to the SHJ and DASH solar cells summarized above, solar cells with the TOPCon

η_{max} [%] Se&h		Electron-selective contacts						
		P-diffused n^+	a-Si:H(i)/a-Si:H(n)	th-SiO _x /poly-Si(n^+) PECVD	th-SiO _x /poly-Si(n^+) LPCVD	chem-SiO _x /poly-Si(n^+) LPCVD	SiO _x /TiO _y	MgO _x
Hole-selective contacts	Al- p^+	24.5 (PERC) 11.7	26.8 12.8	26.9 12.8	27.1 12.9	27.1 13.0	26.3 12.5	24.9 11.9
	a-Si:H(i/p)	24.7 11.8	27.5 (HIT) 13.2	27.7 13.3	27.9 13.5	28.0 13.5	26.8 12.8	25.1 12.0
	SiO _x /poly-Si(p^+)	24.9 11.9	28.1 13.6	28.3 13.8	28.7 14.2	28.7 14.2	27.3 13.1	25.4 12.1
	SiO _x /Si:C (p^+)	24.9 11.9	28.0 13.5	28.2 13.7	28.5 14.0	28.6 14.1	27.2 13.0	25.3 12.1
	a-Si:H(i)/MoO _x	24.4 11.7	26.5 12.6	26.6 12.7	26.8 12.8	26.8 12.8	26.0 12.4	24.7 11.8
	MoO _x	24.1 11.6	25.9 12.3	26.0 12.4	26.1 12.4	26.1 12.4	25.5 12.2	24.4 11.7
	PEDOT:PSS	24.1 11.6	26.0 12.4	26.1 12.4	26.2 12.5	26.2 12.5	25.6 12.2	24.5 11.7

Fig. 19. Combined selectivity $S_{e\&h}$ and maximum efficiency η_{max} of solar cells composed of different electron / hole-selective contact materials [267]. Reproduced with permission.

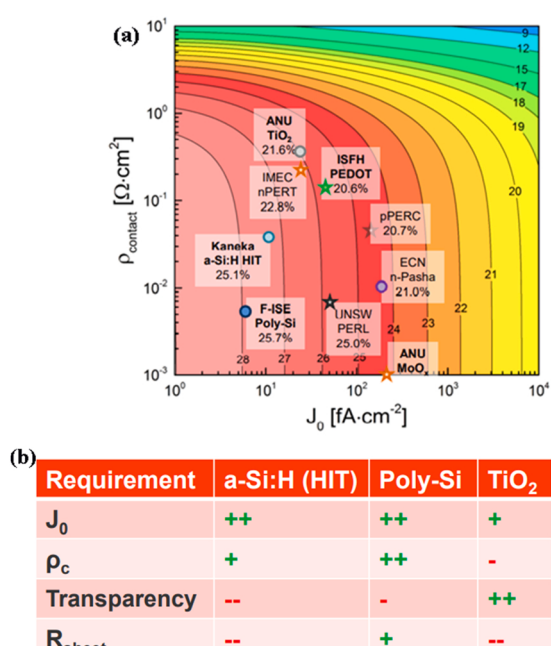


Fig. 20. (a). J_0 , ρ_c and the highest efficiency for various passivating contacts. (b). comparison of properties (J_0 , ρ_c , transparency and sheet resistance R_{sheet}) of different contact materials, the green plus sign indicates excellent performance, while the red minus sign indicates poor performance [268].

Reproduced with permission. Copyright 2017, Wiley.

architecture have a higher overall conversion efficiency over a larger area and therefore have better prospects for industrial application. Recently, the conversion efficiency of LONGi's monocrystalline double-sided n-type TOPCon solar cells reached 25.09% as tested by the ISFH Institute in Germany, which is the first time that the efficiency of wafer-based commercial size TOPCon cells exceeded 25%, which proves that the TOPCon structure will occupy an important position in the industrial production map [289].

As a typical representative of the passivation contact concept, TOPCon has been incorporated into solar cells of different architectures: (1). TOPCon cell with a homojunction emitter at the front and a passivating

rear contact; (2). IBC cell with both electron and hole passivation contacts on the back side; (3). solar cell with TOPCon top / rear contacts (double-side contacted). Up to now, the efficiency records for the above cell configurations are 25.8% (ISE), 26.1% (ISFH), and 22.6% (EPFL), respectively [269,277,280]. However, these records were obtained based on complicated processes, and there is still a long way to go before it is truly applicable to industry.

Compared with the a-Si:H-based contacts, poly-Si / SiO_x contacts are more thermally stable. However, this structure generally requires a high-temperature process to condition the material properties for the passivating contacts, especially for achieving the desirable doping. Besides, another nonnegligible drawback of poly-Si / SiO_x contacts is that the bandgap of poly-Si is parallel to that of c-Si, which is expected to cause severe absorption losses when arranged at front side of devices. The heavily doped properties of poly-Si (to form good contacts to improve carrier selectivity) can also result in significant free-carrier adsorption, which still needs to be considered [112]. Considered the adsorption losses problem, researchers have long been committed to finding more transparent carrier-selective materials. Hydrogenated nanocrystalline Si (nc-Si:H) is regarded as an ideal candidate that circumvents the severe adsorption losses. Higher transparency is a unique advantage of nc-Si:H. Besides, it also ensures higher doping efficiency, lower contact resistivity, and suppressed Schottky barrier at the interface with TCO compared with a-Si:H [194,290]. Interestingly, the transparent will further improve when alloying with oxygen, i.e., constituting hydrogenated nanocrystalline Si oxide (nc-SiO_x:H). In the study of L. Mazzarella et al., a large J_{SC} improvement was obtained when p-type nc-SiO_x:H was substituted for a-Si:H [291]. Alternatively, the combination of an ultrathin SiO_x layer and hydrogenated nanocrystalline Si carbide (nc-SiC_x:H) can provide excellent passivating properties after annealing at high temperatures, which generally applied as hole-selective passivating contacts with excellent J_0 and ρ_c results [119,290]. However, unsatisfactory transparency is still an important aspect that restricts its applications, practically when applied at rear side. In addition to enable an excellent surface passivation, poly-Si / SiO_x can also improve the bulk properties [292,293]. Interestingly, there exists differences for the passivation property of poly-Si with different doping types. More specifically, phosphorus-doped poly-Si outperforms boron-doped poly-Si from the available passivation results [294].

In terms of the thickness of the oxide layer, two limiting cases can be divided: (1). the oxide layer is untra-thin [114]; (2). the oxide layer is

Table 3

Summary of c-Si solar cells featuring TOPCon architecture.

Organization	Poly-Si layer, doping	Interfacial SiO _x	Post-dep. anneal	V _{OC} (V)	J _{SC} (mA/cm ²)	FF	Efficiency (%)	Area (cm ²)	Year
Both-side contacted TOPCon cells									
ISE	n-SiC _x PECVD	wet-chemical	FGA	0.724	42.9	0.831	25.8	4.00	2010[269]
ISE	n-SiC _x PECVD	PECVD	FGA	0.674	41.1	0.805	22.3	4.00	2017[270]
ISE	n-SiC _x PECVD	wet-chemical	FGA	0.697	41.4	0.811	23.4	100.00	2018[271]
ANU	n-poly PECVD +POCl ₃ diff.	wet-chemical	FGA	0.705	42.4	0.826	24.7	4.00	2019[272]
EPFL	p-SiC _x PECVD	wet-chemical	FGA	0.698	39.4	0.795	21.9	4.00	2018[137]
Trina Solar	LPCVD	—	—	—	—	—	24.6	244.00	2019[273]
Jinko Solar	LPCVD	—	—	0.724	40.7	0.824	24.2	244.00	2019[274]
Trina Solar	LPCVD	thermal	FGA	0.717	40.2	0.820	23.6	244.00	2019[275]
MeyerBurger	PECVD	—	—	0.696	41.3	0.810	23.3	—	2019[276]
Jolywood	LPCVD	—	—	0.694	40.2	0.821	23.1	239.00	2019[276]
GCI	—	—	—	0.698	40.3	0.816	23.0	—	2019[276]
SERIS	PECVD	PECVD	FGA	0.696	40.5	0.809	22.8	244.30	2019[97]
ECN	n-poly LPCVD	thermal	—	0.676	39.7	0.804	21.5	239.00	2016[109]
GIT	n-poly PECVD	wet-chemical	FGA	0.683	39.7	0.781	21.2	239.00	2016[115]
ANU	n-poly PECVD	thermal	FGA	0.675	38.4	0.804	20.8	4.00	2015[118]
ISE	n-poly PECVD	wet-chemical	SiN _x , Al ₂ O ₃ or H-plasma	0.714	42.4	0.808	24.3	4.00	2017[283]
EPFL	p-SiC _x PECVD	wet-chemical	SiN _x , Al ₂ O ₃ or H-plasma	0.708	38.7	0.799	21.9	4.84	2017[134]
SUSU	n-poly HWCVD	ozone	FGA +nSiC _x :H	0.724	37.0	0.800	21.4	4.00	2020[285]
CCZU	n-poly LPCVD	thermal	FGA	0.689	39.9	0.814	22.4	245.70	2020[286]
Trina Solar	n-poly LPCVD	thermal	—	0.712	40.9	0.793	23.2	247.79	2020[287]
IBC solar cells with poly-Si contacts									
ISFH	Poly-Si LPCVD+ implantation	dry oxidation	FGA	0.727	42.6	0.843	26.1	4.00	2018[277]
ISE	Poly-Si LPCVD+ implantation	wet-chemical	FGA	0.720	41.3	0.796	23.7	4.00	2017[278]
SunPower	—	—	—	0.737	41.3	0.827	25.2	153.00	2016[279]
Trina Solar	n-poly LPCVD	—	—	0.716	42.3	0.828	25.0	239.00	2018[271]
TOPCon top / rear cells									
EPFL	SiC _x PECVD	wet-chemical	FGA	0.720	38.8	0.810	22.6	4.00	2018[280]
TetraSun	—	—	—	0.702	38.8	0.809	22.0	239.00	2016[281]
ISFH	Poly-Si LPCVD+ implantation	—	—	0.714	38.5	0.811	22.3	244.00	2017[282]
ALST	Poly-Si PECVD	ALD	H-plasma	0.624	39.0	0.795	19.1	1.02	2020[284]
ALST	Poly-Si PECVD	ALD	H-plasma	0.655	39.0	0.780	18.8	1.00	2019[288]
LONGi	—	—	—	0.720	41.6	0.838	25.1	242.77	2021
									[289]

relatively thick thus tunneling is insufficient and pinholes are needed to ensure smooth transport of carriers [107]. In both cases, the dopant diffuses into the c-Si during the annealing process. In case (1), the shallow diffused layer can enhance the tunneling current while for case (2), it can reduce the recombination in the vicinity of pinholes [129, 295]. While the application prospect of TOPCon structure has been recognised, some pivotal principles about the interfacial oxide are still under intense debate (optimal thickness, the stoichiometry of the oxide, and the charge transport mechanisms). It is generally accepted that direct tunneling and defect assisted tunneling are two responsible transport ways in which carriers pass through the ultrathin oxide layer, which is supported by numerical simulation results [295–297]. However, some researchers proposed that transport with the aid of pinholes could also occupies part of the carrier transport in the oxide [129,130, 298]. Noted that tunneling is less likely for thick oxides, it is generally believed that tunneling occurs when the oxide is thin enough (< 2 nm) [298]. A predictive model was presented in 2016, which could actually predict two operating regimes [130]. When the pinhole density is high enough ($> 1 \times 10^9 \text{ cm}^{-2}$), $\log(J_0)$ increases linearly with the decrease in $\log(\rho_c)$. While for pinhole density is extremely low ($< 1 \times 10^7 \text{ cm}^{-2}$), there is no longer a functional relationship between J_0 and the pinhole density, and J_0 only depends on the recombination at the c-Si / SiO_x interface. The changes in the two operating regimes predicted by Green et al. are the same, but the boundary line of hole areal density is different [298,299]. Actually, both models have some applicability and the effect depends on the passivating contact structure (i.e., case 1 and case 2). After the above discussion, it can be concluded that it is extremely hard to summarize the mechanism of carrier transport into a detailed theory.

Poly-Si contacts can guarantee both the ideal values of J_0 and ρ_c , which makes the system highly competitive in different types of passivation contacts [125,300]. The introduction of atomic hydrogen into poly-Si junctions is a common means of enhancing the passivation

effect, for example by stacking a hydrogen-rich layer (SiN_x or Al₂O₃), followed by an appropriate annealing treatment [109,117,301]. Besides, exposure to hydrogen plasma at around 400 °C is also an effective means of replenishing atomic hydrogen. In contrast, the improvement of the passivation effect by means of molecular hydrogen supplementation, e.g. by forming gas annealing, is not as obvious. Notably, the importance of the c-Si / SiO_x interface state density for the passivation quality is also reflected in the difference in J_0 for poly-Si junctions on different orientations of Si surfaces [302,303]. Additionally, research of Feldmann et al. has proved that the recombination at the c-Si / SiO_x interface is leading the change of J_0 , while the Auger recombination in the shallow diffusion region related to high-temperature annealing only accounts for a little portion [304]. In addition to the interface state density, the capture cross section of the interface state is another factor determining the surface recombination velocity [305]. Minimizing recombination at the c-Si / SiO_x interface is a key priority in realizing the gratifying passivation effect of poly-Si based contacts. Furthermore, minority carriers are required to avoid reaching the poly-Si, where the high density of defects makes it prone to cause recombination [306–308]. At the same time, the majority carriers should have unimpeded access to the poly-Si, thus obtaining the desired selectivity. In generally, potential innovations aiming to the preparation of different functional layers and doping techniques are being pursued to further optimize the oxide / poly-Si contacts.

Currently, as shown in Table 3, two mainstream deposition techniques are being applied and developed in the preparation of doped poly-Si layers, of which LPCVD is widely used in thin film deposition processes in the semiconductor industry. This has become a well-established deposition method, widely used in the photovoltaic industry; however, it also has unavoidable disadvantages such as slightly high process temperature and inadequate deposition rates. Another alternative technique is PECVD, although it has the problem of blistering

at high hydrogen content, but it has been studied and found that this problem has been solved via raising the deposition temperature or alloying [309].

3.6. Technical challenges and future development directions

In terms of metallization, TOPCon solar cells in the laboratory are mainly achieved by evaporation. However, this method is more costly and alternatives need to be found for mass production. For now, screen-printing and fast-firing is a promising choice. Others schemes such as plating are not yet mature and are still under investigation [310]. The TCO is an essential contact material in TOPCon solar cells because it reduces the reflection and enhances the lateral conductivity ensuring the collection of carriers simultaneously. Sputter is the commonly used deposition method for TCOs, but it has an adverse effect on surface passivation property.

Another advantage of TOPCon solar cells is that their production process can be compatible with existing production lines and existing (obsolete) lines can be upgraded [275]. The TOPCon device contains a dielectrically passivating front homojunction and a passivating contact on the back side. Due to the full-area metallization feature (lab level), the performance is largely independent of the wafer resistance, and *FF* remains high even for wafer with high resistance [99]. However, the structure of industrialization requires screen-printed metal grids on both sides and, hence, is inherently bifacial but also needs wafers with low resistance. Moreover, the designed thickness is also quite different from the lab version. A doped poly-Si interlayer with thickness over than 100 nm is typically needed to reduce the recombination losses caused by metallization. This has a negative impact on the final performance in two aspects: there is a trade-off between the introduction of heavy doping and the losses of free carrier absorption; besides, bifaciality degradation is undesirable which is attributed to the parasitic absorption originating from the thick poly-Si layer [138,311,312]. The oxygen doping of the poly-Si layer is an available strategy to reduce free carrier adsorption losses, but the mechanisms involved remain to be studied [313]. The solar cell architecture containing double-sided poly-Si contacts has the same advantages as the SHJ solar cells (i.e., excellent V_{OC}), and is compatible with the existing SHJ production line. Besides, TOPCon concept is also compatible with the high temperature conditions of subsequent processes, which broadens the process window of TCO preparation and screen printing. Besides, the IBC concept achieves maximum efficiency, which was pioneered by SunPower [315]. In 2018, Haase et al. realized a 26.1% POLO efficiency record via combining IBC concept [277]. However, the patterning of the rear electrodes is the drawback of IBC concept, which makes this technology costly and temporarily unsuitable for industrial production. To simplify the process sequence, many methods are still under investigation, e.g. printing of local poly-Si (liquid Si) [316].

The doping level of the poly-Si layer has a strong impact on the electrical performance of the poly-Si / SiO_x junction. A low dopant concentration (below 10^{19} cm^{-3}) results in high J_0 and ρ_c and an insufficient internal potential whereas a high concentration (above 10^{20} cm^{-3}) can lead to excessive oxide breakup and dopant penetration into the c-Si substrate, resulting in increased J_0 and also deteriorating the internal potential [282,314]. Dopant incorporation can be achieved by a variety of methods, such as in situ deposition together with the Si film, ion implantation, or thermal diffusion.

From the process of improving the efficiency records of TOPCon solar cells internationally in recent years, we can see that the improvement of large-area solar cells has accelerated significantly in the last two years, but the pace of large-scale industrialization has not progressed very fast. This is mainly due to the fact that the current TOPCon technology is not yet fully developed, where the process is still relatively complex. However, the efficiency of the production line is already improving significantly, mainly due to the introduction of the main grid technology, which will bring a greater efficiency improvement, and the introduction

of some new processes, which will simplify the process and thus reduce process costs. In addition, the price of TOPCon solar cells remains at a high level. A pressing task for TOPCon solar cells is therefore currently to simplify the preparation process in order to minimise costs. Three different industrial processes for TOPCon solar cells are given in Fig. 21: (1). LPCVD preparation of poly-Si films combined with a conventional total diffusion process. This process uses LPCVD to prepare back-surface SiO_2 films and to prepare poly-Si films. The SiO_2 film is prepared using LPCVD, followed by an intrinsic amorphous Si film in the temperature range of 600–700 °C. The back surface is then subjected to one-sided diffusion, which has a crystalline annealing effect on the amorphous Si film as the diffusion temperature can reach 850 °C, so it can be annealed without separate annealing, followed by etching of the poly-Si wrapped around the front surface. Since the etching process also has a corrosive thinning effect on the PN junction on the original front surface, special attention should be paid to this single-sided etching process, and the phosphor silica glass on the back surface should be removed after the etching. In addition, the phosphorus diffusion process may also not crystallise the Si film on the back surface sufficiently, perhaps requiring a higher temperature crystallisation anneal prior to diffusion. Once the above process has been completed the usual double-sided coating and double-sided screen printing process is carried out to prepare the

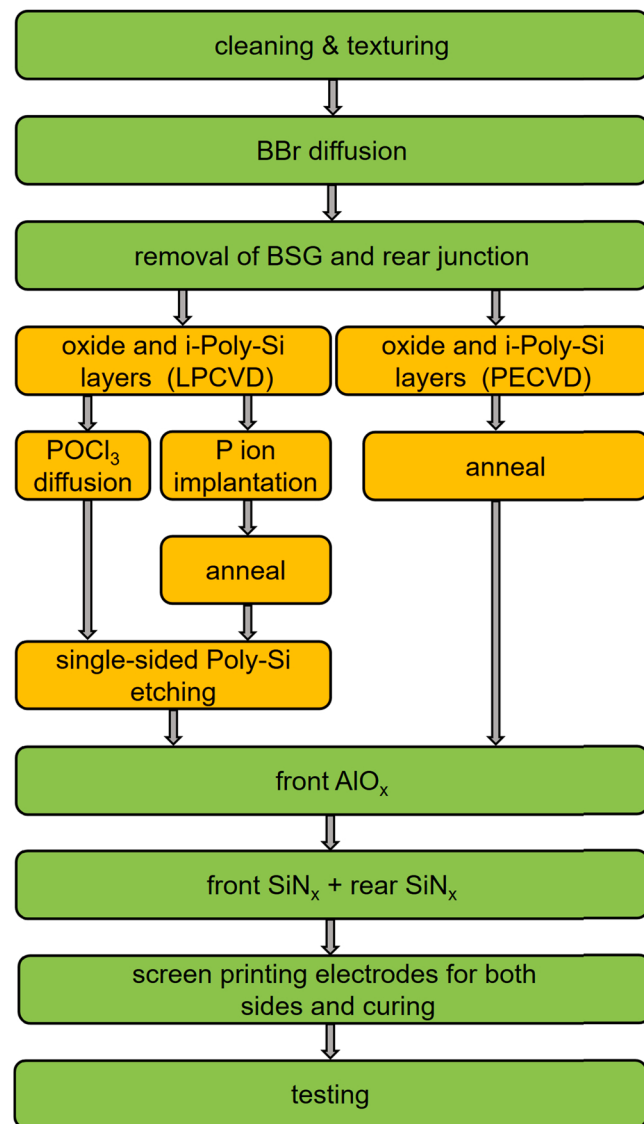


Fig. 21. Three different industrial processes for TOPCon solar cells.

electrodes. Notably, for n-type TOPCon devices where Al_2O_3 and SiN_x layers are required on the front surface, a very thin but well passivated layer is required and the Al_2O_3 layer prepared using the ALD method is advantageous; (2). LPCVD preparation of poly-Si films combined with boron expansion and ion implantation of phosphorus. The difference between this technology and the first is that ion implantation is used instead of phosphorus expansion. As ion implantation is operated on a single side, the doped ions are not bypassed, but the intrinsic amorphous Si grown by LPCVD is still bypassed and therefore requires single-sided etching to remove the bypassed layer on the positive surface of the (i) poly-Si. The ion implantation equipment in this process increases the cost, but the bypass phenomenon is less severe; (3). PECVD process for preparing poly-Si films with in-situ doping. 2019 saw several companies introduce processes for preparing amorphous Si films using PECVD, which allows the preparation of SiO_x films and the deposition of phosphorus-doped amorphous Si films in one go on the same PECVD machine, followed by annealing for crystallisation. The low deposition temperature and the single-sided deposition characteristics of PECVD make the process much simpler, with 9 process steps instead of 11 for diffusion or ion implantation.

There has also been some progress in understanding the mechanism of the TOPCon solar cell and its process details, thus providing technical support for the tuning of the industrial process: (1). Influencing factors of characteristics of passivated tunnel layer. Passivation properties and conductive properties are a contradiction in terms. The previous understanding was that the oxide tunneling junction was completely passivated, with no doping of the oxide layer adjacent to the c-Si side, while the latest understanding is that some dopant atoms penetrate the oxide layer and enter the c-Si region after annealing. If the oxide layer is too thick, the dopant atoms will not be able to diffuse into the c-Si region making the conductive properties poor, so subsequent high temperature annealing is required to create pinholes to enhance the conductivity. As shown in research of Feldmann et al., the passivation effect decreases significantly after high temperature annealing when wet nitric acid oxidation is used, while thermal oxidation (TO) still has good passivation properties even at higher temperatures [317]. The hydrogen passivation treatment after the formation of the poly-Si layer is also a very important step, which is done by annealing the stacked passivation layer using Al_2O_3 / SiN_x , which is the same mechanism as the back passivation of PERC solar cells; (2). Metal contact issues. Another contradiction in TOPCon solar cells is the relationship between metal sintering and the poly-Si thickness. When the poly-Si layer is too thin it can lead to metal atoms penetrating this layer directly into the mono c-Si, reducing the passivation effect, while if the poly-Si layer is too thick it not only increases deposition costs but also leads to a loss of light absorption. This is particularly true when preparing poly-Si layers on the front surface, as demonstrated in the POLO concept. To resolve this contradiction, one option is to prepare a thin poly-Si layer with a TCO layer on the outside to enhance its conductive properties. However, the use of TCO also encounters some challenges (magnetron sputtering can damage poly-Si surfaces; optimize deposition process and annealing process to achieve contact resistance less than $50 \text{ m}\Omega \text{ cm}^2$; optimize TCO to be the source of H; to make $iV_{OC} \sim 730 \text{ mV}$ after annealing; no additional annealing process required; TCO is not resistant to high temperatures, so the electrode sintering temperature cannot be too high. The development of a silver paste for medium to low temperatures is a challenge, which can be somewhat higher than for SHJ devices, but not as high as for PERC devices, which generally within the range of 250–350 °C). Considering that all laboratory high-efficiency TOPCon solar cells use metal electrodes prepared by evaporation, which is not adapted to industrialization, and therefore the challenge of bringing industrial TOPCon solar cells to higher efficiencies is still more difficult; (3). The TOPCon solar cell requires three new machines due to the introduction of three new processes, in addition to the conclusion that the boron expansion is more difficult than the phosphorus expansion and requires more diffusion furnaces, which results in a 10% higher

capital expenditure (CAPEX) for the TOPCon solar cell than the PERC solar cell. On the operational side, TOPCon solar cells are another 25% higher than PERC solar cells, which is mainly reflected in the higher cost of double-sided silver paste and higher equipment costs [318]. For TOPCon solar cells to be competitive, therefore, the following is required: simplify the process, reduce equipment prices, reduce silver paste usage (multi-grid technology) and increase efficiency. If TOPCon solar cells can combine high efficiency, no attenuation, low temperature coefficient and high bifacial rate, it is possible that they can have a lower LCOE than PERC on the power station side, making such cells more competitive.

The researchable options can be broken down from theory to practice into the following categories of studies: (1). Basic studies of poly-Si based contacts and TCOs: electrical research of poly-Si based contacts about carrier transport and recombination; optical research of poly-Si based contacts and TCOs, especially for parasitic absorption, and evaluation of approaches to improve transparency; structural research of poly-Si based contacts, the emphasis is on the interfacial oxide layer; modeling of current transport to further condition process parameters; (2). Integration of poly-Si based contacts into high-efficiency devices: exploration of different strategies to prepare poly-Si based contacts; evaluation of three different TOPCon structures; optimization of process sequences and align with existing production lines; application of poly-Si based contacts in connecting sub-cells in monolithic tandem configurations; (3). Assessment of novel module interconnection approaches [319].

Optimizing hydrogenation from the $\text{SiN}_x:\text{H}$ layer during the firing step at the same time as the ρ_c is also a complex issue needs to be considered. Another option is electroplating, possibly combined with a thin seed layer. Metallization by plating has been demonstrated in industrial production, and it allows the use of cheaper metals like copper to avoid the high cost of silver. It also permits the use of thinner poly-Si layers, down to ~20 nm for better optical performance. Nowadays, although poly-Si junctions have mainly applied in n-type cells, p-type Si wafers will remain the workhorse of the industry in the near future, particularly considering the ongoing shift from boron to gallium as the preferred dopant, which may reduce in-field degradation. Hence, the fusion of poly-Si junctions and p-type c-Si wafers is a general trend. There is still room for optimization of the device architecture in the future. A desirable method for optimizing p-type Si cells is to turn the PERC structure upside down, moving the n^+ junction to the back, and the localized p^+ regions to the front. This allows to use n^+ poly-Si at the back without additional optical losses, just like in the n-type TOPCon structure.

Considering the agreeable results of poly-Si based contacts and the vibrant exploration in universities, research institutes and companies, this contact concept is expected to become mainstream in industrial use. In terms of industrialization, time will tell if TOPCon can outperform PERC in terms of both cost and efficiency with the innovation of various technologies. In scientific terms, more study is needed to figure out why p-TOPCon posses inferior passivation properties, especially for textured surface. Moreover, it is vital to determine the minimum thickness of poly-Si while still holding the quasi-Fermi level splitting. Furthermore, the detailed mechanisms of the high temperature annealing that may lead to atomic rearrangement at the Si / SiO_x interface is a subject of ongoing research [15].

4. Passivating contacts for tandem solar cells

4.1. Introduction to tandem architectures

The inevitable spectral losses substantially limit the efficiency of photovoltaic devices. Currently, the efficiency of c-Si devices is gradually approaching its empirical limit (only about 2.7% difference), indicating limited room for improvement. Fig. 22 depicts that the loss in efficiency of single-junction solar cells mainly comes from the

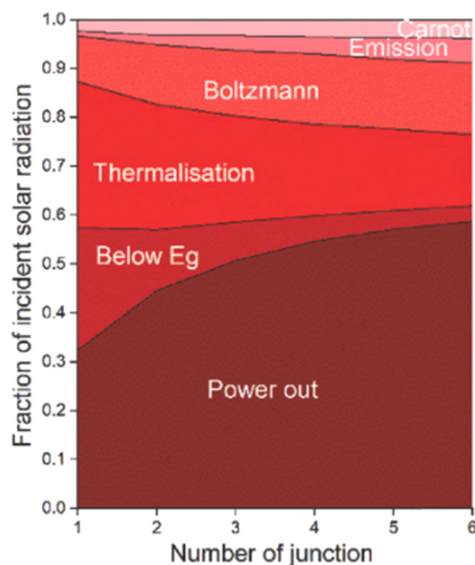


Fig. 22. Efficiency limit and loss processes of non-concentrated multi-junction devices under AM1.5 illumination [320].

Reproduced with permission. Copyright 2011, Wiley.

thermalisation loss of photons above the bandgap energy and the loss of photons below the bandgap energy that cannot be absorbed and utilized [320]. Multi-junction cell structures, where materials with different bandgaps are used to absorb sunlight of different energies, help to circumvent these losses and improve the conversion efficiency. The simplest of these is the tandem structure, which uses a wide bandgap top-cell combined with a narrow bandgap bottom-cell. The concept of the tandem structure was originally proposed by Jackson and has received a lot of attention for its broad spectral absorption, high V_{OC} , high conversion efficiency and low cost [321]. The theoretical limit of its conversion efficiency is up to 46.1%, greater than the Shockley-Queisser limit (about 33%) for single-junction devices, at a potentially low LCOE [322]. Specifically, the so-called tandem structure means that the solar spectrum is divided into several consecutive parts, and the solar cell is prepared in turn with the material whose bandgap best matches the spectrum of each part, and is prepared or stacked from the top to the bottom in the order of the bandgap from the largest to the smallest, with the top wide bandgap cell absorbing the short band light and the long band light being absorbed through by the bottom narrow bandgap cell, thus distributing the spectrum more rationally [323,324].

The efficiency of single-junction devices can not exceed the limit of Shockley-Queisser, which can be attributed to the absorption losses of low-energy carriers and thermalisation losses of high-energy carriers (Fig. 23a). Combining suitable (e.g., low-cost, ideal performance, etc.) wide-bandgap top-cell with narrow-bandgap bottom-cell (represented by Si) has been proved to be a promising strategy to enhance the conversion efficiency. In this configuration, the top-cell absorbs the high-energy photons, while the passing low-energy photons will be absorbed in bottom-cell (Fig. 23b). In generally, the tandem architectures can be divided into two categories: two terminal (2 T or monolithic) and four-terminal (4 T) as illustrated in Fig. 23c. For 2 T tandem, the top-cell is commonly fabricated monolithically on top of the bottom-cell. A recombination layer is required to connect the series sub-cells. This structure has only two external contacts and only the top contact needs to be transparent, which helps to reduce manufacturing costs and parasitic absorption losses. According to the Kirchhoff law, the photocurrent is determined by the smaller one of the sub-cells in this series-integrated device. Therefore, the properties of each sub-cell (bandgap, thickness, etc.) should be precisely controlled to realize the match of photocurrent at the MPP [328]. In terms of V_{OC} , the overall value is the

difference between the sum of the sub-cells and the voltage loss of tunnel junction. However, the manufacturing technique is relatively complex. During the growth process the top-cell, the bottom-cell is used as the substrate, therefore, the requirements for surface conditions are stringent, because it will affect the subsequent deposition. In addition, the deposition of the top-cell is required not to deteriorate the bottom-cell. Moreover, the design of the recombination layer is a tough problem, as it needs to ensure both low electrical resistance and excellent transparency to allow the smooth passage of low-energy photons [329]. Hence, the 4 T architecture with mechanically stacked tandem was subsequently proposed. The two sub-cells are physically separated so that their electrical properties are independent, and the overall conversion efficiency is the simple superimposition of the two sub-cells. The top-cell must be transparent, and 4 external contacts are required whereas 3 of them are required to be transparent (except for the rear electrode of the bottom-cell). Additionally, there is also an elaborate optically coupled 4 T-based structure in recent reports [330–332]. The sub-cells are optically coupled by an optical splitter, it includes a dichroic mirror which splits incident light. By rational allocation of the split incident light into sub-cells, the multijunction cell maximizes the use of the incident light. Unfortunately, this concept is too costly for production in industrial scale [322]. Compared with 4 T architecture, a 2 T device may have an efficiency superiority due to the absorption loss of 2 extra transparent layers. A simulation work done by Hörantner et al. compared the device performance of the two architectures in practical simulation, indicating that 2 T device ensure a significant performance improvement compared with c-Si technique, but that is advantageous to tune the parameters (layer thicknesses, bandgaps, etc.) according to the installation site. And it is justified to lean towards 2 T tandem [329]. Interestingly, three-terminal (3 T) configuration is also considered as another option, and its principle is that excess current lost in the 2 T concept is collected by a third electrode. Unfortunately, 3 T devices are far less common owing to the complexity of process [333].

The detailed balance principle applies to analysis the theoretical maximum conversion efficiencies for 2 T and 4 T architectures with the evolution of the bandgaps [327,334,335]. Fig. 24 shows the prediction results for 2 T and 4 T configurations done by Eperon et al. [327]. It can be seen that the highest conversion efficiencies for both configurations can be over 46%. Moreover, both two architectures exhibit board contours with conversion efficiencies over 33% (Shockley-Queisser limit for single-junction device under 1 sun illumination), providing sufficient flexibility for the bandgaps of sub-cells [336]. The 4 T device has a wider selection window than the 2 T device, which is limited by the current matching principle, and the sub-cells can operate at their respective MPPs.

For such tandem architectures, Si-based solar cells are the most appropriate candidates compared with other photovoltaics materials in serving as low bandgap bottom-cell owing to properties of ideal bandgap, high V_{OC} , cost competitiveness, high efficiency, non-toxicity, good stability and superior long-band spectral response [10,57,337–340]. As illustrated in Fig. 25, integrating ultraviolet-visible (UV-Vis) tuned top-cell material with high infrared (IR) transparency with IR tuned Si bottom-cell is considered as a feasible pathway to promote roadmap can clearly extend beyond 30% efficiency [341].

To date, in terms of top-cell materials, there are two main types of material that have stimulated research in Si-based tandem devices: III-V semiconductors and perovskites. The detailed introduction and the research status of the two pathways are listed in the next sections.

4.2. III-V / c-Si tandem solar cells

4.2.1. Research status and progress

The tremendous challenge for building tandem architectures is to find suitable top-cell with properties of cheap, ideal-performance and wide-bandgap. According to previous simulations, top-cells with suitable bandgap (1.70–1.85 eV) are theoretically suited to Si bottom-cells,

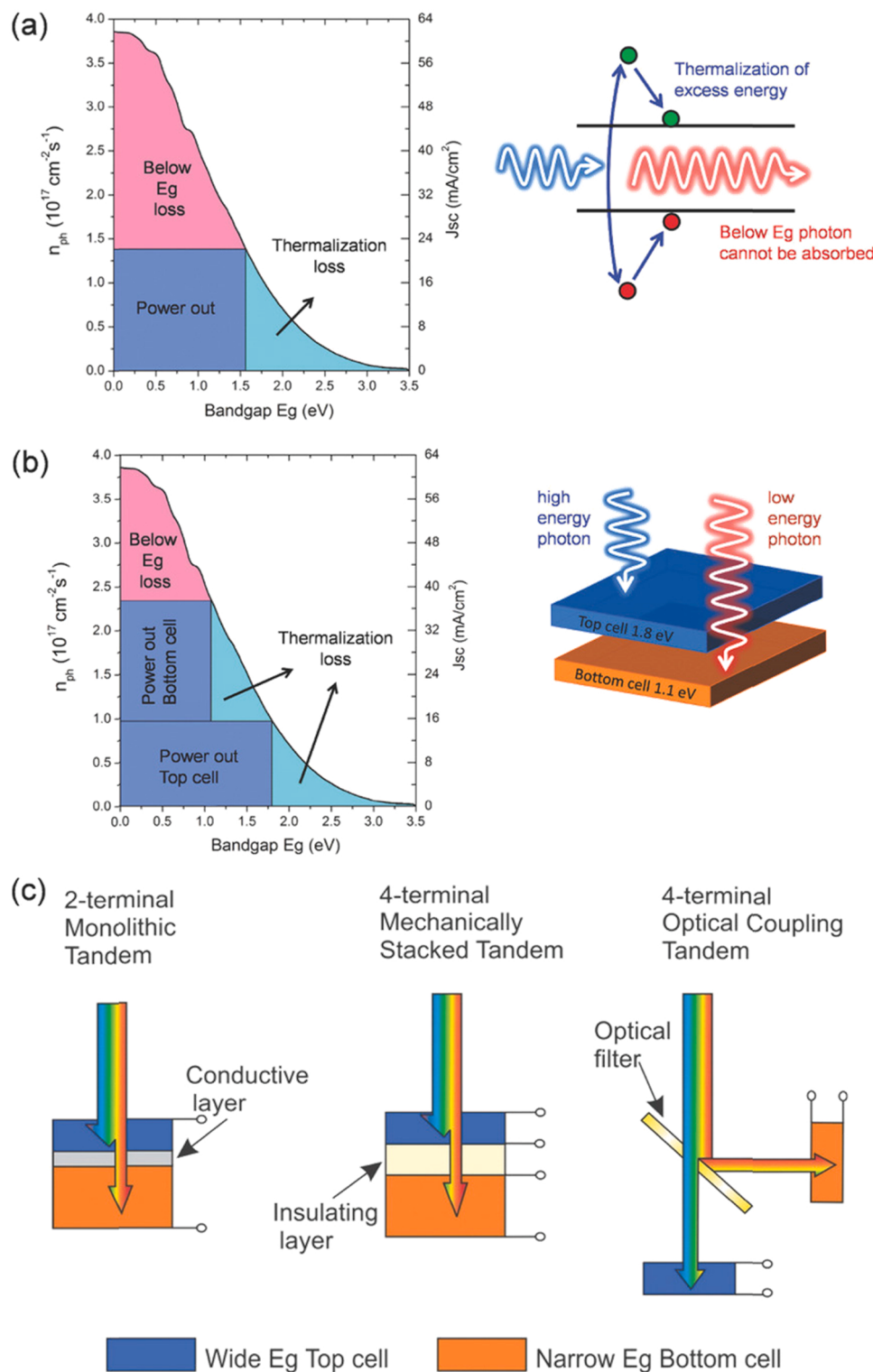


Fig. 23. Thermalization and below- E_g losses of (a) single-junction device and (b) dual-junction tandem device. n_{ph} represents the absorbed photon flux [325]. (c) Three different tandem configurations. The colored arrows showing how the solar spectrum is transmitted and absorbed by the top and the bottom cells [326]. Reproduced with permission. Copyright 2016, Nature Publishing Group.

resulting in modules with the potential to achieve conversion efficiencies greater than 30% [326,363,364]. It has been proved that III-V photovoltaics materials are a reliable high-efficiency technology despite its high costs, which already applied in many fields such as aerospace engineering, with champion efficiency up to 38.8% for a five-junction device measured at 1 sun and 46% for a four-junction device

measured at 508 suns [365]. The III-V-based devices have ideal spectral efficiency, so from the efficiency point of view, III-V solar cell seems to be an ideal tandem partner of Si [326]. In addition to the efficiency benefits, III-V solar cells are known to have excellent reliability and suitable bandgaps. Moreover, considerable research has been done on III-V solar cells, its maturity provides convenience for the research of

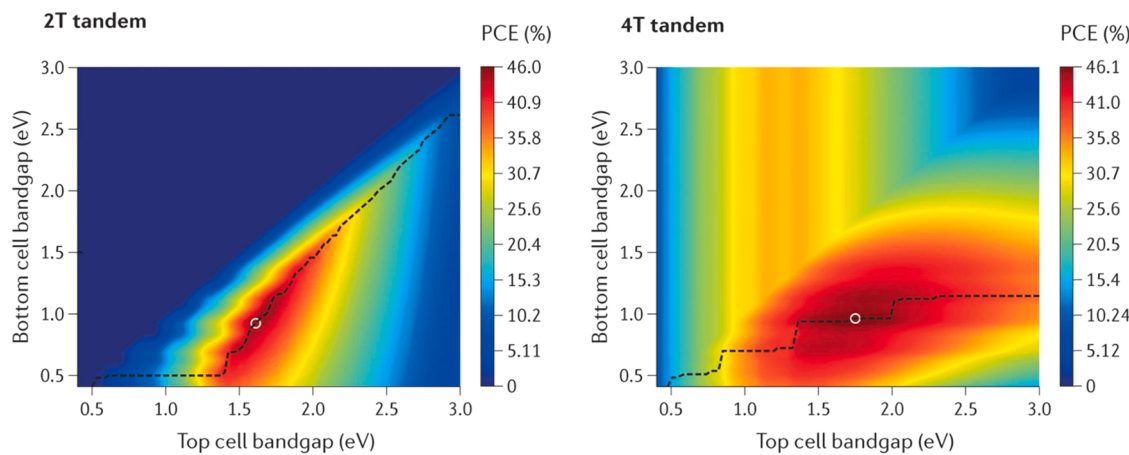


Fig. 24. Evolution of theoretical maximum power conversion efficiency for two-terminal (2 T) and four-terminal (4 T) tandem devices when changing the bandgap of sub-cells. Adsorption loss is not considered [327].

Reproduced with permission. Copyright 2017, Nature Publishing Group.

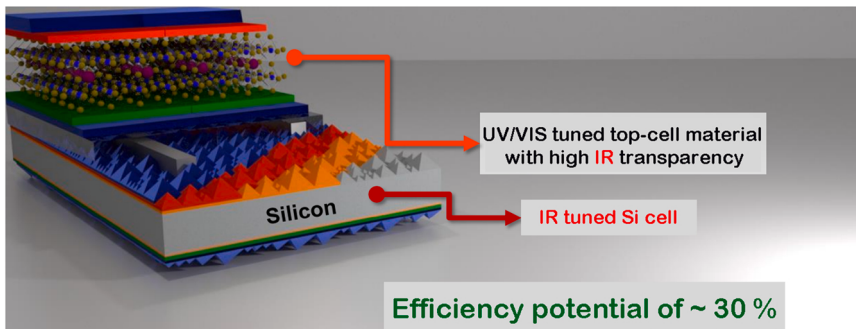


Fig. 25. Schematic of future trends in tandem solar cell structures achieving conversion efficiency in excess of 30% (passivating contact Si bottom-cell + suitable top-cell tandem).

tandem devices [366].

After two decades of continuous research, high-efficiency III-V devices are extensively integrated into multi-junction solar cells, and some representative solar cells for III-V / Si tandem architecture in recent years are summarized in Table 4 [367]. To unify the high-efficiency merits of III-V semiconductor solar cells with the Si bottom-cell, strategies to apply III-V on Si have been investigated by generations of scientists [368]. Unfortunately, the lattice mismatch between Si and common III-V materials is still a grand challenge. To ensure ideal performance, monolithically epitaxial prepared III-V multijunction solar cells generally require the same lattice constant for all the grown layers to achieve desirable crystallinity. Seen from Fig. 26, the range of III-V materials compatible with Si is relatively small. Besides, the thermal expansion coefficients between the two are also quite different, which aggravate the lattice mismatch problem. This is due to the fact that the epitaxial process usually involves a heating and cooling process, which may cause bowing, bending or cracking of the growing materials. Therefore, strain still exists even for lattice-matched growth. Currently, mainstream approaches include heteroepitaxy, wafer bonding and mechanical stacking, while there also exists many new strategies which promise to solve this problem.

Indeed, III-V materials can directly grow on Si without regard to lattice mismatch. The direct heteroepitaxy process typically consists two steps: the GaAs layer (typically 10 nm) is firstly prepared under low-temperature (~ 400 °C) condition to promote the nucleation, followed by a high-temperature (~ 700 °C) process to realize an epitaxial layer with better uniformity. Following this initial growth, thermal cyclic annealing (TCA) and strain-layer super lattices (SLSs) are applied to

control the stresses in the lattice to reduce the density of defects arising from the growth process [369–372]. However, various defects that can be reduced but not avoided, have led scientists to search for suitable buffer layer to achieve an asymptotic change in lattice constant between Si and III-V semiconductors [373,374]. $\text{Si}_x\text{Ge}_{1-x}$ and $\text{GaAs}_y\text{P}_{1-y}$ have proved to be two promising graded buffer layer materials. The method of direct growth has recently been rapidly developed, with reports of efficiencies as high as 24.3% [375,376].

Wafer bonding technology involves the chemical and physical bonding of two mirror-polished homogeneous or heterogeneous wafers. After the wafers are joined, the atoms at the interface are reacted by external forces to form a covalent bond and to achieve a specific bonding strength at the interface. This approach can avoid most of the defects caused by lattice mismatches, and parasitic resistance and optical loss can also be reduced due to the thin bonding layer between two wafers. Fig. 27 shows a flowchart of preparing wafer-bonded III-V on Si substrate. The surfaces of Si and III-V solar cells with high cleanliness can be activated after ion bombardment, followed by a pressing process under high-temperature condition, which can realize mechanical strong interconnection with high conductivity [377]. Wafer-bonded 3 J GaInP / GaAs / Si solar cells were first proposed in 2013, and since then this technology has received a lot of attention and research [377]. Typically, the technique of band bonding was used to obtain a surprising 34.5% record efficiency for two-terminal Si-based tandem devices, and its structure is illustrated in Fig. 28 [359]. The top-cell is a GaAs / GaInP dual junction device while the bottom-cell features TOPCon structure with ideal V_{OC} , FF and J_{SC} .

Mechanical stack is also a commonly used approach, which uses

Table 4

Summary of representative solar cells for III–V / Si tandem structure.

R&D Institute and photovoltaics industry	Cell structure	Bottom-cell type	Interconnect	V_{OC} (V)	J_{SC} (mA/cm ²)	FF	Efficiency (%)	Area (cm ²)	Year
TTI	GaAs / Si (1 J)	n-Si	heteroepitaxy	0.930	27.0	0.800	20.1	1.00	2001 [342]
TTI	GaAs / Si (1 J)	n-Si	heteroepitaxy	0.940	33.2	0.791	18.3	1.00	2001 [342]
NIT	AlGaAs / Si (2 J)	n-Si	heteroepitaxy	1.570	23.6	0.772	21.2	–	1995 [343]
UTokyo	GaAs // Si (2 J)	SHJ	wafer bonding	1.550	27.9	0.580	25.2	1.00	2012 [344]
ISE	GaInP / GaAs / Si (2 J)	n-Si	heteroepitaxy	2.450	11.2	0.753	16.4	4.00	2014 [345]
ISE	GaInP / GaAs / Si (2 J)	n-Si	wafer bonding	2.385	12.7	0.859	26.0	4.00	2014 [345]
ISE	GaInP / GaAs // Si (3 J)	SHJ	wafer bonding	3.335	14.2	0.826	27.9	0.05	2013 [346]
McMaster	GaInP / GaAs // Si (3 J)	SHJ	metal interconnect	2.740	11.8	0.790	25.5	0.64	2014 [347]
OSU	GaAsP // Si (2 J)	SHJ	heteroepitaxy	1.620	10.2	0.795	12.9	0.04	2016 [348]
USC	GaAs-NW // Si (2 J)	SHJ	nanowires	0.960	20.6	0.578	11.4	0.01	2015 [349]
OCU	GaInP / GaAs // Si (3 J)	SHJ	wafer bonding	2.847	10.9	0.818	25.5	0.25	2015 [350]
AIST	GaInP / GaAs // Si (3 J)	SHJ	PdNP array	2.810	10.5	0.790	23.2	0.14	2016 [351]
NREL	GaInP // Si(2 J)	SHJ	4 T by epoxy	1.456 // 0.667	14.15 22.7	0.879 0.762	29.8 18.1// 11.7	1.00	2016 [352]
ISE	GaInP / GaAs // Si (3 J)	SHJ	wafer bonding	3.046	11.9	0.830	30.2	3.96	2017 [353]
Yale	GaAsP / Si (1 J)	p-Si	heteroepitaxy	1.150	13.3	0.790	12.0	0.10	2016 [354]
Sharp	GaInP / GaAs // Si (3 J)	SHJ	epoxy	2.446 // 0.694	13.9 // 8.3	0.847 // 0.766	28.6 // 4.4	3.60	2016 [355]
ISE	GaInP / GaAs // Si (3 J)	SHJ	wafer bonding	3.046	11.7	0.875	31.3	3.98	2017 [356]
EPFL	GaInP / GaAs // Si (3 J)	SHJ	4 T by epoxy	2.520 // 0.681	13.6// 22.0	0.875 // 0.785	35.9 30.0 // 5.9	1.00	2017 [357]
EPFL	GaAs // Si (2 J)	SHJ	4 T by epoxy	1.092 // 0.683	28.9// 11.1	0.850 // 0.792	32.8 26.8 // 6.0	1.00	2017 [357]
TTI	GaInP / GaAs // Si (3 J)	SHJ	4 T	2.330 // 0.520	13.7 // 7.6	0.801 // 0.652	28.2 25.6 // 2.6	0.95	2017 [358]
ISE	GaInP / AlGaAs // Si (3 J)	TOPCon	wafer bonding	3.230	12.81	0.832	34.5	3.99	2018 [359]
ISE	GaInP / GaAs // Si (3 J)	SHJ	epoxy	2.647	12.21	0.802	25.9	3.99	2019 [360]
ISE	GaInP / AlGaAs // Si (3 J)	TOPCon	wafer bonding	3.177	12.40	0.864	34.1	4.00	2020 [361]
ALST	InGaP / AlGaAs // Si (3 J)	TOPCon	PdNP array	2.380 // 0.650	12.72	0.800	30.8	1.00	2020 [362]

Notes: For the “cell structure” section, “//” denotes the stack of III–V on active Si substrates, while that on inactive Si is represented by “/”, and the content in brackets indicates the number of junctions. For 4 T architecture, the figures of merit of the sub-cells are shown as (top-cell) // (bottom-cell).

adhesive materials to stack sub-cells and can prevent the lattice dislocation defects. The efficiency record (35.9%) for Si-based tandem devices was obtained via this approach [357]. A 2 J GaAs / GaInP device was realised on GaAs, which was then shifted to glass substrate. Finally, the substrate was attached to a SHJ solar cell using an adhesive, the schematic of its structure is illustrated in Fig. 29. Despite the significant efficiency advantages, the concept is still some way from being transferred to industrial applications. And if the adhesive conducts poorly, additional terminals are needed for the sub-cells, which would create extra cost in making modules [358].

In 2017, researchers developed a mechanically stacked, but electrically interconnected III–V–Si solar cell via Pd nanoparticles array, and it can serve as adhesive and conductive interconnection layer simultaneously [378]. A GaAs / GaInP // Si (Al-BSF) design was made, and final efficiency was only 25.1% due to the poor electrical performance of bottom-cell. Later, Makita et al. fabricated an InGaP / AlGaAs // Si 3 J device (Fig. 30) using Pd nanoparticle array, and finally obtained an efficiency of 30.8% [362]. The apparent improvements were realized via

the optimization of the GaAs-based device and employment of a TOPCon-based Si device.

4.3. Technical challenges and future development directions

The performance of the bottom-cell is critical to the overall outputs of the entire tandem device. Notably, the choice of Si bottom-cells has gradually evolved from the earliest Si substrates to SHJ structures, and that other passivating contact structures, represented by TOPCon, have come into view and demonstrate grand application potential (several different structures of tandem solar cell efficiency records have used TOPCon-based bottom-cells) [359,361,362].

The high-efficient III–V on Si solar cells have made remarkable progress. However, they have met with limited success to-date, primarily due to the high material and fabrication costs caused by the difficulty in growing material. In other words, the difficulties to note are not only to achieve efficiency gains, but to do so at an appreciable cost.

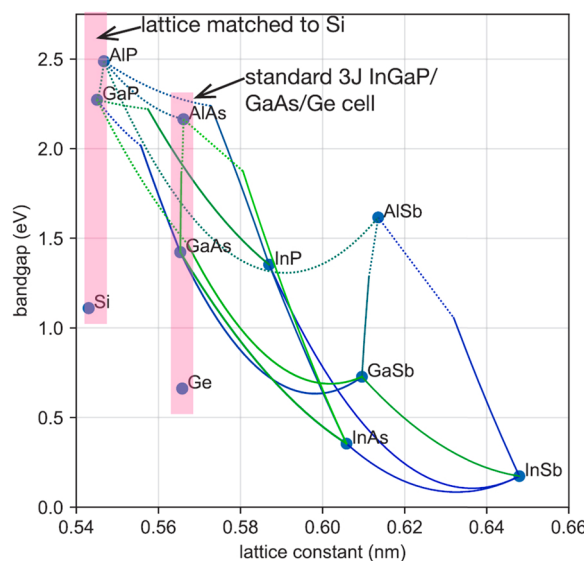


Fig. 26. Bandgaps versus lattice constants for Si, germanium and III-V materials [358].

Reproduced with permission. Copyright 2018, IOP Publishing.

4.4. Perovskite / c-Si tandem solar cells

4.4.1. Research status and progress

Since T. Miyasaka successfully produced the first perovskite solar cell in 2009, numerous researchers have been involved in this research, pursuing efficiency, stability and industrialization [15]. Perovskite is considered as a prime candidate for pairing with Si in tandems for the following reasons: (1). Organic-inorganic perovskite films have high absorption coefficients, carrier mobility, carrier diffusion length, defect tolerance, etc. The basic properties of perovskite materials can be found in other reviews [328,341]. (2). After just a few years of development, the efficiency of single-junction perovskite devices has rapidly enhanced from initial 3.8% to more than 20%, and now have reached 25.5%, and there is room for further improvement [421]. (3). Perovskite materials can be prepared by a variety of processes, including chemical methods such as spin coating, slit coating and squeegee coating, and vacuum deposition methods such as thermal vapour deposition and CVD, and all of these preparation methods are carried out at low temperatures, making it easy to achieve high quality perovskite solar cells on all types of substrates at low manufacturing costs [422–425]. (4). Perovskite films with ABX_3 crystal structure have an adjustable bandgap, which can be varied between 1.4 and 2.2 eV by composition control to enable the precise regulation. All these characteristics drive the perovskite devices as the ideal choice for top-cells. Research frenzy starts a race for

efficiency, as shown in Table 5, presenting the notable achievements for perovskite / Si tandem devices.

The solar cells of this concept were first published in 2015 with a 4 T configuration using a nip-based top-cell, realizing an efficiency of 13.4% [380,409]. The bottom-cell was a standard double-side textured SHJ solar cell. Soon after that, the first perovskite / Si monolithic tandem was developed using the same silver nanowire electrode [389]. The TiO_2 layer was prepared using ALD and the mesoporous layer via spin coating and subsequent sintering. The presence of a high-temperature process limits the use of SHJ devices as bottom-cells, and a Si tunnel junction formed by PECVD was applied to connect the sub-cells. This solar cell realized a 13.7% efficiency, and the parasitic absorption losses of the charge transport layers greatly limited the performance. At the end of 2015, Albrecht et al. first used a low-temperature planar perovskite device, its most distinctive feature is the use of SnO_2 prepared by ALD as the electron transport layer, realizing an efficiency of 18.1% [390]. The use of a SHJ solar cell as bottom-cell also exploited the optical and electrical properties of the entire device. Soon later, Werner et al. realized a new efficiency record (21.2%) of monolithic tandem device using a double-layered electron transport layer and IZO as intermediate recombination layer [391]. In addition to the structure and process of the device, researchers focused on the perovskite materials containing cesium (Cs) cations to widen the bandgap at the meantime, which helps acquire high reproducibility. In 2016, a perovskite material containing Cs-formamidinium (FA) double cation was proposed, opening the bandgap to the theoretical optimal values for top-cell materials (≈ 1.74 eV) [382].

Stability issues are a topic that cannot be avoided when using perovskite materials in solar cells, particularly for tandem devices. A research in 2016 showed that perovskite devices with double-sided electrodes (applicable in the tandem architecture) outperformed conventional devices featuring single metal rear electrode in terms of thermal stability [411]. This is due to the fact that the TCO rear electrode effectively blocks the penetration of water and prevents the volatilisation of organic compounds.

When converted to a pin structure, the parasitic absorption losses for the 2 T configuration will get substantial reduction. In this structure, Bush et al. were the first to prepare a solar cell with an efficiency of 18.0% [411]. Subsequent research by a number of groups based on this has driven rapid advances in conversion efficiency. Bush et al. optimized their device in both optics and electronics, boosting the efficiency to 25%. In 2018, the perovskite top-cell was deposited on a Si substrate with double-sided texture via a composite preparation process combining evaporation and spin coating [396]. Surprisingly, the front textured surface resulted in an attractive J_{SC} and final conversion efficiency of 25.2%.

Researchers of Helmholtz Zentrum Berlin (HZB) currently hold the efficiency record of 29.15% for perovskite / Si tandem devices (1 cm^2), which means that 30% efficiency threshold is within reach [418].

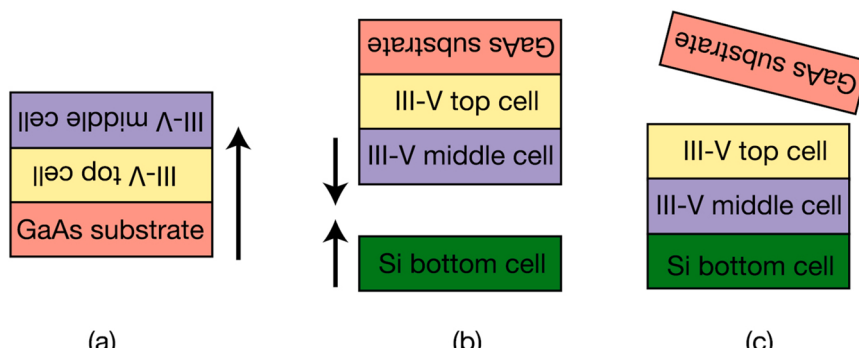


Fig. 27. Flowchart of the wafer bonding. (a) III-V epitaxial growth, (b) wafer bonding, (c) GaAs wafer lift-off [358].

Reproduced with permission. Copyright 2018, IOP Publishing.

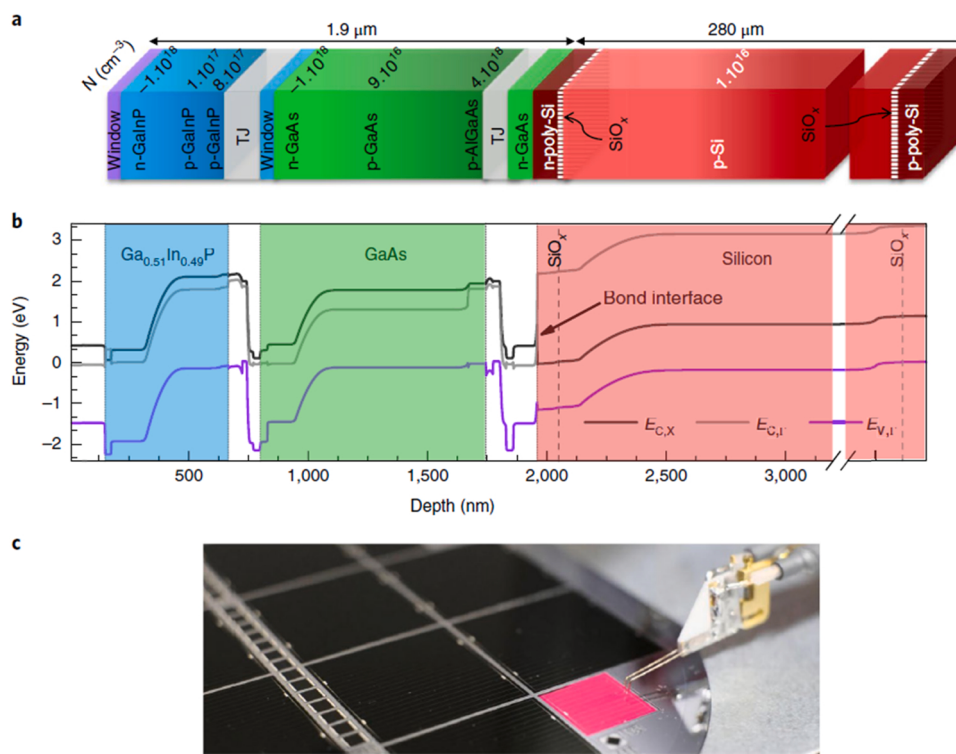


Fig. 28. Introduction to the 2 T III-V // Si 3 J device. (a) Structure schematic of the device. The left side of the device is the light receiving surface and sub-cells are connected by tunnel junctions. (b) The corresponding energy band structure. (c) Physical view of this cell on a wafer [359]. Reproduced with permission. Copyright 2018, Nature Publishing Group.

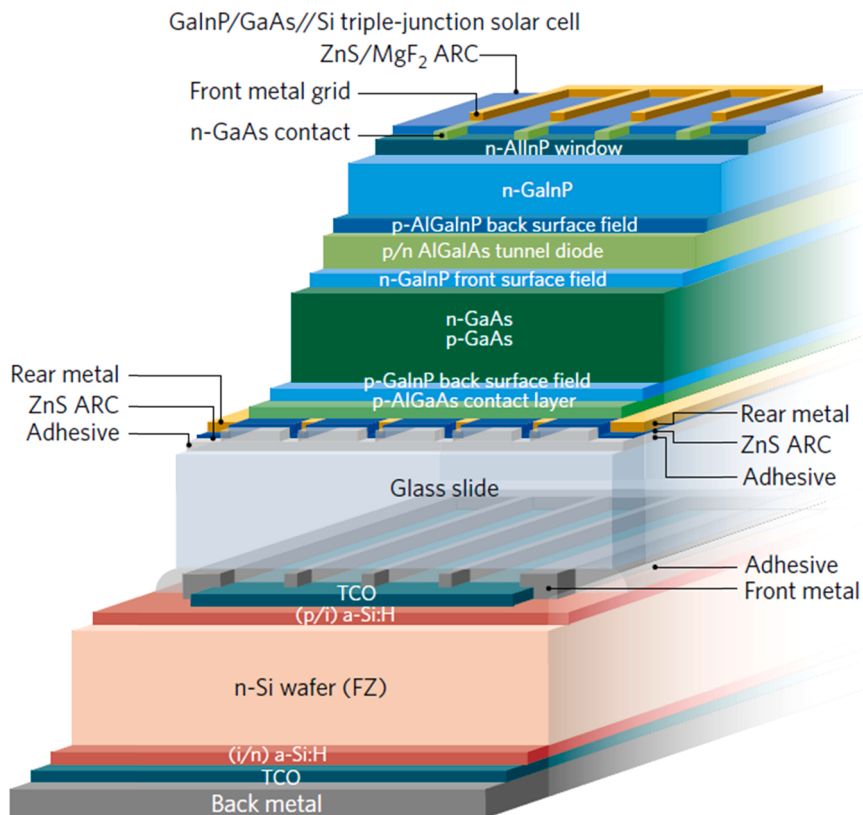


Fig. 29. Schematic of the 4 T GaInP / GaAs // Si 3 J device [357]. Reproduced with permission. Copyright 2017, Nature Publishing Group.

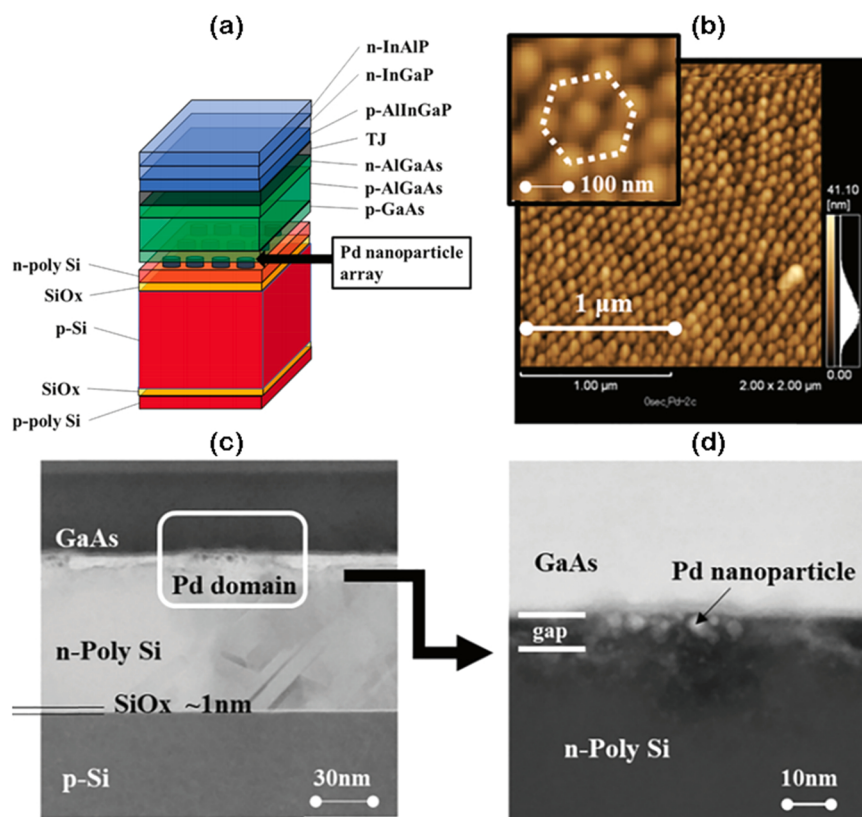


Fig. 30. (a) Structure of the InGaP / AlGaAs // TOPCon Si 3 J solar cell constructed using smart stack technology. Images of the bonding interfaces: (b) atomic force microscopy (AFM) image of the Pd nanoparticle array on Si bottom-cell; (c) cross-section of the bonding interface obtained by TEM; (d) cross-section of the bonding interface obtained by high-angle annular dark-field scanning transmission electron microscope (HAADF-STEM) [362]. Reproduced with permission. Copyright 2020, Wiley.

However, the specific structure of the cell is not given. The improvement in cell performance is mainly attributed to the improved special electrode contact layer and intermediate layer.

As reviewed above, the performance of perovskite / Si tandem devices has made impressive progress. Unfortunately, the champion efficiency of 29.15% is still a long way from theoretical limit of 43% [387]. In practice, all photons cannot ideally be harvested in their entirety through the coordination of the sub-cells. Parasitic absorption, reflection losses and unabsorbed losses are considered as major challenges that still limit performance. In response to this, scientists have explored many aspects to conduct the performance optimization.

The development of tandem device necessarily needs the compatibility of the single-junction solar cell manufacturing processes, especially for the two-terminal monolithic structure. The high-temperature processes typically used for deposition of perovskite layers limit the choice of Si bottom-cells to diffused-junction or “tunnel oxide” solar cells (commonly compatible with processes up to ≈ 200 °C) for monolithic tandem configurations. As the quality of the perovskite material itself and the quality of the interface improves, scaffold-free solar cells are gradually beginning to replace the original mesoporous perovskite solar cells, which can be prepared at low temperatures (< 200 °C) and are compatible with high-efficiency Si bottom-cells [385,426–428]. Common charge transport layer materials can all be deposited at low temperatures, including spiro-OMeTAD, PEDOT:PSS, NiO_x, n-TiO₂, SnO₂, C60 and (phenyl-C61-butylric-acid-methyl-ester) PCBM, etc. [429, 430].

Since perovskite solar cells with metal electrodes cannot be used in tandem configurations, much initial work has focused on using transparent electrodes instead of metal ones. As the transparent electrode of tandem devices, it needs to meet the following basic conditions: (1) high transmittance in a wide spectral range of 400 ~ 1 200 nm, so that the incident solar energy can be effectively absorbed and utilized by sub-cells; (2) high conductivity to realize the effective collection of carriers; (3) low-loss and low-temperature preparation technology [431].

TCO films by sputtering are the most widely studied transparent electrode systems, mainly ITO films. However, the high square resistance of ITO films prepared at low temperatures can affect the performance of perovskite solar cells. Therefore, researchers have started to search for high conductivity, low temperature TCO film systems, the most promising of which include IZO and hydrogen-doped indium oxide (IO:H) [381,385]. Ballif's group has prepared amorphous IZO films with ideal mobility square resistance at a low temperature of 60 °C [381]. The average absorption of the electrodes is less than 3% in the range of 400–1200 nm. The electrode was applied to a translucent perovskite device and realized a 10.3% efficiency. The J_{SC} and FF values are inferior compared to Au electrodes, due to the weaker back reflection and higher square resistance of the back electrode IZO, respectively. In addition, the average transmittance of the top-cell exceeds 60% in range of 800–1200 nm, which facilitates the use of near-infrared light in the c-Si bottom-cell. The amorphous IO:H film with a mobility greater than 50 cm² / (V·s) and a square resistance of 25.7 Ω / sq was prepared by Fu et al. at room temperature [432]. The electrode was applied to a translucent device and realized a 14.1% conversion efficiency, while the average transmittance of the top-cell was 72% in the range of 800–1150 nm. The researchers attempted to deposit IZO and IO:H films directly onto the carrier transport layer of the perovskite solar cell via a low temperature and low sputtering power process, but found that sputtering damage had an adverse effect on the FF , so a transition layer is required to be deposited before sputtering the TCO. For n-i-p structured perovskite solar cells, MoO_x or WO_x materials are generally vapour deposited on the hole transport layer (HTL), while for p-i-n structured perovskite solar cells, materials such as ZnO nanoparticles or SnO₂ films are deposited by atomic beam deposition on the electron selective layer [393,411].

Ultrathin metals are another class of transparent electrode materials. To achieve ultrathin metal films with high transmission and conductivity, the key is to reduce the threshold thickness for the transition from three-dimensional to two-dimensional growth mode and to achieve

Table 5

Summary of 4 T and 2 T perovskite / Si tandem devices.

Mechanically stacked 4 T solar cells							
Organization	Perovskite composition	E _g (eV)	Si technology	Efficiency (top + bottom = total, %)	Area (top; bottom, cm ²)	Year	
EPFL	MAPbI ₃	1.55	SHJ	6.2 + 7.2 = 13.4	0.25; 4.00	2014[379]	
Stanford	MAPbI ₃	1.55	Multi-Si	12.7 + 4.3 = 17.0	0.39; 0.39	2014[380]	
EPFL	MAPbI ₃	1.55	SHJ	10.4 + 7.8 = 18.2	0.25; 4.00	2015[381]	
Oxford	FACsPbI _{3-x} Br _x	1.74	SHJ	12.5 + 7.3 = 19.8	0.09; -	2016[382]	
ANU	MAPbI ₃	1.55	PERL	12.2 + 7.9 = 20.1	0.25; 4.00	2016[383]	
UNL	MAPbI ₃	1.55	SHJ	16.5 + 6.5 = 23.0	0.075; 4.00	2016[384]	
EPFL	MAPbI ₃	1.55	SHJ	16.4 + 8.8 = 25.2	0.25; 4.00	2016[385]	
EPFL	MAPbI ₃	1.55	SHJ	14.5 + 8.5 = 23.0	1.00; 4.00	2016[385]	
ANU	CsMAFAPbI _{3-x} Br _x	1.63	IBC-SHJ	16.6 + 7.9 = 24.5	0.36; 4.00	2016[386]	
ANU	RbCsMAFAPbI _{3-x} Br _x	1.74	IBC	16.0 + 10.4 = 26.4	0.16; 4.00	2017[387]	
IMEC	MAPbI ₃	1.55	IBC	12.0 + 8.2 = 20.2	4.00; 4.00	2017[388]	
EPFL	MAPbI ₃	1.55	SHJ	6.2 + 7.2 = 13.4	0.25; 4.00	2014[409]	
IMEC	CsFAPbI _{Br}	1.72	IBC	13.8 + 13.3 = 27.1	0.13; 4.00	2019[410]	
Stanford	MAPbI ₃	1.55	SHJ	12.3 + 5.7 = 18.0	0.25; 4.00	2016[411]	
HZB	MAPbI ₃	1.55	SHJ	6.2 + 7.0 = 13.2	0.16; 1.00	2015[412]	
Kaneka	MAPbI ₃	1.55	SHJ	7.5 + 20.5 = 28.0	0.20; 1.00	2015[413]	
Monolithically integrated 2 T solar cells							
R&D Institute and photovoltaics industry	Perovskite composition	Recombination layer	E _g (eV)	Si technology	Efficiency (%)	Area (cm ²)	
MIT	MAPbI ₃	n ⁺⁺ /p ⁺⁺ Si tunnel	1.55	Homojunction	13.7	1.00	2015[389]
HZB	FAMAPbI _{3-x} Br _x	ITO	1.56	SHJ	18.1	0.12	2015[390]
EPFL	MAPbI ₃	IZO	1.55	SHJ	21.2	0.17	2015[391]
EPFL	MAPbI ₃	IZO	1.55	SHJ	20.5	1.43	2016[385]
EPFL	MAPbI ₃	ZTO	1.55	Homojunction	16.0	1.43	2016[392]
Stanford	CsFAPbI _{3-x} Br _x	ITO	1.63	SHJ	23.6	1.00	2017[393]
EPFL	CsFAPbI _{3-x} Br _x	nc-Si tunnel	1.63	SHJ	22.8	0.25	2017[394]
EPFL	CsFAPbI _{Br}	nc-Si tunnel	1.63	SHJ	18.0	12.93	2017[394]
EPFL	Cs _x FA _{1-x}	nc-Si tunnel	1.60	TOPCon	24.9	1.42	2019[395]
EPFL	Pb (I, Br) ₃						
EPFL	Cs _x FA _{1-x}	nc-Si tunnel	1.60	SHJ	25.2	1.42	2018[396]
PKU	Pb (I, Br) ₃						
PKU	FA _x MA _{1-x}	ITO	1.69	SHJ	20.6	0.10	2017[397]
PKU	Pb _y Br _{3-y}						
PKU	FA _{0.5} MA _{0.38}	ITO	1.69	SHJ	22.2	0.10	2018[398]
PKU	Cs _{0.12}						
PKU	PbI _{2.04} Br _{0.96}						
NKU	Cs _{0.08} FA _{0.69} MA _{0.23}	ITO	1.67	SHJ	20.4	0.24	2019[399]
ANU	Pb (I _{0.69} Br _{0.23})						
ANU	Cs _{0.17} Rb _{0.05} FA _{0.75}	ITO	1.63	PERC	22.3	1.00	2017[400]
Stanford	MA _{0.15} PbI _{1.8} Br _{1.2}						
Stanford	FA _{0.75} Cs _{0.25}	ITO	1.68	SHJ	25.0	1.00	2018[401]
HZB	Pb (I _{0.8} Br _{0.2}) ₃						
HZB	Cs _{0.05} (FA _{0.83}	ITO	1.63	SHJ	25.4	1.09	2019[402]
HZB	MA _{0.17}) _{0.95}						
HZB	Pb (I _{1-x} Br _x) ₃						
UNC	Cs _{0.15} (FA _{0.83}	ITO	1.64	SHJ	25.4	-	2019[403]
UNC	MA _{0.17}) _{0.85}						
HZB	Pb (I _{0.8} Br _{0.2}) ₃						
HZB	Cs _{0.05} MA _{0.17} FA _{0.83}	ITO	1.63	SHJ	25.5	0.81	2018[404]
HZB	Pb _{1.1} (I _{0.82} Br _{0.17}) ₃						
HZB	Cs _{0.05} (MA _{0.82} FA _{0.17})	ITO	1.63	SHJ	26.0	0.77	2019[405]
UNSW	MAPbI ₃	Interlayer-free	1.55	Homojunction	19.1	4.00	2018[406]
UNSW	(FAPbI ₃) _{0.83}	Interlayer-free	1.59	Homojunction	21.8	16.00	2018[407]
ANU	(MAPbBr ₃) _{0.17}						
ANU	Cs _{0.17} Rb _{0.05} FA _{0.75}	Interlayer-free	1.63	TOPCon	24.5	1.00	2018[408]
ANU	MA _{0.15} PbI _{1.8} Br _{1.2}						
ISE	FA _{0.75} Cs _{0.25} Pb (I _{0.8} Br _{0.2}) ₃	ITO	1.68	SHJ	25.1	6.25	2020[414]
ISE	Cs _{0.07} Rb _{0.03} FA _{0.765} MA _{0.135} PbI _{2.55}	ITO	1.70	SHJ	21.0	0.25	2020[415]
FAU	Br _{0.45}						
NRL	-	ITO	-	SHJ	21.0	1.00	2019[416]
NRL	FA _{0.8} Cs _{0.2} Pb (I _{1-x} Br _x) ₃	ITO	1.63	TOPCon	20.7	9.00	2020[417]
HZB	-	-	-	-	29.2	1.06	2020[418]
UofT	-	ITO	1.68	SHJ	25.2	0.83	2021[419]
Kaust	-	nc-Si tunnel	-	SHJ	25.1	0.83	2020[420]

Notes: IZO and ZTO refer to indium zinc oxide and zinc tin oxide, respectively.

continuous growth of lower thickness (< 10 nm) films [433]. Ultrathin metals are also used in the study of transparent electrodes for tandem devices due to their low loss thermal vapour deposition process, which does not require additional transition layers. Chen et al. used a high surface energy Cu seed layer to reduce the threshold thickness of Au films for continuous growth, resulting in a 7 nm Au film with a broad spectral transmittance of 400–1100 nm [384]. The final efficiency using this electrode was 16.5%, with a slightly lower J_{SC} compared to the reference cell with a thick metal electrode, which is mainly due to the weak reflection of the ultrathin metal electrode, resulting in a poor spectral response in the 600–800 nm band. Yang et al. used a high surface energy Au seed layer to reduce the threshold thickness of the Ag continuous film, and further used a MoO_x layer to improve the transmission of ultrathin Ag at 400–1100 nm [434]. The cell efficiency using it as a transparent electrode is 11.5%, which has a lower J_{SC} compared to the reference cell with a conventional opaque metal electrode, mainly due to the light feed from the ultrathin metal electrode, which makes more parasitic absorption. However, compared to the TCO back electrode, the ultrathin metal IR absorption is stronger, resulting in a lower transmission rate of the top-cell at 800–1200 nm. For example, the transmission rate of the translucent perovskite solar cell prepared by Chen et al. is only about 60% in the 800–1200 nm in the NIR band, making the effective utilisation of the c-Si bottom-cell for long waves lower, thus reducing the entire efficiency of the tandem devices [384].

The metal nanowires, represented by AgNWs, are an alternative transparent electrode material due to their properties such as a transmittance of more than 90% at 550 nm, a square resistance of less than $20 \Omega / \text{sq}$, and low cost of preparation by solution method [380,435, 436]. Guo et al. used a spraying method to prepare AgNWs on the backside, combined with ZnO as a dielectric layer, resulting in an efficiency of 8.49%, with a slight decrease in J_{SC} and FF compared to the perovskite solar cell with thick metal electrodes [435]. McGehee et al. applied AgNWs to the electrodes using a mechanical transfer method and realized an efficiency of 12.7%, which is comparable to the efficiency of the reference cell [380]. Meanwhile, the transmittance of perovskite solar cells at 800 ~ 1 200 nm is 60~80%, of which the peak transmittance at 800 nm is 77%, which is conducive to the effective use of near-infrared light in the bottom-cell. However, perovskite is soluble in polar solvents, which limits the film forming process of AgNWs. More seriously, AgNWs is conducive to the chemical reaction of perovskite to form metal halides, which leads to poor stability. All of these bring challenges to the application of AgNWs. Guo et al. found in their experiments that the performance of translucent perovskite devices decreased significantly after 1 day in a glove box filled with N_2 , even with a ZnO nanoparticle barrier [435]. It has been suggested that inert metal nanowires (Ni, Cr) could be used to mitigate the degradation problem of perovskite solar cells [437]. Therefore, if AgNWs are to be successfully applied in perovskite devices, the stability and large area reproducible preparation of AgNWs electrodes must be addressed.

In addition, carbon-based transparent conductive films, such as carbon nanotubes and graphene, can also be used as transparent electrodes on the back of perovskite solar cells, but their high square resistance of $> 100 \Omega / \text{sq}$ affects the effective collection of carriers and the series resistance, thus reducing the J_{SC} and FF [412,438,439]. Lang et al. used graphene deposited by CVD as the transparent electrode. Through the field-effect doping of Spiro-OMeTAD, combined with the stabilization of adsorbed doping by the polymer coating, the graphene square resistance was reduced by 24% [439]. However, compared with the reference cell using Au electrodes, the FF of the perovskite solar cell with graphene electrode still decreased significantly (from 62.9% to 52.7%). Therefore, it was proposed that the metal gate line could further reduce the series resistance and thus increase the FF .

As the most usual hole transport material, spiro-OMeTAD has obvious parasitic absorption problems when placed on the light incident side. The parasitic absorption strongly limits the performance of the entire tandem device [440]. To reduce parasitic absorption, alternative

hole transport layer alternatives include small-molecule semiconductors, such as NPB, spiro-TTB, or TaTm, as well as the inorganic NiO_x and copper thiocyanate materials with high bandgaps [441–445]. Thin layers of fullerenes, e.g. PCBM or C_{60} , have also been proved to be an suitable choice [385,393].

The current composition of the commonly used high-efficiency perovskite device is MAPbI_3 (bandgap = 1.55 eV), however the ideal bandgap for the top-cell is 1.73 eV, so it is important to prepare a perovskite top-cell with wider bandgap while ensuring the high quality of the functional layer and interface to obtain the corresponding V_{OC} gain and high conversion efficiency [326]. For ABX_3 -type perovskite materials, modulation of the bandgap can be achieved by compositional optimization. The partial substitution of iodine with bromine at the X-position increases the bandgap of methylammonium-based perovskite materials to 1.55–2 eV. However, these compounds suffer from photogenic or thermogenic phase instability, mainly due to the migration of I ions under light, the so-called Hoke effect [446]. Subsequently, it was found that a breakthrough in phase stability could be achieved by introducing Cs cations at the A-site [447–449]. However, the current wide bandgap perovskite devices generally exist huge deviations between V_{OC} and E_g and low conversion efficiency. Controlling the crystallization process of perovskite is beneficial to improve the structural properties of perovskite materials. Combined with interface passivation layer or energy level matching interface materials to improve the interface properties can effectively increase V_{OC} and conversion efficiency [450–457]. By introducing a polar formamide co-solvent into the $\text{FA}_{0.81}\text{MA}_{0.14}\text{Cs}_{0.05}\text{PbBr}_{1.2}\text{I}_{1.8}$ perovskite precursor solution, Kim et al. formed the black perovskite crystalline phase directly during film formation, avoiding the formation of a yellow intermediate phase, thereby reducing the defect density of states of the perovskite, with the conversion efficiency of 17.8% [455]. By introducing butylammonium bromide (BABr) on the perovskite surface and a 2D perovskite layer at the interface of the 3D perovskite and HTLs, the 2D / 3D heterojunction passivation defect does not affect the extraction of holes, resulting in a stable efficiency of 19.4% [457]. The ratio of V_{OC} to the limit value based on Shockley-Queisser theory is more than 90%, which is the highest level of wide bandgap perovskite solar cells reported in all literatures. Although there is a consensus on the use of wide bandgap perovskite top-cells in tandem structure, the current bandgap for wide bandgap top-cells in two-terminal monolithically solar cells is mostly 1.63 eV. This is mainly due to the fact that theoretical simulations have found that when the bandgap of perovskite top-cells exceeds 1.7 eV, the thickness of the perovskite layer required to match the current of bottom-cell increases dramatically, and at the optimum bandgap (1.73 eV), the matching thickness is 1500 nm and it is currently not possible to produce a high-quality perovskite layer at the micron level.

Additionally, the thickness of perovskite absorber layer strongly affects the photo-current of the top-cells. In case of ideal bandgap, the thickness is required to be about 1 μm , which is a certain difficulty in experiment under the precondition of maintaining good material quality [458]. For low bandgap materials, a thinner thickness of the absorber layer is preferred. Moreover, the high thickness of the perovskite layer tends to create nonuniformities and pinholes during deposition, which can significantly damage the performance of the device [459,460].

In addition to parasitic losses, reflection losses at multiple interfaces in a tandem structure also have an effect on the J_{SC} value. For monolithically integrated two-terminal solar cells, for example, it is generally accepted that the reflection loss comes from three main sources: the front surface reflection R_1 , the reflection at the interface between the two solar cells R_2 , and the rear surface reflection R_3 (as shown in device A in Fig. 31). R_3 is mainly the unabsorbed photons at $\lambda > 950$ nm through the perovskite and c-Si solar cells, R_2 is mainly the unabsorbed photons at $\lambda > 700$ nm through the perovskite solar cell, and R_1 is mainly from the photons at short wavelengths. To reduce R_3 , the backside can be structured with a textured surface (as in device B in Fig. 31), which increases the optical path in the c-Si under the effect of

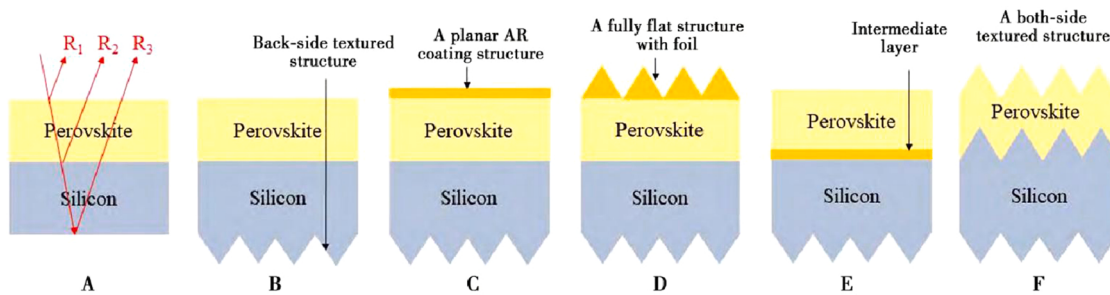


Fig. 31. Different structures of perovskite / Si tandem devices for reducing reflection loss: A is a fully flat device; B is back-side textured device; C is device using a planar anti-reflection coating in the front side; D is device using a structured foil in the front side; E is device with an intermediate layer; F is both-side textured device [404,461].

oblique incidence as well as total internal reflection, thus increasing the J_{SC} . This is currently the most common structure used for tandem devices. To reduce R₁, a flat reflective layer or structured foil can be introduced on the front surface (e.g. devices C and D in Fig. 31). The reflective foil is usually LiF₂ or MgF₂ and is simple to prepare, but usually only effective for a single wavelength. The foil with the structure usually imitates the pyramid structure and improves the J_{SC} of the sub-cells through the dual action of reflection reduction and light trapping [462]. However, this method also increases the optical path of the other layers except the absorption layer, causing the seriousness of parasitic absorption, and the gain of J_{SC} cannot be effectively achieved sometimes. Both of these structures have received extensive attention at present, but which structure has the advantage has not been determined. To reduce R₂, an interface layer with matching refractive index and thickness can be introduced at the interface of the two solar cells (device E in Fig. 31), where the refractive index of the intermediate layer needs to be between the perovskite carrier transport layer and the Si film to effectively reduce the interface reflection and increase the J_{SC} of the c-Si bottom-cell. Theoretical simulations have shown that materials with refractive indices of 2.6–2.8 can achieve optimal current matching, while the refractive indices of the currently used interlayer materials, TCO and nc-Si films, are not optimal. Mazzarella et al. proposed the use of SiO_x films containing nano-Si, which could effectively reduce the reflectance in the range of 700–1100 nm, increase the J_{SC} by 1.4 mA/cm² and achieve an efficiency of 25.2% compared to the reference tandem device with an nc-Si interlayer [402]. An alternative approach to reducing reflection losses is the application of a c-Si bottom-cell with bifacial textured (e.g. device F in Fig. 31), where the combined effect of light trapping and reflection reduction increases the J_{SC} of both the sub-cells. At present, the EPFL group has prepared the perovskite layer by a two-step method using thermal evaporation combined with coating, and prepared other functional layers such as carrier transport layer by thermal evaporation, sputtering or ALD, so as to realize the preparation of high-quality perovskite solar cells on bifacial textured c-Si solar cells [396]. In combination with optical management such as an intermediate interface layer and a MgF₂ reflective reduction layer, a J_{SC} of 19.5 mA / cm² and an efficiency of 25.2% were achieved for the tandem device. For mechanically stacked four-terminal solar cells, there is no electrical coupling between the sub-cells, and the top-cells are generally high-efficiency perovskite devices, while the bottom-cells are high-efficiency c-Si devices with bifacial textured. However, for four-terminal stacked devices, there is an optical coupling effect, i.e. the light passing through the top-cells has an effect on the performance of the bottom-cells, so the same methods of reducing reflection losses as described above apply, such as introducing a reflective reduction film or a structured foil on the top-cell surface. Slightly different from the two-terminal devices, the interface between the four-terminal sub-cells is an air medium, and a refractive index mismatch with the adjacent film will result in greater interfacial reflections, so introducing a refractive index-matched film at the interface

can help to increase the J_{SC} and efficiency of the bottom-cell, and then boosting the overall efficiency. Jaysankar et al. introduced a structured foil on the light incident side of the top-cell, combined with an intermediate matching layer with a refractive index of about 1.5, effectively reducing the reflection and increasing the J_{SC} and efficiency of the bottom-cell, thus increasing the tandem device efficiency from 23.1% to 23.9% [463]. In conclusion, to reach the theoretical limit of the path length given by the Yablonovitch formula of $4n^2$ (n is the refractive index of the absorber), an effective light trapping strategy must be used [440,461,462].

4.5. Technical challenges and future development directions

The choice of c-Si bottom-cell is crucial for the entire perovskite / Si tandem architecture. It is still uncertain which type of c-Si bottom-cell is most suitable for use in tandem structures. The current efficiency record for tandem structures uses the SHJ technique, but at the same time other passivation contact technologies, such as TOPCon, are gaining attention and application. In addition to efficiency, how to achieve the translation from laboratory to industrial mass production is an important issue. Messner et al. compared different concepts of c-Si bottom-cell, and proposed that the competition for the best c-Si technique for industrial application is still ongoing, the different types of passivating contacts all have great potential, which is counter to the current trend in research where the SHJ technology is in the lead [464]. Other passivating contact types of bottom-cells, represented by TOPCon, deserve more attention.

In conclusion, perovskite / Si tandem devices are considered as a promising pathway to realize over 30% efficiency, but there are still many problems to be solved urgently. The current bandgap of most perovskite top-cells is 1.6 eV, and with the improved performance and stability of 1.7 eV bandgap perovskite devices, the V_{OC} of the top-cell can reach 1.3 V, which in turn enables the V_{OC} of the tandem device to reach 2.0 V. However, the matching perovskite layer is required to exceed 1 μm when the bandgap exceeds 1.7 eV to satisfy the current matching principle. The production of high-quality micrometer-thick perovskite materials remains a challenge. In terms of J_{SC} , a J_{SC} of 19.5 mA / cm² has been obtained, and by further reducing the parasitic losses in TCO and the carrier transport layer and optimising the metal grid structure to reduce the shadow area, a J_{SC} of approximately 21 mA / cm² can be achieved, for a total J_{SC} of 42 mA / cm². Considering that the J_{SC} of c-Si solar cells is 42.65 mA / cm², it shows that the current tandem devices do not broaden the effective use of sunlight, but are still limited to the range of 300–1200 nm. The use of wide bandgap top-cells is expected to broaden the use of the short wavelength spectrum, and in addition the combination of narrower bandgap solar cells, such as germanium-Si or organic solar cells, could broaden the use of the long wavelength spectrum. In the future, multi-junction devices featuring three or more junctions are an effective means to maximize the use of sunlight, but the quantum efficiency of each band needs to be ensured while broadening the utilization of the spectrum. In terms of FF, the

translucent perovskite top-cell electrode can be supplemented with a metal grid wire structure to achieve $FF = 80\%$. Based on the above estimated photovoltaic characteristics parameters, the conversion efficiency of the tandem device would be greater than 33% ($V_{OC} = 2.0$ V, $J_{SC} = 21 \text{ mA/cm}^2$, $FF = 80\%$). To achieve higher performance in tandem solar cells, multiple processes need to be optimised in concert to achieve the final efficiency gain.

In addition to the research on the high efficiency, it is also crucial to carry out research on the process of uniform preparation of high efficiency tandem solar cells over large areas and on their stability. Currently, magnetron sputtering or thermal evaporation techniques for transparent electrodes, as well as slit coating techniques for perovskite and carrier transport layers, are promising for large-area homogeneous preparation. The stacking of perovskite modules on large-area c-Si solar cells of 156 cm²-156 cm is a practical method for the preparation of large-area tandem solar cells. In addition, perovskite face severe stability challenges, as they are susceptible to the effects of light, heat, water and oxygen, and the phase instability of wide bandgap perovskite solar cells is particularly prominent. Therefore, it is necessary to control the characteristics of perovskite layer, carrier transport layer, and organic-inorganic interface, to inhibit the migration of iodide ions and improve the stability of the perovskite solar cell, so as to achieve a lifetime that matches the bottom-cells.

4.6. Potential efficiency improvements from State-of-the-Art surface passivation

Yamaguchi et al. proposed a theoretical analysis model used to compare the nature of efficiency loss for different types of Si-based tandem devices, which considers losses including non-radiative recombination and resistance losses, and the former is quantified by ERE and while the latter is assessed by FF [358]. ERE indicates the proportion of radiation recombination-related carriers to all recombined carriers. It was found that the efficiency of III-V / Si could achieve 38% when the ERE is enhanced by two orders of magnitudes since that of state-of-the-art III-V top-cell is on the order of 10^{-3} . As for perovskite / Si devices, efficiencies of 35.2% (2 J) and 39.2% (3 J) can be achieved if ERE can be enhanced to 10^{-3} . Fig. 32 illustrates the calculated efficiencies under one-sun illumination versus EREs. It can be seen that the ERE of the best III-V / Si device by mechanical stack almost catches up with the state-of-the-art GaInP / GaAs / InGaAs 3 J device, showing that the negative impact of this integration method on the sub-cells is very

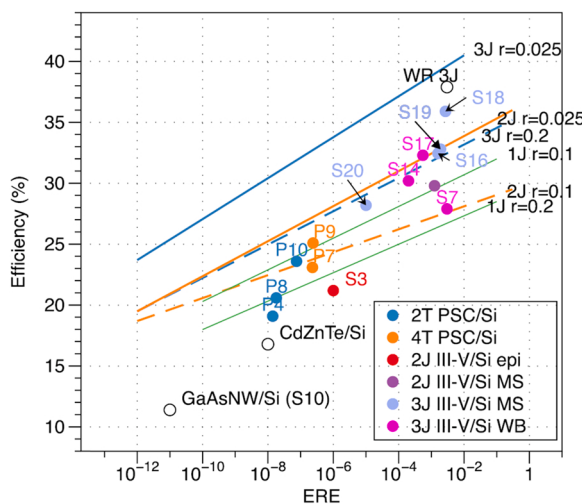


Fig. 32. Calculated efficiencies under one-sun illumination versus external radiative efficiencies (EREs) of different junctions and r (total normalized resistance), along with some notable results of tandem solar cells [358]. Reproduced with permission. Copyright 2018, IOP Publishing.

weak. In terms of wafer bonding, the best III-V / Si tandem devices also realize high EREs. However, the efficiency is lower than that of the reference cell due to the non-optimal bandgap of the top-cell. For III-V / Si tandem devices formed by direct heteroepitaxy, the unsatisfactory EREs result in their poor efficiencies. Based on advanced results in both simulation and experiment, Yan et al. conducted a semi-empirical analysis of the possible and actual conversion efficiencies of perovskite / Si tandem devices with different device designs under AM 1.5 G under certain assumptions, the predicted results are listed in Table 6 [340]. We can see that the conversion efficiency of planar n-i-p perovskite / n-TOPCon is promising to achieve 33.8% ($V_{OC} = 1.91$ V, $FF = 83.3\%$, $J_{SC} = 21.25 \text{ mA/cm}^2$). The PERC devices are an ideal choice in industry application currently, because it is compatible with existing production lines. Besides, TOPCon and SHJ, both with excellent passivation properties, are ideal choices of bottom-cells for obtaining high performance devices. TOPCon, in particular, could become another bottom-cell suitable for mass production as mature production lines are established. Generally, all types of c-Si bottom-cells are expected to be suitable candidates used in perovskite / Si tandem devices with potential over 30% efficiencies due to their own unique advantages, and design optimisation is imperative.

5. Conclusion and perspectives

In this article, different passivating contacts techniques were introduced, which fuel the explosion in efficiencies of Si-based solar cells. Fig. 33 shows the development trend of Si photovoltaics, the continuous technological development makes it keep the vitality of efficiency growth.

Currently, the maximum efficiency of PERC production is approximately 22.9%. The metal / semiconductor interface recombination is the Achilles heel of this concept, limiting its prospects for sustainable development in the future. Fortunately, the efficiency improvement path has been maintained thanks to the emergence of new passivation contact concepts. With the integration of passivating contact technology, novel Si-based solar cells, such as SHJ, DASH or TOPCon, have the ability to outperform conventional PERC. The big question now is which of these concepts will stand out and replace PERC in mass production. Time will give us the answers.

The combination of the passivation contacts concept and the tandem concept can break the theoretical limit of single junction c-Si devices. Compared to single-junction solar cells, the design of tandem structures requires more consideration, such as selection of transparent electrodes, tunnel junction type, material engineering, and the preparation technology. With well-designed passivating contact-based c-Si bottom-cell, the cleverly designed tandem devices promise to break the efficiency bottleneck of 30%. The follow-on issues that need attention are stability and cost.

In summary, Si technology has not only shown outstanding developments in photovoltaics in the past, but also has the great potential to continue to be the leader of photovoltaic markets in the future due to the emergence of passivating contact concepts.

Table 6
The predicted achievable efficiencies of perovskite / Si tandem devices [340].

The bottom-cell type	Specific tandem composition	V_{OC} (V)	J_{SC} (mA/cm ²)	FF	Efficiency (%)
homojunction	planar p-i-n perovskite / p-PERC	1.836	20.2	0.814	30.1
	planar n-i-p perovskite / n-TOPCon	1.910	21.3	0.833	33.8
heterojunction	planar n-i-p perovskite / SHJ	1.923	20.4	0.835	32.8

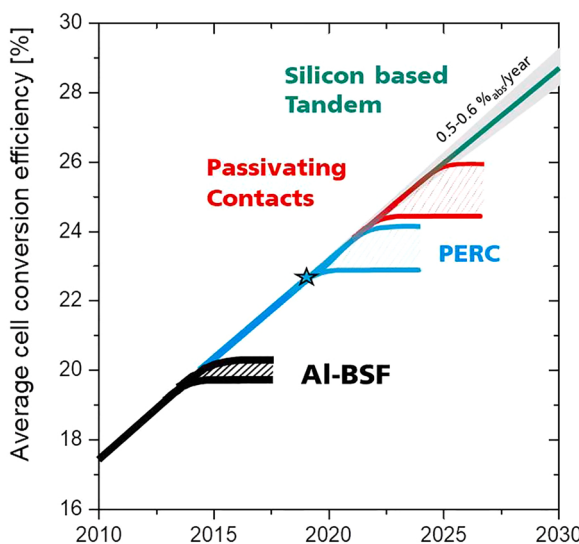


Fig. 33. The development trend of Si photovoltaics [15].

Reproduced with permission. Copyright 2020, AIP Publishing Group.

Declaration of Competing Interest

The authors declare that they have no known competing financial interests or personal relationships that could have appeared to influence the work reported in this paper.

Data Availability

The data that support the findings of this study are available from the corresponding author upon reasonable request.

Acknowledgments

This work was supported by National Key Research and Development Program of China (Grant No. 2018YFB1500402), and National Natural Science Foundation of China (62074084).

References

- [1] Nadarajah Kannan, Divagar Vakeesan, Solar energy for future world: a review, *Renew. Sustain. Energy Rev.* 62 (2016) 1092–1105.
- [2] Sung Hae Kim, Jin-Young Jung, Ralf B. Wehrspohn, All-room-temperature processed 17.25%-crystallize silicon solar cell, *ACS Appl. Energy Mater.* 3 (2020) 3180–3185.
- [3] E. Elangovan, G. Goncalves, R. Martins, RF sputtered wide work function indium molybdenum oxide thin films for solar cell applications, *Sol. Energy* 82 (2009) 726–731.
- [4] A. Martin, Green, The path to 25% silicon solar cell efficiency: history of silicon cell evolution, *Prog. Photovolt. Res. Appl.* 17 (2009) 183–189.
- [5] Keiichiro Masuko, Masato Shigematsu, Taiki Hashiguchi, Achievement of more than 25% conversion efficiency with crystalline silicon heterojunction solar cell, *IEEE J. Photovolt.* 4 (2014) 1433–1435.
- [6] Pedro Henrique Alves Verissimo, Rafael Antunes Campos, Area and LCOE considerations in utility-scale, single-axis tracking PV power plant topology optimization, *Sol. Energy* 211 (2020) 433–445.
- [7] Corsin Battaglia, Andres Cuevas, Stefaan De Wolf, High-efficiency crystalline silicon solar cells: status and perspectives, *Energy Environ. Sci.* 9 (2016) 1552–1576.
- [8] Deokjae Choi, Hyun Yoon, Ka-Hyun Kim, ITO-free carrier-selective contact for crystalline silicon solar cells, *J. Mater. Chem. A* 7 (2019) 2192–2199.
- [9] Bin Liu, Shijia Feng, Lifei Yang, Bifacial passivation of n-silicon metal-insulator-semiconductor photoelectrodes for efficient oxygen and hydrogen evolution reactions, *Energy Environ. Sci.* 13 (2020) 221–228.
- [10] Kunta Yoshikawa, Wataru Yoshida, Toru Irie, Exceeding conversion efficiency of 26% by heterojunction interdigitated back contact solar cell with thin film Si technology, *Sol. Energy Mater. Sol. Cells* 173 (2017) 37–42.
- [11] Kunta Yoshikawa, Hayato Kawasaki, Wataru Yoshida, Silicon heterojunction solar cell with interdigitated back contacts for a photoconversion efficiency over 26%, *Nature Energy* 2 (2017) 17032.
- [12] Armin Richter, Martin Hermle, Stefan Gulnz, Reassessment of the limiting efficiency for crystallize silicon solar cells, *IEEE J. Photovolt.* 3 (2013) 1184–1191.
- [13] Antonio Luque, Will we exceed 50% efficiency in photovoltaics? *J. Appl. Phys.* 110 (2011), 031301.
- [14] F. Fertig, F. Kersten, R. Lantzsch, LID and LETID in PERC: Suppression by Q. ANTUM TECHNOLOGY, presented at AsiaChem 5th PERC+ and TOPCon Forum, Hangzhou, China, 8 August 2019.
- [15] Martin Hermle, Frank Feldmann, Martin Bivour, Passivating contacts and tandem concepts: approaches for the highest silicon-based solar cell efficiencies, *Appl. Phys. Rev.* 7 (2020), 021305.
- [16] Jia Chen, Zhe Ren Du, Fujun Ma, Accurate extraction of the series resistance of aluminum local back surface field silicon wafer solar cells, *Sol. Energy Mater. Sol. Cells* 133 (2015) 113–118.
- [17] Yifeng Chen, Hui Shen, P. Pietro Altermatt, Analysis of recombination losses in screen-printed aluminum-alloyed back surface fields of silicon solar cells by numerical device simulation, *Sol. Energy Mater. Sol. Cells* 120 (2014) 356–362.
- [18] Xin Gu, Xuegong Yu, Deren Yang, Efficiency improvement of crystallize silicon solar cells with a back-surface field produced by boron and aluminum co-doping, *Scr. Mater.* 66 (2012) 394–397.
- [19] Xin Gu, Xuegong Yu, Jinglin Xu, Towards thinner and low bowing silicon solar cells: form the boron and aluminum co-doped back surface field with thinner metallization film, *Prog. Photovolt.* 21 (2013) 456–461.
- [20] Daniel Kray, Martin Hermle, W. Stefam, Glunz, Theory and experiments on the back side reflectance of silicon wafer solar cells, *Prog. Photovolt.* 16 (2007) 1–15.
- [21] Thomas G. Allen, James Bullock, Xinbo Yang, Passivating contacts for crystallize silicon solar cells, *Nature Energy* 4 (2019) 914–928.
- [22] Matthias Muller, Gerd Fischer, Bernd Bitnar, Loss analysis of 22% efficient industrial PERC solar cells, *Energy Procedia* 124 (2017) 131–137.
- [23] Haibing Huang, Jun Lv, Yameng Bao, 20.8% industrial PERC solar cell: ALD Al_2O_3 rear surface passivation, efficiency loss mechanisms analysis and roadmap to 24%, *Sol. Energy Mater. Sol. Cells* 161 (2017) 14–30.
- [24] Jan Benick, Bram Hoex, M.C.M. van de Sanden, High efficiency n-type Si solar cells on Al_2O_3 -passivated boron emitters, *Appl. Phys. Lett.* 92 (2008), 253504.
- [25] Bart Vermang, Hans Goverde, Loic Tous, Approach for Al_2O_3 rear surface passivation of industrial p-type Si PERC above 19%, *Prog. Photovolt.* 20 (2012) 269–273.
- [26] Maksym M. Plakhotnyuk, Nadine Schuler, Evgeniy Shkodin, Surface passivation and carrier selectivity of the thermal-atomic-layer-deposited TiO_2 on crystalline silicon, *Jpn. J. Appl. Phys.* 56 (2017), 08MA11.
- [27] Rahul Pandey, Rishu Chaujar, Rear contact silicon solar cells with a-SiCxH based front surface passivation for near-ultraviolet radiation stability, *Superlattices Microstruct.* 122 (2018) 111–123.
- [28] F. Feldmann, M. Simon, M. Bivour, Carrier-selective contacts for Si solar cells, *Appl. Phys. Lett.* 104 (2014), 181105.
- [29] R.M. Swanson, Approaching the 29% limit efficiency of silicon solar cells, in: Proceedings of the 31st IEEE Photovoltaic Specialists Conference, Lake Buena Vista, FL, USA: IEEE, (2005) 889–894.
- [30] M. Bivour, M. Reusch, S. Schroer, Doped layer optimization for silicon heterojunctions by injection-level-dependent open-circuit voltage measurements, *IEEE J. Photovolt.* 4 (2014) 566–574.
- [31] Moustafa Ghannam, Yaser Abdulraheem, Fundamental constraints imposed by energy barriers on the fill factor and on the efficiency of silicon heterojunction solar cells, *Sol. Energy Mater. Sol. Cells* 171 (2017) 228–238.
- [32] Uli Wurfel, Andres Cuevas, Peter Wurfel, Charge carrier separation in solar cells, *IEEE J. Photovolt.* 5 (2015) 461–469.
- [33] S. Sterk, J. Knoloch, W. Wetling, Optimization of the rear contact pattern of high-efficiency silicon solar cells with and without local back surface field, *Prog. Photovolt.* 2 (1994) 19–26.
- [34] Andres Cuevas, Di Yan, Misconceptions and misnomers in solar cells, *IEEE J. Photovolt.* 3 (2013) 916–923.
- [35] Erkan Aydin, Michèle De Bastiani, Stefaan De Wolf, Defect and contact passivation for perovskite solar cells, *Adv. Mater.* 31 (2019), 1900428.
- [36] Lu Wan, Cuili Zhang, Kunpeng Ge, Conductive hole-selective passivating contacts for crystalline silicon solar cells, *Adv. Energy Mater.* 10 (2020), 1903851.
- [37] Christoph Messmer, Martin Bivour, Jonas Schon, Numerical simulation of silicon heterojunction solar cells featuring metal oxides as carrier-selective contacts, *IEEE J. Photovolt.* 8 (2018) 456–464.
- [38] James Bullock, Mark Hettick, Jonas Geissbuhler, Efficient silicon solar cells with dopant-free asymmetric heterocontacts, *Nat. Energy* 1 (2016) 15031.
- [39] M.A. Green, R.B. Godfrey, MIS silicon solar cells, *Jpn. J. Appl. Phys.* 17 (1978) 295–298.
- [40] T. Raymond, Tung, The physics and chemistry of the Schottky barrier height, *Appl. Phys. Rev.* 1 (2014), 011304.
- [41] W.F. Egelhoff Jr., Core-level binding-energy shifts at surfaces and in solids, *Surf. Sci. Rep.* 6 (1987) 253–415.
- [42] D.K. Schroder, D.L. Meier, Solar cell contact resistance: a review, *IEEE Trans. Electron Devices* 31 (1984) 637–647.
- [43] Corsin Battaglia, Xingtian Yin, Maxwell Zheng, Hole selective MoO_x contact for silicon solar cells, *Nano Lett.* 14 (2014) 967–971.
- [44] Thomas G. Allen, James Bullock, Peiting Zheng, Calcium contacts to n-type crystalline silicon solar cells, *Prog. Photovolt.* 25 (2017) 636–644.
- [45] Di Yan, Andres Cuevas, Empirical determination of the energy band gap narrowing in highly doped n⁺ silicon, *J. Appl. Phys.* 114 (2013), 044508.

- [46] Di Yan, Andres Cuevas, Empirical determination of the energy band gap narrowing in p⁺ silicon heavily doped with boron, *J. Appl. Phys.* 116 (2014) 194505.
- [47] A. Wolf, A. Kimmerle, S. Lohmuller, Status and perspective of emitter formation by POCl₃-diffusion, in: Proceedings of the 31st European Photovoltaic Solar Energy Conference and Exhibition, 2015, pp. 414–419.
- [48] International Technology Roadmap for Photovoltaic (ITRPV), (2020) (<https://itrpv.vdma.org/>).
- [49] Jan Haschke, Olivier Dupre, Mathieu Boccard, Silicon heterojunction solar cells: recent technological development and practical aspects - from lab to industry, *Sol. Energy Mater. Sol. Cells* 187 (2018) 140–153.
- [50] Keiichiro Masuko, Masato Shigematsu, Taiki Hashiguchi, Achievement of more than 25% conversion efficiency with crystalline silicon heterojunction solar cell, *IEEE J. Photovolt.* 4 (2014) 1433–1435.
- [51] Martin Bivour, Sebastian Schroer, Martin Hermle, Silicon heterojunction rear emitter solar cells: less restrictions on the optoelectrical properties of front side TCOs, *Sol. Energy Mater. Sol. Cells* 122 (2014) 120–129.
- [52] Nathan L. Chang, Matthew Wright, Renate Egan, The technical and economic viability of replacing n-type with p-type wafers for silicon heterojunction solar cells, *Cell Rep. Phys. Sci.* 1 (2020), 100069.
- [53] Eiji Kobayashi, Stefaan De Wolf, Jacques Levrat, Light-induced performance increase of silicon heterojunction solar cells, *Appl. Phys. Lett.* 109 (2016), 153503.
- [54] Christophe Ballif, Mathieu Boccard, Matthieu Despeisse, The amazing improvement of silicon heterojunction technology: ready for a true mass market launch, in: Proceedings of the IEEE 7th World Conference on Photovoltaic Energy Conversion, (2018) 2104–2107.
- [55] REC, (<https://www.recgroup.com/en/alpha>).
- [56] Panasonic, (<https://na.panasonic.com/us/energy-solutions/solar/hit-panels>).
- [57] Mikio Taguchi, Ayumi Yano, Satoshi Tohoda, 24.7% record efficiency HIT solar cell on thin silicon wafer, *IEEE J. Photovolt.* 4 (2013) 96–99.
- [58] Omid Madani Ghahfarokhi, Kambulakwao Chakanga, Stefan Geissendoerfer, DC-sputtered ZnO:Al as transparent conductive oxide for silicon heterojunction solar cells with a-Si:H emitter, *Prog. Photovolt.* 23 (2015) 1340–1352.
- [59] Ronald A. Sinton, Contactless determination of current-voltage characteristics and minority-carrier lifetimes in semiconductors from quasi-steady-state photoconductance data, *Appl. Phys. Lett.* 69 (1996) 2510–2512.
- [60] Heike Angermann, Frank Wunsch, Marinus Kunst, Effect of wet-chemical substrate pretreatment on electronic interface properties and recombination losses of a-Si:H/c-Si and a-Si:H/c-Si hetero-interfaces, *Phys. Status Solidi C* 8 (2011) 879–882.
- [61] Sara Olibet, Evelyne Vallat-Sauvain, Luc Fesquet, Properties of interfaces in amorphous/crystalline silicon heterojunctions, *Phys. Status Solidi A* 207 (2010) 651–656.
- [62] T.F. Schulze, C. Leendertz, N. Mingirulli, Impact of Fermi-level dependent defect equilibration on V_{OC} of amorphous/crystalline silicon heterojunction solar cells, *Energy Procedia* 8 (2011) 282–287.
- [63] B. von Roedern, G.H. Bauer, Material requirements for buffer layers used to obtain solar cells with high open circuit voltages, *MRS Online Proc. Libr.* 557 (1999) 761.
- [64] Domenico Caputo, Giampiero de Cesare, Mario Tucci, Built-in enhancement in a-Si:H solar cell by chromium silicide layer, *IEEE Electron Device Lett.* 31 (2010) 689–691.
- [65] J.A. del Alamo, R.M. Swanson, The physics and modeling of heavily doped emitters, *IEEE Trans. Electron Devices* 31 (1984) 1878–1888.
- [66] Markus Reusch, Martin Bivour, Martin Hermle, Fill factor limitation of silicon heterojunction solar cells by junction recombination, *Energy Procedia* 38 (2013) 297–304.
- [67] W. Fuhs, K. Niemann, J. Stuke, Heterojunctions of amorphous silicon and silicon single crystals, *AIP Conference Proceedings*, 20, 1974, p. 345.
- [68] L. Korte, E. Conrad, H. Angermann, Advances in a-Si:H/c-Si heterojunction solar cell fabrication and characterization, *Sol. Energy Mater. Sol. Cells* 93 (2009) 905–910.
- [69] Z.C. Holman, A. Descoeuilles, L. Barraud, Current losses at the front of silicon heterojunction solar cells, *IEEE J. Photovolt.* 2 (2012) 7–15.
- [70] Martin Bivour, Jan Templer, Heiko Steinkemper, Molybdenum and tungsten oxide: high work function wide band gap contact materials for hole selective contacts of silicon solar cells, *Sol. Energy Mater. Sol. Cells* 142 (2015) 34–41.
- [71] James Hack, Christoph Luderer, Christian Reichel, Determining limitations of capacitance-voltage measurements of built-in voltage as an alternative to surface photovoltaic for a-Si:H/c-Si heterojunctions, *Sol. Energy Mater. Sol. Cells* 219 (2019), 110794.
- [72] Martin Bivour, Sebastian Schroer, Martin Hermle, Numerical analysis of electrical TCO / a-Si:H(p) contact properties for silicon heterojunction solar cells, *Energy Procedia* 38 (2013) 658–669.
- [73] R. Robler, C. Leendertz, L. Korte, Impact of the transparent conductive oxide work function on injection-dependent a-Si:H/c-Si band bending and solar cell parameters, *J. Appl. Phys.* 113 (2013), 144513.
- [74] Hiroyuki Fujiwara, Michio Kondo, Effects of a-Si:H layer thicknesses on the performance of a-Si:H / c-Si heterojunction solar cells, *J. Appl. Phys.* 101 (2007), 054516.
- [75] Warren B. Jackson, Robert Nemanich, Marissa Jenna, Schottky barriers on phosphorus-doped hydrogenated amorphous silicon: the effects of tunneling, *Phys. Rev. B* (1986) 6936–6945.
- [76] Hassan Imran, Tarek M. Abdolkader, Nauman Z. Butt, Carrier-selective NiO/Si and TiO₂/Si contacts for silicon heterojunction solar cells, *IEEE Trans. Electron Devices* 63 (2016) 3584–3590.
- [77] Xinbo Yang, Qinyu Bi, Haider Ali, High-performance TiO₂-based electron-selective contacts for crystalline silicon solar cells, *Adv. Mater.* 28 (2016) 5891–5897.
- [78] Jimmy Melskens, Bas W.H. van de Loo, Bart Macco, Passivating contacts for crystalline silicon solar cells: from concepts and materials to prospects, *IEEE J. Photovolt.* 8 (2018) 373–388.
- [79] Ji-Hwan Yang, Sang Jung Kang, Yunho Hong, Doping-free intrinsic amorphous silicon thin-film solar cell having a simple structure of Glass/SnO₂/MoO₃/i-a-Si/LiF/Al, *IEEE Electron Device Lett.* 35 (2014) 96–98.
- [80] James Bullock, Christian Samundsett, Andres Cuevas, Proof-of-concept p-type silicon solar cells with molybdenum oxide local rear contacts, *IEEE J. Photovolt.* 5 (2015) 1591–1594.
- [81] Han-Don Um, Namwoo Kim, Kangmin Lee, Dopant-free all-back-contact Si nanohole solar cells using MoO_x and LiF films, *Nano Lett.* 16 (2016) 981–987.
- [82] Weiliang Wu, Wenjie Lin, Jie Bao, Dopant-free multilayer back contact silicon solar cells employing V₂O_x/metal/V₂O_x as an emitter, *RSC Adv.* 7 (2017) 23851–23858.
- [83] Gerard Masmijta, Luis G. Gerling, Pablo Ortega, V₂O_x-based hole-selective contacts for c-Si interdigitated back-contacted solar cells, *J. Mater. Chem. A* 5 (2017) 9182–9189.
- [84] Andres Cuevas, Thomas Allen, James Bullock, Skin care for healthy silicon solar cells, in: Proceedings of the 2015 IEEE 42nd Photovoltaic Specialist Conference, (2015).
- [85] Dieter Neher, Julianne Kniepert, Arik Elimelech, A new figure of merit for organic solar cells with transport-limited photocurrents, *Sci. Rep.* 6 (2016) 24861.
- [86] Luis G. Gerling, Somnath Mahato, Anna Morales-Vilches, Transition metal oxides as hole-selective contacts in silicon heterojunctions solar cells, *Sol. Energy Mater. Sol. Cells* 145 (2016) 109–115.
- [87] Corsin Battaglia, Silvia Martin de Nicolas, Stefaan De Wolf, Hole selective MoO_x contact for silicon heterojunction solar cells, in: Proceedings of the IEEE 40th Photovoltaic Specialists Conference, (2014).
- [88] Teng Sun, Rongbin Wang, Ruiyuan Liu, Investigation of MoO_x/n-Si strong inversion layer interfaces via dopant-free heterocontact, *Phys. Status Solidi RRL* 11 (2017), 1700107.
- [89] Shengsheng Zhao, Yuzeng Xu, Junfan Chen, Research progress of crystalline silicon solar cells with dopant-free asymmetric heterocontacts, *Acta Phys. Sin.* 68 (2019), 048801.
- [90] Mark T. Greiner, Michael G. Helander, Wing-Man Tang, Universal energy-level alignment of molecules on metal oxides, *Nat. Mater.* 11 (2012) 76–81.
- [91] Ramachandran Ammapet Vijayan, Stephanie Essig, Stefaan De Wolf, Hole-collection mechanism in passivating metal-oxide contacts on Si solar cells: insights from numerical simulations, *IEEE J. Photovolt.* 8 (2018) 473–482.
- [92] Lisa Neusel, Martin Bivour, Martin Hermle, Selectivity issues of MoO_x based hole contacts, *Energy Procedia* 124 (2017) 425–434.
- [93] Martin Bivour, Florian Zahringer, Paul Ndione, Sputter-deposited WO_x and MoO_x for hole selective contacts, *Energy Procedia* 124 (2017) 400–405.
- [94] SERIS, (<http://www.seris.sg/>).
- [95] Yuguo Tao, Vijaykumar Upadhyaya, Keenan Jones, Tunnel oxide passivated rear contact for large area n-type front junction silicon solar cells providing excellent carrier selectivity, *AIMS Mater. Sci.* 3 (2016) 180–189.
- [96] Armin Richter, Jan Benick, Frank Feldmann, n-Type Si solar cells with passivating electron contact: Identifying sources for efficiency limitations by wafer thickness and resistivity variation, *Sol. Energy Mater. Sol. Cells* 173 (2017) 96–105.
- [97] Naomi Nandakumar, John Rodriguez, Thomas Kluge, Approaching 23% with large-area monoPoly cells using screen-printed and fired rear passivating contacts fabricated by inline PECVD, *Prog. Photovolt.* 27 (2019) 107–112.
- [98] Shujian Huang, Eun-Chel Cho, Gavin Conibeer, Structural and photoluminescence properties of superlattice structures consisting of Sn-rich SiO₂ and stoichiometric SiO₂ layers, *Thin Solid Films* 520 (2011) 641–645.
- [99] Stefan W. Glunz, Frank Feldmann, Armin Richter, The irresistible charm of a simple current flow pattern – 25% with a solar cell featuring a full-area back contact, in: Proceedings of the 31st European Photovoltaic Solar Energy Conference, (2015).
- [100] Bert Stegemann, Karim M. Gad, Patrice Balamou, Ultra-thin silicon oxide layers on crystalline silicon wafers: comparison of advanced oxidation techniques with respect to chemically abrupt SiO₂/Si interfaces with low defect densities, *Appl. Surf. Sci.* 395 (2017) 78–85.
- [101] Jingnan Tong, Xi Wang, Zi Ouyang, Ultra-thin tunnel oxides formed by field-induced anodisation for carrier-selective contacts, *Energy Procedia* 77 (2015) 840–847.
- [102] Hikaru Kobayashi Asuha, Osamu Maida, Masao Takahashi, Nitric acid oxidation of Si to form ultrathin silicon dioxide layers with a low leakage current density, *J. Appl. Phys.* 94 (2003) 7328–7335.
- [103] J.L. Hernandez, D. Adachi, Kunta Yoshikawa, High efficiency copper electropolished heterojunction solar cells, in: Proceedings of the 28th European Photovoltaic Solar Energy Conference and Exhibition, (2013) 741.
- [104] Ruy Sebastian Bonilla, Christian Reichel, Martin Hermle, Controlled field effect surface passivation of crystalline n-type silicon and its application to back-contact silicon solar cells, in: Proceedings of the IEEE 40th Photovoltaic Specialists Conference, (2014).
- [105] Yuguo Tao, Vijaykumar Upadhyaya, Ying-Yuan Huang, Carrier selective tunnel oxide passivated contact enabling 21.4% efficient large-area N-type silicon solar

- cells, in: Proceedings of the IEEE 43rd Photovoltaic Specialists Conference (PVSC), (2016).
- [106] R. Peibst, Y. Larionova, S. Reiter, Implementation of n⁺ and p⁺ poly junctions on front and rear side of double-side contacted industrial silicon solar cells, in: Proceedings of the 32nd European Photovoltaic Solar Energy Conference and Exhibition, 2016, pp. 323–327.
- [107] Udo Romer, Robby Peibst, Tobias Ohrdes, Recombination behavior and contact resistance of n⁺ and p⁺ poly-crystalline Si/mono-crystalline Si junctions, *Sol. Energy Mater. Sol. Cells* 131 (2014) 85–91.
- [108] Michael Rienacker, Agnes Merkle, Udo Romer, Recombination behavior of photolithography-free back junction back contact solar cells with carrier-selective polysilicon on oxide junctions for both polarities, in: Proceedings of the 6th International Conference on Crystalline Silicon Photovoltaics, (2016).
- [109] M.K. Stodolny, M. Lenes, Y. Wu, n-Type polysilicon passivating contact for industrial bifacial n-type solar cells, *Sol. Energy Mater. Sol. Cells* 158 (2016) 24–28.
- [110] Pradeep Padhamnath, Ankit Khanna, Naomi Nandakumar, Development of thin polysilicon layers for application in monoPolyTM cells with screen-printed and fired metallization, *Sol. Energy Mater. Sol. Cells* 207 (2020), 110358.
- [111] J.Y. Gan, R.M. Swanson, Polysilicon emitters for silicon concentrator solar cells, in: Proceedings of the IEEE Conference on Photovoltaic Specialists, (1990).
- [112] Frank Feldmann, Christian Reichel, Ralph Muller, The application of poly-Si/SiO_x contacts as passivated top/rear contacts in Si solar cells, *Sol. Energy Mater. Sol. Cells* 159 (2017) 265–271.
- [113] Shubham Duttagupta, Naomi Nandakumar, Pradeep Phdhamnath, monoPolyTM cells: large-area crystalline silicon solar cells with fire-through screen printed contact to doped polysilicon surfaces, *Sol. Energy Mater. Sol. Cells* 187 (2018) 76–81.
- [114] Frank Feldmann, Martin Bivour, Christian Reichel, Passivated rear contacts for high-efficiency n-type Si solar cells providing high interface passivation quality and excellent transport characteristics, *Sol. Energy Mater. Sol. Cells* 120 (2014) 270–274.
- [115] Yuguo Tao, Vijaykumar Upadhyaya, Large area tunnel oxide passivated rear contact n-type Si solar cells with 21.2% efficiency, *Prog. Photovolt.* 24 (2016) 830–835.
- [116] R. Peibst, Y. Larionova, S. Reiter, Implementation of n⁺ and p⁺ poly junctions on front and rear side of double-side contacted industrial silicon solar cells, in: Proceedings of the 32nd European Photovoltaic Solar Energy Conference and Exhibition, (2016) 323–327.
- [117] Bill Nemeth, David L. Young, Matthew R. Page, Polycrystalline silicon passivated tunneling contacts for high efficiency silicon solar cells, *J. Mater. Res.* 31 (2016) 671–681.
- [118] Di Yan, Andres Cuevas, James Bullock, Phosphorus-diffused polysilicon contacts for solar cells, *Sol. Energy Mater. Sol. Cells* 142 (2015) 75–82.
- [119] Wantang Wang, Baoguo Zhang, Yunhui Shi, Tengda Ma, Jiakai Zhou, Ru Wang, Hanxiao Wang, Nengyuan Zeng, Improvement in chemical mechanical polishing of 4H-SiC wafer by activating persulfate through the synergistic effect of UV and TiO₂, *J. Mater. Process. Technol.* 295 (2021), 117150.
- [120] Bernd Steinhauser, Jana-Isabell Polzin, Frank Feldmann, Excellent surface passivation quality on crystalline silicon using industrial-scale direct-plasma TOPCon deposition technology, *Sol. RRL* 2 (2018), 1800068.
- [121] A. Merkle, S. Seren, H. Knauss, Atmospheric pressure chemical vapor deposition of in-situ doped amorphous silicon layers for passivating contacts, in: Proceedings of the 35th European Photovoltaic Solar Energy Conference and Exhibition, (2018) 785–791.
- [122] Di Yan, Andres Cuevas, Sieu Pheng Phang, 23% efficient p-type crystalline silicon solar cells with hole-selective passivating contacts based on physical vapor deposition of doped silicon films, *Appl. Phys. Lett.* 113 (2018), 061603.
- [123] J. Lossen, J. Hob, S. Eisert, Electron beam evaporation of silicon for poly-silicon/SiO₂ passivated contacts, in: Proceedings of the 35th European Photovoltaic Solar Energy Conference and Exhibition, (2018) 418–421.
- [124] F. Kiefer, N. Wehmeyer, T. Brendemuhl, Inkjet printing as a new method for the preparation of POLO contacts, MRS Fall Meeting and Exhibit, (2018).
- [125] Jan Schmidt, Robby Peibst, Rolf Brendel, Surface passivation of crystalline silicon solar cells: Present and future, *Solar Energy Materials and Solar Cells*, 187, 2018, pp. 39–54.
- [126] Yuheng Zeng, Hui Tong, Cheng Quan, Theoretical exploration towards high-efficiency tunnel oxide passivated carrier-selective contacts (TOPCon) solar cells, *Sol. Energy* 155 (2017) 654–660.
- [127] Di Yan, Andres Cuevas, Jesus Ibarra Michel, Polysilicon passivated junctions: the next technology for silicon solar cells, *Joule* 5 (2021) 811–828.
- [128] Josua Stuckelberger, Gizem Nogay, Philippe Wyss, Recombination analysis of phosphorus-doped nanostructured silicon oxide passivating electron contacts for silicon solar cells, *IEEE J. Photovolt.* 8 (2018) 1–8.
- [129] Robby Peibst, Udo Romer, Karl R. Hofmann, A simple model describing the symmetric IV characteristics of p polycrystalline Si/ n monocrystalline Si, and n polycrystalline Si/p monocrystalline Si junctions, *IEEE J. Photovolt.* 4 (2014) 841–850.
- [130] R. Peibst, U. Romer, Y. Larionova, Working principle of carrier selective poly-Si/c-Si junctions: Is tunnelling the whole story? *Sol. Energy Mater. Sol. Cells* 158 (2016) 60–67.
- [131] Stefan W. Glunz, Frank Feldmann, SiO₂ surface passivation layers – a key technology for silicon solar cells, *Sol. Energy Mater. Sol. Cells* 185 (2018) 260–269.
- [132] Manuel Schnabel, Bas W.H. Van de Loo, William Nemeth, Hydrogen passivation of poly-Si/SiO_x contacts for Si solar cells using Al₂O₃ studied with deuterium, *Appl. Phys. Lett.* 112 (2018), 203901.
- [133] Thien N. Truong, Di Yan, Christian Samundset, Hydrogenation of phosphorus-doped polycrystalline silicon films for passivating contact solar cells, *ACS Appl. Mater. Interfaces* 11 (2019) 5554–5560.
- [134] Gizem Nogay, Josua Stuckelberger, Philippe Wyss, Interplay of annealing temperature and doping in hole selective rear contacts based on silicon-rich silicon-carbide thin films, *Sol. Energy Mater. Sol. Cells* 173 (2017) 18–24.
- [135] Leonard Tutsch, Frank Feldmann, Jana Polzin, Implementing transparent conducting oxides by DC sputtering on ultrathin SiO_x/poly-Si passivating contacts, *Sol. Energy Mater. Sol. Cells* 200 (2019), 109960.
- [136] Zhi Zhang, Mingdun Liao, Yuqing Huang, Improvement of surface passivation of tunnel oxide passivated contact structure by thermal annealing in mixture of water vapor and nitrogen environment, *Sol. RRL* 3 (2019), 1900105.
- [137] Andrea Ingenito, Gizem Nogay, Quentin Jeangros, A passivating contact for silicon solar cells formed during a single firing thermal annealing, *Nat. Energy* 3 (2018) 800–808.
- [138] Maciej K. Stodolny, J. Anker, C.J. Tool, Novel schemes of P⁺ poly-Si hydrogenation implemented in industrial 6" bifacial front-and-rear passivating contacts solar cells, in: Proceedings of the International Conference EU PVSEC for Photovoltaic Research, 2018, pp. 1–4.
- [139] Yevgeniya Larionova, Mircea Turcu, Sina Reiter, On the recombination behavior of p⁺-type polysilicon on oxide junctions deposited by different methods on textured and planar surfaces, *Phys. Status Solidi A* 214 (2017), 1700058.
- [140] T. Sawada, N. Terada, S. Tsuge, High-efficiency a-Si/c-Si heterojunction solar cell, in: Proceedings of 1994 IEEE 1st World Conference on Photovoltaic Energy Conversion – WCPEC, (1994).
- [141] T. Kinoshita, D. Fujishima, A. Yano, The approaches for high efficiency HIT solar cell with very thin (<100 μm) silicon wafer over 23%, in: Proceedings of the 26th European Photovoltaic Solar Energy Conference and Exhibition, 2011, pp. 871–874.
- [142] Daisuke Adachi, Jose Luis Hernandez, Kenji Yamamoto, Impact of carrier recombination on fill factor for large area heterojunction crystalline silicon solar cell with 25.1% efficiency, *Appl. Phys. Lett.* 107 (2015), 233506.
- [143] Kunta Yoshiikawa, Hayato Kawasaki, Wataru Yoshida, Silicon heterojunction solar cell with interdigitated back contacts for a photoconversion efficiency over 26%, *Nat. Energy* 2 (2017) 17032.
- [144] Thomas Mueller, Johnson Wong, Armin G. Aberle, Heterojunction silicon wafer solar cells using amorphous silicon suboxides for interface passivation, *Energy Procedia* 15 (2012) 97–106.
- [145] Jonas Geissbuhler, Stefaan De Wolf, Antonin Faes, Silicon heterojunction solar cells with copper-plated grid electrodes: status and comparison with silver thick-film techniques, *IEEE J. Photovolt.* 4 (2014) 1055–1062.
- [146] Fanying Meng, Jinning Liu, Leilei Shen, High-quality industrial n-type silicon wafers with an efficiency of over 23% for Si heterojunction solar cells, *Front. Energy* 11 (2017) 78–84.
- [147] Jiunn Benjamin Heng, Jianming Fu, Bob Kong, >23% high-efficiency tunnel oxide junction bifacial solar cell with electroplated Cu gridlines, *IEEE J. Photovolt.* 5 (2014) 82–86.
- [148] Stanislau Y. Herasimenka, Clarence J. Tracy, William J. Dauksher, A simplified process flow for silicon heterojunction interdigitated back contact solar cells: Using shadow masks and tunnel junctions, in: Proceedings of the IEEE 40th Photovoltaic Specialist Conference (PVSC), (2014).
- [149] Cao Yu, Miao Yang, Yue Zhang, Development of high efficiency rear-emitter n-type silicon heterojunction solar cells, in: Proceedings of the IEEE 42nd Photovoltaic Specialist Conference (PVSC), (2015).
- [150] Eiji Kobayashi, N. Nakamura, Yoshimi Watabe, Reduction of optical and electrical losses in silicon heterojunction solar cells by hydrogenated tungsten-doped In₂O₃, in: Proceedings of the 28th European Photovoltaic Solar Energy Conference, (2012).
- [151] J. Chang, F.-S. Chen, M.-Y. Chen, Investigation of interface between sputtered NiV/Ag and TCO layer in back side metallization for high efficiency heterojunction solar cell, in: 31st European Photovoltaic Solar Energy Conference and Exhibition, (2015) 890–892.
- [152] Nicola Mingirulli, Jan Haschke, Ralf Gogolin, Efficient interdigitated back-contacted silicon heterojunction solar cells, *Phys. Status Solidi RRL* 5 (2011) 159–161.
- [153] Seung-Yoon Lee, Hongsik Choi, Hongmei Li, Analysis of a-Si:H/TCO contact resistance for the Si heterojunction back-contact solar cell, *Sol. Energy Mater. Sol. Cells* 120 (2014) 412–416.
- [154] Samuel Harrison, Oriol Nos, Guillaume D. Alonzo, Back contact heterojunction solar cells patterned by laser ablation, *Energy Procedia* 92 (2016) 730–737.
- [155] Bertrand Paviet-Salomon, Andrea Tomasi, Antoine Descoedres, Back-contacted silicon heterojunction solar cells: optical-loss analysis and mitigation, *IEEE J. Photovolt.* 5 (2015) 1293–1303.
- [156] Harihasudan Sivararamakrishnan Radhakrishnan, Twan Bearda, Menglei Xu, Module-level cell processing of silicon heterojunction interdigitated back-contacted (SHJ-IBC) solar cells with efficiencies above 22%: Towards all-dry processing, in: Proceedings of the IEEE 43rd Photovoltaic Specialists Conference, (2016) 1182–1187.
- [157] Junichi Nakamura, Naoki Asano, Takeshi Hieda, Development of heterojunction back contact Si solar cells, *IEEE J. Photovolt.* 4 (2014) 1491–1495.
- [158] Jan-Willem A. Schuttauf, Karine H.M. van der Werf, Inge M. Kielen, Excellent crystalline silicon surface passivation by amorphous silicon irrespective of the

- technique used for chemical vapor deposition, *Appl. Phys. Lett.* 98 (2011), 153514.
- [159] Jianhui Chen, Jing Yang, Yanjiao Shen, Investigation of post-annealing enhancement effect of passivation quality of hydrogenated amorphous silicon, *Acta Phys. Sin.* 64 (2015), 198801.
- [160] Damian Pysch, Christoph Meinhard, Nils-Peter Harder, Analysis and optimization approach for the doped amorphous layers of silicon heterojunction solar cells, *J. Appl. Phys.* 110 (2011), 094516.
- [161] H. Tasaki, W.Y. Kim, M. Hallerdt, Computer simulation model of the effects of interface states on high-performance amorphous silicon solar cells, *J. Appl. Phys.* 63 (1988) 550–560.
- [162] C. Leendertz, N. Mingirulli, T.F. Schulze, Discerning passivation mechanisms at a-Si:H/c-Si interfaces by means of photoconductance measurements, *Appl. Phys. Lett.* 98 (2011), 202108.
- [163] Wilfried Favre, Jean Coignus, Nathalie Nguyen, Influence of the transparent conductive oxide layer deposition step on electrical properties of silicon heterojunction solar cells, *Appl. Phys. Lett.* 102 (2013), 181118.
- [164] Andreas Janotta, Rainer Janssen, Matthias Schmidt, Doping and its efficiency in a-SiO_xH, *Phys. Rev. B* 69 (2004), 115206.
- [165] R.R. King, R.A. Sinton, R.M. Swanson, Studies of diffused phosphorus emitters: saturation current, surface recombination velocity, and quantum efficiency, *IEEE Trans. Electron Devices* 37 (1990) 365–371.
- [166] Jagannath Panigrahi, Vamsi K. Komarala, Progress on the intrinsic a-Si:H films for interface passivation of silicon heterojunction solar cells: a review, *J. Non-Cryst. Solids* 574 (2021), 121166.
- [167] R. Varache, J.P. Kleider, M.E. Gueunier-Farret, Silicon heterojunction solar cells: Optimization of emitter and contact properties from analytical calculation and numerical simulation, *Mater. Sci. Eng.: B* 178 (2013) 593–598.
- [168] Simon Kirner, Manuel Hartig, Luana Mazzarella, The influence of ITO dopant density on J-V characteristics of silicon heterojunction solar cells: experiments and simulations, *Energy Procedia* 77 (2015) 725–732.
- [169] Andreas Klein, Christoph Korber, Andre Wachau, Transparent conducting oxides for photovoltaics: manipulation of Fermi level, work function and energy band alignment, *Materials* 3 (2010) 4892–4914.
- [170] L. Zhao, C.L. Zhou, H.L. Li, H.W. Diao, W.J. Wang, Design optimization of bifacial HIT solar cells on p-type silicon substrates by simulation, *Sol. Energy Mater. Sol. Cells* 92 (2008) 673–681.
- [171] Kurt-Ulrich Ritzau, Martin Bivour, Sebastian Schroer, TCO work function related transport losses at the a-Si:H/TCO-contact in SHJ solar cells, *Sol. Energy Mater. Sol. Cells* 131 (2014) 9–13.
- [172] Moustafa Ghannam, Ghadah Shehadah, Yaser Abdulraheem, On the possible role of the interfacial inversion layer in the improvement of the performance of hydrogenated amorphous silicon/crystalline silicon heterojunction solar cells [HIT], *Sol. Energy Mater. Sol. Cells* 132 (2015) 320–328.
- [173] Lin Yiren, Tan Xin, Liu Aimin, Influence of the asymmetrical defect state distribution at the a-Si:H/cSi interface on the performance of homo-heterojunction solar cells, *Surf. Sci.* 682 (2019) 51–59.
- [174] Xixing Wen, Xiangbin Zeng, Wugang Liao, An approach for improving the carriers transport properties of a-Si:H/c-Si heterojunction solar cells with efficiency of more than 27%, *Sol. Energy* 96 (2013) 168–176.
- [175] Hiroyuki Fujiwara, Tetsuya Kaneko, Michio Kondo, Application of hydrogenated amorphous silicon oxide layers to c-Si heterojunction solar cells, *Appl. Phys. Lett.* 91 (2007), 133508.
- [176] Weihong Chang, Hanmin Tian, Guochuan Fang, Simulation of innovative high efficiency perovskite solar cell with Bi-HTL: NiO and Si thin films, *Sol. Energy* 186 (2019) 323–327.
- [177] Jeehan Kim, Ahmed Abou-Kandil, Keith Fogel, The role of high work-function metallic nanodots on the performance of a-Si:H solar cells: offering ohmic contact to light trapping, *ACS Nano* 4 (2010) 7331–7336.
- [178] Raphael Lachaume, Wilfried Favre, Pascal Scheiblin, Influence of a-Si:H/ITO interface properties on performance of heterojunction solar cells, *Energy Procedia* 38 (2013) 770–776.
- [179] Venkanna Kanboina, Ramakrishna Madaka, Pratima Agarwal, High open circuit voltage c-Si/a-Si:H heterojunction solar cells: influence of hydrogen plasma treatment studied by spectroscopic ellipsometry, *Sol. Energy* 166 (2018) 255–266.
- [180] John Robertson, Band offsets, Schottky barrier heights, and their effects on electronic devices, *J. Vac. Sci. Technol. A* 31 (2013), 050821.
- [181] S. Martin de Nicolas, D. Munoz, A.S. Ozanne, Optimization of doped amorphous silicon layers applied to heterojunction solar cells, *Energy Procedia* 8 (2011) 226–231.
- [182] Stefaan De Wolf, Michio Kondo, Boron-doped a-Si:H/c-Si interface passivation: degradation mechanism, *Appl. Phys. Lett.* 91 (2007), 112109.
- [183] M.J. Powell, S.C. Deane, Improved defect-pool model for charged defects in amorphous silicon, *Phys. Rev. B* 48 (1993) 10815–10827.
- [184] Benedicte Demaurex, Johannes P. Seif, Sjoerd Smit, Atomic-layer-deposited transparent electrodes for silicon heterojunction solar cells, *IEEE J. Photovolt.* 4 (2014) 1387–1396.
- [185] Benedicte Demaurex, Stafaan De Wolf, Antoine Descoedres, Damage at hydrogenated amorphous/crystalline silicon interfaces by indium tin oxide overlayer sputtering, *Appl. Phys. Lett.* 101 (2012), 171604.
- [186] Hiroyuki Fujiwara, Michio Kondo, Effects of a-Si:H layer thicknesses on the performance of a-Si:H/c-Si heterojunction solar cells, *J. Appl. Phys.* 101 (2007), 054516.
- [187] Emanuele Centurioni, Daniele lencinella, Rita Rizzoli, Silicon heterojunction solar cell: a new buffer layer concept with low-temperature epitaxial silicon, *IEEE Trans. Electron Devices* 51 (2004) 1818–1824.
- [188] F. Zignani, Agostino Desalvo, Emanuele Centurioni, Silicon heterojunction solar cells with p nanocrystalline thin emitter on monocrystalline substrate, *Thin Solid Films* 451 (2004) 350–354.
- [189] O.A. Masolva, J. Alvarez, E.V. Gushina, Observation by conductive-probe atomic force microscopy of strongly inverted surface layers at the hydrogenated amorphous silicon/crystalline silicon heterojunctions, *Appl. Phys. Lett.* 97 (2010), 252110.
- [190] J.K. Arch, F.A. Rubinelli, J.-Y. Hou, Computer analysis of the role of p-layer quality, thickness, transport mechanisms, and contact barrier height in the performance of hydrogenated amorphous silicon p-i-n solar cells, *J. Appl. Phys.* 69 (1991) 7057–7066.
- [191] D.C. Walter, B. Lim, K. Bothe, Lifetimes exceeding 1 ms in 1-Ω cm boron-doped Cz-silicon, *Sol. Energy Mater. Sol. Cells* 131 (2014) 51–57.
- [192] Mehdi Leilaieoun, William Weigand, Mathieu Boccard, Contact resistivity of the p-type amorphous silicon hole contact in silicon heterojunction solar cells, *IEEE J. Photovolt.* 10 (2020) 54–62.
- [193] S. Martin de Nicolas, D. Munoz, A.S. Ozanne, Optimisation of doped amorphous silicon layers applied to heterojunction solar cells, *Energy Procedia* 8 (2011) 226–231.
- [194] Gizem Nogay, Johannes Peter Seif, Yannick Riesen, Nanocrystalline silicon carrier collectors for silicon heterojunction solar cells and impact on low-temperature device characteristics, *IEEE J. Photovolt.* 6 (2016) 1654–1662.
- [195] W.E. Spear, P.G. Le Comber, Substitutional doping of amorphous silicon, *Solid State Commun.* 17 (1975) 1193–1196.
- [196] Alexandros Cruz, Er-Chien Wang, Anna B. Morales-Vilches, Effect of front TCO on the performance of rear-junction silicon heterojunction solar cells: insights from simulations and experiments, *Sol. Energy Mater. Sol. Cells* 195 (2019) 339–345.
- [197] Jan Haschke, Christoph Messmer, Jean Cattin, Injection-dependent lateral resistance in front-junction solar cells with nc-Si:H and a-Si:H hole selective contact, in: Proceedings of the IEEE 46th Photovoltaic Specialists Conference, (2019).
- [198] Atse Louwen, Wilfried van Sark, Ruud Schropp, A cost roadmap for silicon heterojunction solar cells, *Sol. Energy Mater. Sol. Cells* 147 (2016) 295–314.
- [199] Eiji Kobayashi, Stefaan De Wolf, Jacques Levrat, Increasing the efficiency of silicon heterojunction solar cells and modules by light soaking, *Sol. Energy Mater. Sol. Cells* 173 (2017) 43–49.
- [200] European Commission, Critical Raw Materials. (https://ec.europa.eu/growth/sector/raw-materials/specific-interest/critical_en).
- [201] Jorg Schube, Maximilian Weil, Tobias Fellmeth, Intense pulsed light meets the metallization of silicon heterojunction solar cells, in: Proceedings of the IEEE 46th Photovoltaic Specialists Conference, (2019).
- [202] Joost Hermans, P. Papet, Karlos Perez Pacheco, Inkjet printing of Ag nanoparticle inks for heterojunction solar cell metallization 2015 SNEC PV Power Expo. 2015.
- [203] Zhenhao Zhang, Marco Huber, Mirza Corda, Key equipments for O₃-based wet-chemical surface engineering and PVD processes tailored for high-efficiency silicon heterojunction solar cells, *Energy Procedia* 130 (2017) 31–35.
- [204] Ziqiu Ren, Na Wang, Peicheng Wei, Ultraviolet-ozone modification on TiO₂ surface to promote both efficiency and stability of low-temperature planar perovskite solar cells, *Chem. Eng. J.* 393 (2020), 124731.
- [205] Hideki Matsumura, Koichi Higashimine, Koichi Koyama, Comparison of crystalline-silicon/amorphous-silicon interface prepared by plasma enhanced chemical vapor deposition and catalytic chemical vapor deposition, *J. Vac. Sci. Technol. B* 33 (2015), 031201.
- [206] Qi Wang, Hot-wire CVD amorphous Si materials for solar cell application, *Thin Solid Films* 517 (2009) 3570–3574.
- [207] Xinyu Wang, Xudong Sui, Shuaitung Zhang, Effect of deposition pressures on uniformity, mechanical and tribological properties of thick DLC coatings inside of a long pipe prepared by PECVD method, *Surf. Coat. Technol.* 375 (2019) 150–157.
- [208] K. Iwata, T. Sakemi, A. Yamada, Improvement of ZnO TCO film growth for photovoltaic devices by reactive plasma deposition (RPD), *Thin Solid Films* 480–481 (2005) 199–203.
- [209] K. Bendjebar, W.L. Rahal, D. Rached, Numerical analysis of metal-semiconductor junctions ITO/p-a-Si:H and n-c-Si/Al on silicon heterojunction solar cells, *Optik* 212 (2020), 164741.
- [210] Takashi Koida, Yuko Ueno, Hajime Shibata, In₂O₃-based transparent conducting oxide films with high electron mobility fabricated at low process temperatures, *Phys. Status Solidi A* 215 (2018), 1700506.
- [211] Monica Morales-Masis, Silvia Martin De Nicolas, Jakub Holovsky, Low-temperature high-mobility amorphous IZO for silicon heterojunction solar cells, *IEEE J. Photovolt.* 5 (2015) 1340–1347.
- [212] Eiji Kobayashi, Yoshimi Watabe, Tetsuya Yamamoto, Cerium oxide and hydrogen co-doped indium oxide films for high-efficiency silicon heterojunction solar cells, *Sol. Energy Mater. Sol. Cells* 149 (2016) 75–80.
- [213] Thanaporn Tohsophon, Ali Dabirian, Steffan De Wolf, Environmental stability of high-mobility indium-oxide based transparent electrodes, *APL Mater.* 3 (2015), 116105.
- [214] Kurt-Ulrich Ritzau, Torge Behrendt, Daniele Palaferri, Hydrogen doping of indium tin oxide due to thermal treatment of hetero-junction solar cells, *Thin Solid Films* 599 (2016) 161–165.
- [215] Jan Jeurink, Florian Wagner, Sunah Park, MF-sputtered AZO for a-Si SHJ solar cells, *Energy Procedia* 55 (2014) 777–785.

- [216] Takahiro Mishima, Mikio Taguchi, Hitoshi Sakata, Development status of high-efficiency HIT solar cells, *Sol. Energy Mater. Sol. Cells* 95 (2011) 18–21.
- [217] Manabu Yoshida, Hideo Tokuhisa, Uichi Itoh, Novel low-temperature-sintering type Cu-alloy pastes for silicon solar cells, *Energy Procedia* 21 (2012) 66–74.
- [218] A. De Rose, T. Geipel, D. Eberlein, Interconnection of silicon heterojunction solar cells by infrared soldering - solder joint analysis and temperature study, in: Proceedings of the 36th European Photovoltaic Solar Energy Conference and Exhibition, (2019), pp. 229–234.
- [219] Yuqiang Liu, Yajuan Li, Yiliang Wu, High-efficiency silicon heterojunction solar cells: materials, devices and applications, *Mater. Sci. Eng.: R: Rep.* 142 (2020), 100579.
- [220] Boon Heng Teo, Ankit Khanna, Vinodh Shanmugam, Development of nanoparticle copper screen printing pastes for silicon heterojunction solar cells, *Sol. Energy* 189 (2019) 179–185.
- [221] Emilio Pulli, Elena Rozzi, Federico Bella, Transparent photovoltaic technologies: current trends towards upscaling, *Energy Convers. Manag.* 219 (2020), 112982.
- [222] Peichen Yu, Chia-Ying Tsai, Jan-Kai Chang, 13% efficiency hybrid organic/silicon-nanowire heterojunction solar cell via interface engineering, *ACS Nano* 7 (2013) 10780–10787.
- [223] Lining He, Changyu Jiang, Rusli, Highly efficient Si-nanorods/organic hybrid core-sheath heterojunction solar cells, *Appl. Phys. Lett.* 99 (2011), 021104.
- [224] Jianhui Chen, Linlin Yang, Kunpeng Ge, On the light-induced enhancement in photovoltaic performance of PEDOT:PSS/Si organic-inorganic hybrid solar cells, *Appl. Phys. Lett.* 111 (2017), 183904.
- [225] Jian He, Pingqi Gao, Zhenhai Yang, Silicon/organic hybrid solar cells with 16.2% efficiency and improved stability by formation of conformal heterojunction coating and moisture-resistant capping layer, *Adv. Mater.* 29 (2017) 1606321.
- [226] Dimitri Zielke, Alexandra Pazidis, Florian Werner, Organic-silicon heterojunction solar cells on n-type silicon wafers: The BackPEDOT concept, *Sol. Energy Mater. Sol. Cells* 131 (2014) 110–116.
- [227] Dimitri Zielke, Claudia Niehaves, Wilfried Lovenich, Organic-silicon solar cells exceeding 20% efficiency, *Energy Procedia* 77 (2015) 331–339.
- [228] Hui Tong, Zhenhai Yang, Xixi Wang, Dual functional electron-selective contacts based on silicon oxide/magnesium: tailoring heterointerface band structures while maintaining surface passivation, *Adv. Energy Mater.* 8 (2018), 1702921.
- [229] Yimao Wan, C. Samundsett, James Bullock, Magnesium fluoride electron-selective contacts for crystalline silicon solar cells, *ACS Appl. Mater. Interfaces* 8 (2016) 14671–14677.
- [230] Jonas Geissbuhler, Jeremie Werner, Silvia Martin de Nicolas, 22.5% efficient silicon heterojunction solar cell with molybdenum oxide hole collector, *Appl. Phys. Lett.* 107 (2015), 081601.
- [231] James Bullock, Di Yan, Andres Cuevas, n- and p-type silicon solar cells with molybdenum oxide hole contacts, *Energy Procedia* 77 (2015) 446–450.
- [232] Xinbo Yang, Klaus Weber, N-type silicon solar cells featuring an electron-selective TiO₂ contact, in: Proceedings of the 21 IEEE 42nd Photovoltaic Specialist Conference (PVSC), 2015, pp. 1–4.
- [233] Corsin Battaglia, Silvia Martin de Nicolas, Stefaan De Wolf, Silicon heterojunction solar cell with passivated hole selective MoO_x contact, *Appl. Phys. Lett.* 104 (2014), 113902.
- [234] Xinbo Yang, Peiting Zheng, Qunyu Bi, Silicon heterojunction solar cells with electron selective TiO_x contact, *Sol. Energy Mater. Sol. Cells* 150 (2016) 32–38.
- [235] Yimao Wan, C. Samundsett, James Bullock, Conductive and stable magnesium oxide electron-selective contacts for efficient silicon solar cells, *Adv. Energy Mater.* 7 (2017), 1601863.
- [236] Fengyou Wang, Shanzhen Zhao, Bofei Liu, Silicon solar cells with bifacial metal oxides carrier selective layers, *Nano Energy* 39 (2017) 437–443.
- [237] James Bullock, Yimao Wan, Zhaoran Xu, Stable dopant-free asymmetric heterointerface silicon solar cells with efficiencies above 20%, *ACS Energy Lett.* 3 (2018) 508–513.
- [238] Fengchao Li, Zongheng Sun, Yurong Zhou, Lithography-free and dopant-free back-contact silicon heterojunction solar cells with solution-processed TiO₂ as the efficient electron selective layer, *Sol. Energy Mater. Sol. Cells* 203 (2019), 110196.
- [239] Jian He, Md. Anower Hossain, Hao Lin, 15% efficiency ultrathin silicon solar cells with fluorine-doped titanium oxide and chemically tailored poly(3,4-ethylenedioxythiophene):poly(styrenesulfonate) as asymmetric heterointerface, *ACS Nano* 13 (2019) 6356–6362.
- [240] Wenjie Lin, Mathieu Boccard, Sihua Zhong, Degradation mechanism and stability improvement of dopant-free ZnO/LiF_x/Al electron nanocontacts in silicon heterojunction solar cells, *ACS Appl. Nano Mater.* 3 (2020) 11391–11398.
- [241] Wenjie Lin, Weiliang Wu, Zongtao Liu, Chromium trioxide hole-selective heterointerfaces for silicon solar cells, *ACS Appl. Mater. Interfaces* 10 (2018) 13645–13651.
- [242] Jingye Li, Tianyu Pan, Jilei Wang, Bilayer MoO_x/CrO_x passivating contact targeting highly stable silicon heterojunction solar cells, *ACS Appl. Mater. Interfaces* 12 (2020) 36778–36786.
- [243] Mrutyunjay Nayak, Sourav Mandal, Ashutosh Pandey, Nickel oxide hole-selective heterointerface for silicon solar cells: role of SiO_x interlayer on device performance, *Sol. RRL* 3 (2019), 1900261.
- [244] Sihua Zhong, Julie Dreon, Quentin Jeangros, Mitigating plasmonic absorption losses at rear electrodes in high-efficiency silicon solar cells using dopant-free contact stacks, *Adv. Funct. Mater.* 30 (2020), 1907840.
- [245] Xinbo Yang, Yuanbao Lin, Jiang Liu, A highly conductive titanium oxynitride electron-selective contact for efficient photovoltaic devices, *Adv. Mater.* 32 (2020), 2002608.
- [246] Weiliang Wu, Wenjie Lin, Sihua Zhong, Dopant-free back-contacted silicon solar cells with an efficiency of 22.1%, *Phys. Status Solidi RRL* 14 (2020), 1900688.
- [247] Julie Dréon, Quentin Jeangros, Jean Cattin, 23.5%-efficient silicon heterojunction silicon solar cell using molybdenum oxide as hole-selective contact, *Nano Energy* 70 (2020), 104495.
- [248] Takuya Matsui, Martin Bivour, Martin Hermle, Atomic-layer-deposited TiO_x nanolayers function as efficient hole-selective passivating contacts in silicon solar cells, *ACS Appl. Mater. Interfaces* 12 (2020) 49777–49785.
- [249] Shuangying Cao, Jingye Li, Juan Zhang, Stable MoOX-based heterointerfaces for p-Type crystalline silicon solar cells achieving 20% efficiency, *Adv. Funct. Mater.* 30 (2020) 2004367.
- [250] Francesca Menchini, Maria Luisa Grilli, Theodoros Dikonomos, Application of NiO_x thin films as p-type emitter layer in heterojunction solar cells, *Phys. Status Solidi C* 13 (2016) 1006–1010.
- [251] Xuewen Yin, Zhibo Yao, Qiang Luo, High efficiency inverted planar perovskite solar cells with solution-processed NiO_x hole contact, *ACS Appl. Mater. Interfaces* 9 (2017) 2439–2448.
- [252] Wei Chen, Yongzhen Wu, Youfeng Yue, Efficient and stable large-area perovskite solar cells with inorganic charge extraction layers, *Science* 350 (2015) 944–948.
- [253] Xinbo Yang, Klaus Weber, Ziv Hameiri, Industrially feasible, dopant-free, carrier-selective contacts for high-efficiency silicon solar cells, *Prog. Photovolt.* 25 (2017) 896–904.
- [254] Yuqiang Liu, Jie Zhang, Haihua Wu, Low-temperature synthesis TiO_x passivation layer for organic-silicon heterojunction solar cell with a high open-circuit voltage, *Nano Energy* 34 (2017) 257–263.
- [255] Firoz Khan, Seong-Ho Baek, Jae Hyun Kim, Investigation of the surface passivation mechanism through an Ag-doped Al-rich film using a solution process, *Nanoscale* 8 (2016) 1007–1014.
- [256] Yimao Wan, C. Samundsett, James Bullock, Conductive and stable magnesium oxide electron-selective contacts for efficient silicon solar cells, *Adv. Energy Mater.* 7 (2016), 1601863.
- [257] Jingnan Tong, Yimao Wan, Jie Cui, Solution-processed molybdenum oxide for hole-selective contacts on crystalline silicon solar cells, *Appl. Surf. Sci.* 423 (2017) 139–146.
- [258] Zhimin Liang, Mingze Su, Yangyang Zhou, Interaction at the silicon/transition metal oxide heterojunction interface and its effect on the photovoltaic performance, *Phys. Chem. Chem. Phys.* 41 (2015) 27409–27413.
- [259] Mark T. Greiner, Lily Chai, Michael G. Helander, Transition metal oxide work functions: the influence of cation oxidation state and oxygen vacancies, *Adv. Funct. Mater.* 22 (2012) 4557–4568.
- [260] Mathieu Boccard, Laura Ding, Priyanga Koswatta, Evaluation of metal oxides prepared by reactive sputtering as carrier-selective contacts for crystalline silicon solar cells, in: Proceedings of the IEEE 42nd Photovoltaic Specialist Conference (PVSC), 2015, pp. 1–3.
- [261] Fengxian Xie, Wallace C.H. Choy, Chuandao Wang, Low-temperature solution-processed hydrogen molybdenum and vanadium bronzes for an efficient hole-transport layer in organic electronics, *Adv. Mater.* 25 (2013) 2051–2055.
- [262] Antonios M. Anastasia Soultati, Douvas, G. Georgiadou Dimitra, Solution-processed hydrogen molybdenum bronzes as highly conductive anode interlayers in efficient organic photovoltaics, *Adv. Energy Mater.* 4 (2014), 1300896.
- [263] J. Meyer, M. Kroger, S. Hamwi, Charge generation layers comprising transition metal-oxide/organic interfaces: Electronic structure and charge generation mechanism, *Appl. Phys. Lett.* 96 (2010), 193302.
- [264] Stephen McDonnell, Angelica Azcatl, Rafik Addou, Hole contacts on transition metal dichalcogenides: interface chemistry and band alignments, *ACS Nano* 8 (2014) 6265–6267.
- [265] Rongyue Liu, Manlin Tian, Xinglong Zhang, Solution-processed composite electrodes composed of silver nanowires and aluminum-doped zinc oxide nanoparticles for thin-film solar cells applications, *Sol. Energy Mater. Sol. Cells* 174 (2018) 584–592.
- [266] Sukanta De, Thomas M. Higgins, Philip E. Lyons, Silver nanowire networks as flexible, transparent, conducting films: extremely high DC to optical conductivity ratios, *ACS Nano* 3 (2009) 1767–1774.
- [267] Jan Schmidt, Robby Peibst, R. Brendel, Surface passivation of crystalline silicon solar cells: past, present and future, in: Proceedings of the 9th International Conference on Crystalline Silicon Photovoltaics, (2019).
- [268] Bart Macco, Bas W. H. van de Loo, Wilhelmus M.M. Kessels, Atomic Layer Deposition for High-efficiency Crystalline Silicon Solar Cells // *Atomic Layer Deposition in Energy Conversion Applications (Ltd)*, John Wiley & Sons, 2017.
- [269] Keith R. McIntosh, Pietro P. Altermat, A freeware 1D emitter model for silicon solar cells, in: Proceedings of the 35th IEEE Photovoltaic Specialists Conference, (2010).
- [270] Jan Benick, Armin Richter, Ralph Müller, High-efficiency n-type HP mc silicon solar cells, *IEEE J. Photovolt.* 7 (2017) 1171–1175.
- [271] Martin A. Green, Yoshihiro Hishikawa, Ewan D. Dunlop, Solar cell efficiency tables, *Prog. Photovolt.* 27 (2019) 3–12.
- [272] Di Yan, Sieu Pheng Phang, Yimao Wan, High efficiency n-type silicon solar cells with passivating contacts based on PECVD silicon films doped by phosphorus diffusion, *Sol. Energy Mater. Sol. Cells* 193 (2019) 80–84.
- [273] Trinasolar, (<https://www.trinasolar.com/us/resources/newsroom/trina-solar-announces-new-efficiency-record-2458-efficiency-mono-crystalline>).
- [274] Jinkosolar, (<https://ir.jinkosolar.com/news-releases/news-release-details/jin-kosolar-large-area-n-type-topcon-monocrystalline-silicon>).
- [275] Yifeng Chen, Daming Chen, Chengfa Liu, Mass production of industrial tunnel oxide passivated contacts (i-TOPCon) silicon solar cells with average efficiency over 23% and modules over 345 W, *Prog. Photovolt.* 27 (2019) 827–834.

- [276] PV-CellTech 2019, (<https://celtech.solarenergyevents.com/>).
- [277] Felix Haase, Christina Hollemann, Soren Schafer, Laser contact openings for local poly-Si-metal contacts enabling 26.1%-efficient POLO-IBC solar cells, *Sol. Energy Mater. Sol. Cells* 186 (2018) 184–193.
- [278] Christian Reichel¹, Ralph Müller, Frank Feldmann¹, Influence of the transition region between p- and n-type polycrystalline silicon passivating contacts on the performance of interdigitated back contact silicon solar cells, *J. Appl. Phys.* 122 (2017), 184502.
- [279] David D. Smith, Gerly Reich, Maristel Baldrias, Silicon solar cells with total area efficiency above 25 %, in: Proceedings of the IEEE 43rd Photovoltaic Specialists Conference, (2016).
- [280] Gizem Nogay, Andrea Ingenito, Esteban Rucavado, Crystalline silicon solar cells with coannealed electron- and hole-selective SiC_x passivating contacts, *IEEE J. Photovolt.* 8 (2018) 1478–1485.
- [281] O. Schultz-Wittmann, A. Turner, B. Eggleston, High volume manufacturing of high efficiency crystalline silicon solar cells with shielded metal contacts, in: Proceedings of the 32nd European Photovoltaic Solar Energy Conference and Exhibition, 2016, pp. 456–459.
- [282] R. Peibst, Y. Larionova, S. Reiter, Industrial, screen-printed double-side contacted Polo cells, in: Proceedings of the 33rd European Photovoltaic Solar Energy Conference and Exhibition, 2017, pp. 451–454.
- [283] Armin Richter, Jan Benick, Ralph Müller, Tunnel oxide passivating electron contacts as full-area rear emitter of high-efficiency p-type silicon solar cells, *Prog. Photovolt.* 26 (2017) 579–586.
- [284] Mickael Lozach, Shota Nunomura, Role of silicon surface, polished <100> and <111> or textured, on the efficiency of double-sided TOPCon solar cells, *Prog. Photovolt.* 28 (2020) 1001–1011.
- [285] Kaifu Qiu, Manuel Pomaska, Shenghao Li, Development of conductive SiC_x:H as a new hydrogenation technique for tunnel oxide passivating contacts, *ACS Appl. Mater. Interfaces* 12 (2020) 29986–29992.
- [286] Qinjin Wang, Wangping Wu, Ningyi Yuan, Influence of SiO_x film thickness on electrical performance and efficiency of TOPCon solar cells, *Sol. Energy Mater. Sol. Cells* 208 (2020), 110423.
- [287] Chengfa Liu, Daming Chen, Yifeng Chen, Industrial TOPCon solar cells on n-type quasi-mono Si wafers with efficiencies above 23%, *Sol. Energy Mater. Sol. Cells* 215 (2020), 110690.
- [288] Mickael Lozach, Shota Nunomura, Koji Matsubara, Double-sided TOPCon solar cells on textured wafer with ALD SiO_x layer, *Sol. Energy Mater. Sol. Cells* 207 (2020), 110357.
- [289] Johannes P. Seif, Antoine Descoeuilles, Gizem Nogay, Strategies for doped nanocrystalline silicon integration in silicon heterojunction solar cells, *IEEE J. Photovolt.* 6 (2016) 1132–1140.
- [290] Kaining Ding, Manuel Pomaska, Aryak Singh, Mechanism for crystalline Si surface passivation by the combination of SiO₂ tunnel oxide and μc-SiC:H thin film, *Phys. Status Solidi RRL* 10 (2016) 233–236.
- [291] L. Mazzarella, S. Kirner, B. Stannowski, p-type microcrystalline silicon oxide emitter for silicon heterojunction solar cells allowing current densities above 40 mA/cm², *Appl. Phys. Lett.* 106 (2015), 023902.
- [292] Jan Krugener, Felix Haase, Michael Rienacker, Improvement of the SRH bulk lifetime upon formation of n-type POLO junctions for 25% efficient Si solar cells, *Sol. Energy Mater. Sol. Cells* 173 (2017) 85–91.
- [293] An.Yao Liu, Di Yan, Sieu Pheng Phang, Effective impurity gettering by phosphorus- and boron-diffused polysilicon passivating contacts for silicon solar cells, *Sol. Energy Mater. Sol. Cells* 179 (2018) 136–141.
- [294] M. Lenes, R.C. G. Naber, J.R. M. Luchies, LPCVD polysilicon passivated contacts for different solar cell concepts, in: Proceedings of the 6th SiliconPV Conference, (2016).
- [295] H. Steinkeper, F. Feldmann, M. Bivour, Numerical simulation of carrier-selective electron contacts featuring tunnel oxides, *IEEE J. Photovolt.* 5 (2015) 1348–1356.
- [296] H.C. Card, E.H. Rhoderick, Studies of tunnel MOS diodes I. Interface effects in silicon Schottky diodes, *J. Phys. D: Appl. Phys.* 4 (1997) 1589–1601.
- [297] I.R.C. Post, P. Ashburn, G.R. Wolstenholme, Polysilicon emitters for bipolar transistors: a review and re-evaluation of theory and experiment, *IEEE Trans. Electron Devices* 39 (1992) 1717–1731.
- [298] A. Martin Green, Effects of pinholes, oxide traps, and surface states on MIS solar cells, *Appl. Phys. Lett.* 33 (1978) 178–180.
- [299] M.B. Rowlandson, N.G. Tarr, A true polysilicon emitter transistor, *IEEE Electron Device Lett.* 6 (1985) 288–290.
- [300] Anamaria Moldovan, Frank Feldmann, Martin Zimmer, Tunnel oxide passivated carrier-selective contacts based on ultra-thin SiO₂ layers, *Sol. Energy Mater. Sol. Cells* 142 (2015) 123–127.
- [301] Bill Nemeth, David L. Young, Matthew R. Page, Polycrystalline silicon passivated tunneling contacts for high efficiency silicon solar cells, *J. Mater. Res.* 31 (2016) 671–681.
- [302] J.A. Cooper Jr., R.J. Schwartz, Electrical characteristics of the SiO₂-Si interface near midgap and in weak inversion, *Solid-State Electron.* 17 (1974) 641–654.
- [303] Yoshiko Kato, Hidekuni Takao, Kazuaki Sawada, Improvement of metal-oxide semiconductor interface characteristics in complementary metal-oxide semiconductor on Si(111) by combination of fluorine implantation and long-time hydrogen annealing, *Jpn. J. Appl. Phys.* 46 (2006) L108–L110.
- [304] Frank Feldmann, Ralph Müller, Christian Reichel, Ion implantation into amorphous Si layers to form carrier-selective contacts for Si solar cells, *Phys. Status Solidi RRL* 8 (2014) 767–770.
- [305] A.G. Aberle, S. Glunz, W. Warta, Impact of illumination level and oxide parameters on Shockley-Read-Hall recombination at the Si-SiO₂ interface, *J. Appl. Phys.* 71 (1992) 4422–4431.
- [306] M. Dutoit, F. Sollberger, Lateral polysilicon p-n diodes, *J. Electrochem. Soc.* 125 (1978) 1648–1651.
- [307] A.K. Ghosh, C. Fishman, T. Feng, Theory of the electrical and photovoltaic properties of polycrystalline silicon, *J. Appl. Phys.* 51 (1980) 446–454.
- [308] Kyle Preston, Po Dong, Bradley Schmidt, High-speed all-optical modulation using polycrystalline silicon microring resonators, *Appl. Phys. Lett.* 92 (2008), 151104.
- [309] Sungjin Choi, Ohmin Kwon, Kwan Hong Min, Formation and suppression of hydrogen blisters in tunnelling oxide passivating contact for crystalline silicon solar cells, *Sci. Rep.* 10 (2020) 9672.
- [310] Benjamin Grubel, Gisela Cimotti, Varun Arya, Plated Ni/Cu/Ag for TOPCon solar cell metallization, in: Proceedings of the 36th European Photovoltaic Solar Energy Conference, 2019, pp. 1–5.
- [311] Tobias F. Wietler, Byungsul Min, Sina Reiter, High temperature annealing of ZnO: Al on passivating POLO junctions: impact on transparency, conductivity, junction passivation, and interface stability, *IEEE J. Photovolt.* 9 (2019) 89–96.
- [312] Frank Feldmann, Massimo Nicolai, Ralph Müller, Optical and electrical characterization of poly-Si/SiO_x contacts and their implications on solar cell design, *Energy Procedia* 124 (2017) 31–37.
- [313] Guangtao Yang, Peiqing Guo, Paul Proel, Poly-crystalline silicon-oxide films as carrier-selective passivating contacts for c-Si solar cells, *Appl. Phys. Lett.* 112 (2018), 193904.
- [314] Jörg Schubé, Leonhard Tutsch, Tobias Fellmeth, Low-resistivity screen-printed contacts on indium tin oxide layers for silicon solar cells with passivating contacts, *IEEE J. Photovolt.* 8 (2018) 1208–1214.
- [315] Peter J. Cousins, David D. Smith, Hsin-Chiao Luan, Generation 3: Improved performance at lower cost, in: Proceedings of the 35th IEEE Photovoltaic Specialists Conference, 2010, pp. 275–278.
- [316] Felix Haase, Christina Hollemann, Soren Schafer, Transferring the record p-type Si POLO-IBC cell technology towards an industrial level, in: Proceedings of the IEEE 46th Photovoltaic Specialists Conference (PVSC), (2019).
- [317] Frank Feldmann, T. Fellmeth, Bernd Steinhäuser, Large area TOPCon cells realized by a PECVD tube process, in: Proceedings of the 36th European Photovoltaic Solar Energy Conference and Exhibition, (2019).
- [318] Zhe Rui, Yuheng Zeng, Xueqi Guo, On the passivation mechanism of poly-silicon and thin silicon oxide on crystal silicon wafers, *Sol. Energy* 194 (2019) 18–26.
- [319] ISFH, (<https://isfh.de/en/forschung/photovoltaik/arbeitsgruppen/emergente-zelltechnologien/>).
- [320] Louise C. Hirst, Nicholas J. Ekins-Daukes, Fundamental losses in solar cells, *Prog. Photovolt.* 19 (2011) 286–293.
- [321] E. Jackson, Areas for improvement of the semiconductor solar energy converter, in: Proceedings of the Transactions of the Conference on the Use of Solar Energy, 1995, pp. 122–126.
- [322] Colin D. Bailie, M.D. McGehee, High-efficiency tandem perovskite solar cells, *MRS Bull.* 40 (2015) 681–685.
- [323] Arvind Shah, H. Schade, Milan Vanecek, Thin-film silicon solar cell technology, *Prog. Photovolt. Res. Appl.* 12 (2004) 2–3.
- [324] Arvind Shah, P. Torres, R. Tscharner, Photovoltaic technology: the case for thin-film solar cells, *Science* 285 (1999) 692–698.
- [325] C.H. Henry, Limiting efficiencies of ideal single and multiple energy gap terrestrial solar cells, *J. Appl. Phys.* 51 (1980) 4494–4500.
- [326] Zhengshan Jason Yu, Mehdi Leilaoui, Zachary Holman, Selecting tandem partners for silicon solar cells, *Nat. Energy* 1 (2016) 16137.
- [327] Giles E. Eperon, Maximilian T. Hörranter, Henry J. Snaith, Metal halide perovskite tandem and multiple-junction photovoltaics, *Nat. Rev. Chem.* 1 (2017) 0095.
- [328] Jérémie Werner, Bjoern Niesen, Christophe Ballif, Perovskite/silicon tandem solar cells: marriage of convenience or true love story? – an overview, *Adv. Mater. Interface* 5 (2018), 1700731.
- [329] T. Maximilian, Hörranter, J. Snaith Henry, Predicting and optimising the energy yield of perovskite-on-silicon tandem solar cells under real world conditions, *Energy Environ. Sci.* 10 (2017) 1983–1993.
- [330] Ziyu Wang, Zhaoning Song, Yanfa Yan, Perovskite—A perfect top cell for tandem devices to break the S-Q limit, *Adv. Sci.* 6 (2019), 1801704.
- [331] Andreas Pusch, Phoebe Pearce, Nicholas J. Ekins-Daukes, Analytical expressions for the efficiency limits of radiatively coupled tandem solar cells, *IEEE J. Photovolt.* 9 (2019) 679–687.
- [332] Rui Sheng, Anita W.Y. Ho-Bailie, Shujuan Huang, Four-terminal tandem solar cells using CH₃NH₃PbBr₃ by spectrum splitting, *J. Phys. Chem. Lett.* 6 (2015) 3931–3934.
- [333] T. Nagashima, K. Okumura, K. Murata, Three-terminal tandem solar cells with a back-contact type bottom cell, in: Proceedings of the Conference Record of the Twenty-Eighth IEEE Photovoltaic Specialists Conference, 2000.
- [334] S.P. Bremner, M.Y. Levy, C.B. Honsberg, Analysis of tandem solar cell efficiencies under AM1.5G spectrum using a rapid flux calculation method, *Prog. Photovolt.* 16 (2008) 225–233.
- [335] Niraj N. Lal, Yasmina Dkhissi, Wei Li, Perovskite tandem solar cells, *Advanced Energy Materials* 7 (2017) 1602761.
- [336] William Shockley, Hans J. Queisser, Detail. Balance Limit Effic. PN Junction Sol. Cells, 32, 1961, p. 510.
- [337] Yoshiaki Nakao, Tamejiro Hiyama, Silicon-based cross-coupling reaction: an environmentally benign version, *Chem. Soc. Rev.* 40 (2011) 4893–4901.

- [338] D.M. Chapin, C.S. Fuller, G.L. Pearson, A new silicon p-n junction photocell for converting solar radiation into electrical power, *J. Appl. Phys.* 25 (1954) 676–677.
- [339] Armin Richter, Martin Hermle, Stefan W. Glunz, Reassessment of the limiting efficiency for crystalline silicon solar cells, *IEEE J. Photovolt.* 3 (2013) 1184–1191.
- [340] L.L. Yan, C. Han, B. Shi, A review on the crystalline silicon bottom cell for monolithic perovskite/silicon tandem solar cells, *Mater. Today Nano* 7 (2019), 100045.
- [341] Heping Shen, Daniel Walter, Yiliang Wu, Monolithic perovskite/Si tandem solar cells: pathways to over 30% efficiency, *Adv. Energy Mater.* 10 (2020), 1902840.
- [342] Masafumi Yamaguchi, Yoshiro Ohmachi, Takahiko Ohbara, GaAs solar cells grown on Si substrates for space use, *Prog. Photovolt.: Res. Appl.* 9 (2001) 191–201.
- [343] T. Soga, T. Kato, M. Yang, High efficiency AlGaAs/Si monolithic tandem solar cell grown by metalorganic chemical vapor deposition, *J. Appl. Phys.* 78 (1995) 4196–4199.
- [344] Katsuaki Tanabe, Katsuyuki Watanabe, Yasuhiko Arakawa, III-V/Si hybrid photonic devices by direct fusion bonding, *Sci. Rep.* 2 (2012) 349.
- [345] Frank Dimroth, Tobias Roesener, Stephanie Essig, Comparison of direct growth and wafer bonding for the fabrication of GaInP/GaAs dual-junction solar cells on silicon, *IEEE J. Photovolt.* 4 (2014) 620–625.
- [346] Stephanie Essig, Dimroth Frank, Fast atom beam activated wafer bonds between n-Si and n-GaAs with low resistance, *ECS J. Solid State Sci. Technol.* 2 (2013) 178–181.
- [347] Jingfeng Yang, Zhilin Peng, Dan Cheong, Fabrication of high-efficiency III-V on silicon multijunction solar cells by direct metal interconnect, *IEEE J. Photovolt.* 4 (2014) 1149–1155.
- [348] Tyler J. Grassman, Daniel J. Chmielewski, Santino D. Carnevale, GaAs_{0.75}Po_{0.25}/Si dual-junction solar cells grown by MBE and MOCVD, *IEEE J. Photovolt.* 6 (2015) 326–331.
- [349] Maoqing Yao, Sen Cong, Shermin Arab, Tandem solar cells using GaAs nanowires on Si: design, fabrication, and observation of voltage addition, *Nano Lett.* 15 (2015) 7217–7224.
- [350] Naoteru Shigekawa, Jianbo Liang, Ryusuke Onitsuka, Current–voltage and spectral-response characteristics of surface-activated-bonding-based InGaP/GaAs/Si hybrid triple-junction cells, *Jpn. J. Appl. Phys.* 54 (2015), 08KE03.
- [351] Hidenori Mizuno, Kikuo Makita, Takeshi Tayagaki, A "smart stack" triple-junction cell consisting of InGaP/GaAs and crystalline Si, in: Proceedings of the IEEE 44th Photovoltaic Specialists Conference (PVSC), (2017).
- [352] Stephanie Essig, Myles A. Steiner, Christophe Alleb  , Realization of GaInP/Si dual-junction solar cells with 29.8% 1-sun efficiency, *IEEE J. Photovolt.* 6 (2016) 1012–1019.
- [353] Romain Cariou, Jan Benick, Paul Beutel, Monolithic two-terminal III-V/Si triple-junction solar cells with 30.2% efficiency under 1-sun AM1.5g, *IEEE J. Photovolt.* 7 (2017) 367–373.
- [354] Kevin Nay Yaung, Michelle Vaisman, Jordan Lang, GaAsP solar cells on GaP/Si with low threading dislocation density, *Appl. Phys. Lett.* 109 (2016), 032107.
- [355] Tatsuya Takamoto, Hiroyuki Juso, Kohsuke Ueda, IMM triple-junction solar cells and modules optimized for space and terrestrial conditions, in: Proceedings of the IEEE 44th Photovoltaic Specialist Conference (PVSC), (2017).
- [356] Romain Cariou, Jan Benick, Paul Beutel, Wafer bonded III-V on silicon multi-junction cell with efficiency beyond 31%, in: Proceedings of the IEEE 44th Photovoltaic Specialist Conference (PVSC), (2017).
- [357] Stephanie Essig, Christophe Alleb  , Timothy Remo, Raising the one-sun conversion efficiency of III-V/Si solar cells to 32.8% for two junctions and 35.9% for three junctions, *Nat. Energy* 2 (2017) 17144.
- [358] Masafumi Yamaguchi, Kan-Hua Lee, Kenji Araki, A review of recent progress in heterogeneous silicon tandem solar cells, *J. Phys. D: Appl. Phys.* 51 (2018), 133002.
- [359] Romain Cariou, Jan Benick, Frank Feldmann, III-V-on-silicon solar cells reaching 33% photoconversion efficiency in two-terminal configuration, *Nat. Energy* 3 (2018) 326–333.
- [360] Markus Feifel, David Lackner, Jens Ohlmann, Direct growth of a GaInP/GaAs/Si triple-junction solar cell with 22.3% AM1.5g efficiency, *Sol. RRL* 3 (2019), 1900313.
- [361] David Lackner, Oliver Hohn, Ralph Muller, Two-terminal direct wafer-bonded GaInP/AlGaAs//Si triple-junction solar cell with AM1.5g efficiency of 34.1%, *Sol. RRL* 4 (2020), 2000210.
- [362] Kikuo Makita, Hidenori Mizuno, Takeshi Tayagaki, III-V//Si multijunction solar cells with 30% efficiency using smart stack technology with Pd nanoparticle array, *Prog. Photovolt.* 28 (2020) 16–24.
- [363] Niraj N. Lal, Thomas P. White, Kylie R. Catchpole, Optics and light trapping for tandem solar cells on silicon, *IEEE J. Photovolt.* 4 (2014) 1380–1386.
- [364] J.F. Geisz, D.J. Friedman, III-N-V semiconductors for solar photovoltaic applications, *Semicond. Sci. Technol.* 17 (2002) 769–777.
- [365] Stephanie Essig, Jan Benick, Michael Schachtner, Wafer-bonded GaInP/GaAs//Si solar cells with 30% efficiency under concentrated sunlight, *IEEE J. Photovolt.* 5 (2015) 977–981.
- [366] Ibraheem Almansouri, Anita Ho-Baillie, Stephen P. Bremner, Supercharging silicon solar cell performance by means of multijunction concept, *IEEE J. Photovolt.* 5 (2015) 968–976.
- [367] Nikhil Jain, Mantu K. Hudait, III-V multijunction solar cell integration with silicon: present status, challenges and future outlook, *Energy Harvest. Syst.* 1 (2014) 121–145.
- [368] Yu.B. Bolkhovityanov, O.P. Pchelyakov, GaAs epitaxy on Si substrates: modern status of research and engineering, *Phys. -Uspekhi* 51 (2008) 437–456.
- [369] Masahiro Akiyama, Yoshihiro Kawarada, Katsuzo Kaminiishi, Growth of single domain GaAs layer on (100)-oriented Si substrate by MOCVD, *Jpn. J. Appl. Phys.* 23 (1984) L843–L845.
- [370] Masafumi Yamaguchi, Masami Tachikawa, Yoshio Itoh, Thermal annealing effects of defect reduction in GaAs on Si substrates, *J. Appl. Phys.* 68 (1990) 4518–4522.
- [371] Hiroshi Okamoto, Yoshiro Watanabe, Yoshiaki Kadota, Dislocation reduction in GaAs on Si by thermal cycles and InGaAs/GaAs strained-layer superlattices, *Jpn. J. Appl. Phys.* 26 (1987) L1950–L1952.
- [372] Yoshiro Watanabe, Yoshiaki Kadota, Hiroshi Okamoto, Structural properties of GaAs-on-Si in InGaAs/GaAs strained-layer superlattice, *J. Cryst. Growth* 93 (1988) 459–465.
- [373] Jens Ohlmann, Markus Feifel, Thomas Rachow, Influence of metal–organic vapor phase epitaxy reactor environment on the silicon bulk lifetime, *IEEE J. Photovolt.* 6 (2016) 1668–1672.
- [374] T. Soga, T. Kato, M. Yang, High efficiency AlGaAs/Si monolithic tandem solar cell grown by metalorganic chemical vapor deposition, *J. Appl. Phys.* 78 (1995) 4196–4199.
- [375] Markus Feifel, Jens Ohlmann, Jan Benick, Direct growth of III-V/silicon triple-junction solar cells with 19.7% efficiency, *IEEE J. Photovolt.* 8 (2018) 1590–1595.
- [376] Fraunhofer ISE, (<https://www.ise.fraunhofer.de/en/press-media/press-releases/2019/photovoltaic-tri-cell-tandem-solar-cells-record-efficiency-for-silicon-based-multi-junction-solar-cell.html>).
- [377] Karen Derendorf, Stephanie Essig, Eduard Oliva, Fabrication of GaInP/GaAs//Si solar cells by surface activated direct wafer bonding, *IEEE J. Photovolt.* 3 (2013) 1423–1428.
- [378] Hidenori Mizuno, Kikuo Makita, Takeshi Tayagaki, High-efficiency III-V/Si tandem solar cells enabled by the Pd nanoparticle array-mediated "smart stack" approach, *Appl. Phys. Express* 10 (2017), 072301.
- [379] Reza Asadpoura, Raghu V.K. Chavalia, M. Ryyan Khan, Bifacial Si heterojunction-perovskite organic-inorganic tandem to produce highly efficient ($\eta^*_{\text{T}} \sim 33\%$) solar cell, *Appl. Phys. Lett.* 106 (2015), 243902.
- [380] Colin D. Bailie, M. Greyson Christoforo, Jonathan P. Maiola, Semi-transparent perovskite solar cells for tandems with silicon and CIGS, *Energy Environ. Sci.* 8 (2015) 956–963.
- [381] J  r  mie Werner, Guy Dubuis, Arnaud Walter, Sputtered rear electrode with broadband transparency for perovskite solar cells, *Sol. Energy Mater. Sol. Cells* 141 (2015) 407–413.
- [382] David P. McMeekin, Golnaz Sadoughi, Waqas Rehman, A mixed-cation lead mixed-halide perovskite absorber for tandem solar cells, *Science* 351 (2016) 151–155.
- [383] The Duong, Niraj Lal, Dale Grant, Semitransparent perovskite solar cell with sputtered front and rear electrodes for a four-terminal tandem, *IEEE J. Photovolt.* 6 (2016) 679–687.
- [384] Bo Chen, Yang Bai, Zhengshan Yu, Efficient semitransparent perovskite solar cells for 23.0%-efficiency perovskite/silicon four-terminal tandem cells, *Adv. Energy Mater.* 6 (2016), 1601128.
- [385] J  r  mie Werner, Loris Barraud, Arnaud Walter, Efficient near-infrared-transparent perovskite solar cells enabling direct comparison of 4-terminal and monolithic perovskite/silicon tandem cells, *ACS Energy Lett.* 1 (2016) 474–480.
- [386] Jun Peng, The Duong, Xianzhong Zhou, Efficient indium-doped TiO_x electron transport layers for high-performance perovskite solar cells and perovskite-silicon tandems, *Adv. Energy Mater.* 7 (2017), 1601768.
- [387] The Duong, Yiliang Wu, Heping Shen, Rubidium multication perovskite with optimized bandgap for perovskite-silicon tandem with over 26% efficiency, *Adv. Energy Mater.* 7 (2017), 1700228.
- [388] Manoj Jaysankar, Weiming Qiu, Maarten van Eerden, Four-terminal perovskite/silicon multijunction solar modules, *Adv. Energy Mater.* 7 (2017), 1602807.
- [389] Jonathan P. Maiola, Colin D. Bailie, Eric C. Johlin, A 2-terminal perovskite/silicon multijunction solar cell enabled by a silicon tunnel junction, *Appl. Phys. Lett.* 106 (2015), 121105.
- [390] Steve Albrecht, Michael Saliba, Juan-Pablo Corre-Baena, Monolithic perovskite/silicon-heterojunction tandem solar cells processed at low temperature, *Energy Environ. Sci.* 9 (2015) 81–88.
- [391] J  r  mie Werner, Ching-Hsun Weng, Arnaud Walter, Efficient monolithic perovskite/silicon tandem solar cell with cell area >1 cm², *J. Phys. Chem. Lett.* 7 (2016) 161–166.
- [392] J  r  mie Werner, Arnaud Walter, Esteban Rucaido, Zinc tin oxide as high-temperature stable recombination layer for mesoscopic perovskite/silicon monolithic tandem solar cells, *Appl. Phys. Lett.* 109 (2016), 233902.
- [393] Kevin A. Bush, Axel F. Palmstrom, Zhengshan J. Yu, 23.6%-efficient monolithic perovskite/silicon tandem solar cells with improved stability, *Nat. Energy* 2 (2017) 17009, 227.
- [394] Florent Sahli, J  r  mie Werner Brett, A. Kamino, Improv. Opt. Monolith. perovskite/Silicon Tandem Sol. Cells a nanocrystalline Silicon Recomb. Junction 2017 1701609.
- [395] G. Nogay, F. Sahli, J. Werner, 25.1%-efficient monolithic perovskite/silicon tandem solar cell based on a p-type monocrystalline textured silicon wafer and high-temperature passivating contacts, *ACS Energy Lett.* 4 (2019) 844–845.
- [396] Florent Sahli, J  r  mie Werner, Brett A. Kamino, Fully textured monolithic perovskite/silicon tandem solar cells with 25.2% power conversion efficiency, *Nat. Mater.* 17 (2018) 820–826.

- [397] Rundong Fan, Ning Zhou, Lin Zhang, Toward full solution processed perovskite/Si monolithic tandem solar device with PCE exceeding 20%, *Sol. RRL* 1 (2017), 1700149.
- [398] Zhiwen Qiu, Ziqi Xu, Nengxu Li, Monolithic perovskite/Si tandem solar cells exceeding 22% efficiency via optimizing top cell absorber, *Nano Energy* 53 (2018) 798–807.
- [399] Fuhua Hou, Lingling Yan, Biao Shi, Monolithic perovskite/silicon-heterojunction tandem solar cells with open-circuit voltage of over 1.8 V, *ACS Appl. Energy Mater.* 2 (2019) 243–249.
- [400] Yiliang Wu, Di Yan, Jun Peng, Monolithic perovskite/silicon-homojunction tandem solar cell with over 22% efficiency, *Energy Environ. Sci.* 10 (2017) 2472–2479.
- [401] Kevin A. Bush, Salman Manzoor, Kyle Frohma, Minimizing current and voltage losses to reach 25% efficient monolithic two-terminal perovskite–silicon tandem solar cells, *ACS Energy Lett.* 3 (2018) 2173–2180.
- [402] Luana Mazzarella, Yen-Hung Lin, Simon Kirner, Infrared light management using a nanocrystalline silicon oxide interlayer in monolithic perovskite/silicon heterojunction tandem solar cells with efficiency above 25%, *Adv. Energy Mater.* 9 (2019), 1803241.
- [403] Bo Chen, Zhengshan Yu, Kong Liu, Grain engineering for perovskite/silicon monolithic tandem solar cells with efficiency of 25.4%, *Joule* 3 (2019) 177–190.
- [404] Marko Jošt, Eike Könen, Anna Belen Morales-Vilches, Textured interfaces in monolithic perovskite/silicon tandem solar cells: advanced light management for improved efficiency and energy yield, *Energy Environ. Sci.* 11 (2018) 3511–3523.
- [405] Eike Könen, Marko Jošt, Anna Belen Morales-Vilches, Highly efficient monolithic perovskite silicon tandem solar cells: analyzing the influence of current mismatch on device performance, *Sustain. Energy Fuels* 3 (2019) 1995–2005.
- [406] Jianghui Zheng, Cho Fai Jonathan Lau, Hamid Mehrvarz, Large area efficient interface layer free monolithic perovskite/homo-junction-silicon tandem solar cell with over 20% efficiency, *Energy Environ. Sci.* 11 (2018) 2432–2443.
- [407] Jianghui Zheng, Hamid Mehrvarz, Fa-Jun Ma, 21.8% efficient monolithic perovskite/homo-junction-silicon tandem solar cell on 16 cm², *ACS Energy Lett.* 3 (2018) 2299–2300.
- [408] Heping Shen, Stefan T. Omelchenko, Daniel A. Jacobs, In situ recombination junction between p-Si and TiO₂ enables high-efficiency monolithic perovskite/Si tandem cells, *Sci. Adv.* 4 (2018) 12.
- [409] Philipp Löper, Soo-Jin Moon, S. I. Martín de Nicolas, Organic–inorganic halide perovskite/crystalline silicon four-terminal tandem solar cells, *Phys. Chem. Chem. Phys.* 17 (2015) 1619–1629.
- [410] Manoj Jaysankar, Benedicto A.L. Raul, Joao Bastos, Minimizing voltage loss in wide-bandgap perovskites for tandem solar cells, *ACS Energy Lett.* 4 (2019) 259–264.
- [411] Kevin A. Bush, Colin D. Bailie, Ye Chen, Thermal and environmental stability of semi-transparent perovskite solar cells for tandems enabled by a solution-processed nanoparticle buffer layer and sputtered ITO electrode, *Adv. Mater.* 28 (2016) 3937–3943.
- [412] Felix Lang, Marc A. Gluba, Steve Albrecht, Perovskite solar cells with large-area CVD-graphene for tandem solar cells, *J. Phys. Chem. Lett.* 6 (2015) 2745–2750.
- [413] Hisashi Uzu, Mitsuhiro Ichikawa, Masashi Hino, High efficiency solar cells combining a perovskite and a silicon heterojunction solar cells via an optical splitting system, *Appl. Phys. Lett.* 106 (2015), 013506.
- [414] Patricia S.C. Schulze, Alexander J. Bett, Martin Bivour, 25.1% high-efficiency monolithic perovskite silicon tandem solar cell with a high bandgap perovskite absorber, *Sol. RRL* 4 (2020), 2000152.
- [415] Alexander J. Bett, Patricia S.C. Schulze, Kristina M. Winkler, Two-terminal perovskite silicon tandem solar cells with a high-bandgap perovskite absorber enabling voltages over 1.8 V, *Prog. Photovolt.* 28 (2020) 99–110.
- [416] César Omar Ramírez Quiroz, George D. Spyropoulos, Michael Salvador, Interface molecular engineering for laminated monolithic perovskite/silicon tandem solar cells with 80.4% fill factor, *Adv. Funct. Mater.* 29 (2019), 1901476.
- [417] Woojun Yoon, David Scheiman, Young WooOk, Sputtered indium tin oxide as a recombination layer formed on the tunnel oxide/poly-Si passivating contact enabling the potential of efficient monolithic perovskite/Si tandem solar cells, *Sol. Energy Mater. Sol. Cells* 210 (2020), 110482.
- [418] HZB, (<https://www.pv-magazine.com/2020/01/30/tandems-cells-approaching-g-30-efficiency/>).
- [419] Michele De Bastiani, Alessandro J. Mirabelli, Yi Hou, Efficient bifacial monolithic perovskite/silicon tandem solar cells via bandgap engineering, *Nat. Energy* 6 (2021) 167–175.
- [420] Erkan Aydin, Thomas G. Allen, Michele De Bastiani, Interplay between temperature and bandgap energies on the outdoor performance of perovskite/silicon tandem solar cells, *Nat. Energy* 5 (2020) 851–859.
- [421] Mingyu Jeong, In. Woo Choi, Eun Min Go, Stable perovskite solar cells with efficiency exceeding 24.8% and 0.3-V voltage loss, *Science* 369 (2020) 1615–1620.
- [422] Michael Saliba, Taisuke Matsui, Konrad Domanski, Incorporation of rubidium cations into perovskite solar cells improves photovoltaic performance, *Science* 354 (2016) 6309, 209.
- [423] Spencer T. Williams, Adharsh Rajagopal, Chu-Chen Chueh, Current challenges and prospective research for upscaling hybrid perovskite photovoltaics, *J. Phys. Chem. Lett.* 7 (2016) 811–819.
- [424] Dávid Forgács, Lidón Gil-Escrí, Daniel Pérez-Del-Rey, Efficient monolithic perovskite/perovskite tandem solar cells, *Adv. Energy Mater.* 7 (2017), 1602121.
- [425] Matthew R. Leyden, Yan Jiang, Yabing Qi, Chemical vapor deposition grown formamidinium perovskite solar modules with high steady state power and thermal stability, *J. Mater. Chem. A* 4 (2016) 13125–13132.
- [426] Jong H. Kim, Chu-Chen Chueh, Spencer T. Williams, Room-temperature, solution-processable organic electron extraction layer for high-performance planar heterojunction perovskite solar cells, *Nanoscale* 7 (2015) 17343–17349.
- [427] Chen Tao, Stefanie Neutzner, Letizia Coella, 17.6% stabilized efficiency in low-temperature processed planar perovskite solar cells, *Energy Environ. Sci.* 8 (2015) 2365–2370.
- [428] Elham Halvani Anaraki, Ahmad Kermanpur, Ludmilla Steier, Highly efficient and stable planar perovskite solar cells by solution-processed tin oxide, *Energy Environ. Sci.* 9 (2016) 3128–3134.
- [429] Nguyen Ha Khoa, Yuki Tanaka, Wei Peng Goh, A solution processed Ag-nanowires/C₆₀ composite top electrode for efficient and translucent perovskite solar cells, *Sol. Energy* 196 (2020) 582–588.
- [430] Pramila Patil, Dilpreet Singh Mann, Umesh T. Nakate, Hybrid interfacial ETL engineering using PCBM-Sn₂ for high-performance p-i-n structured planar perovskite solar cells, *Chem. Eng. J.* 397 (2020), 125504.
- [431] Monica Morales-Masis, Staafana De Wolf, Rachel Woods-Robinson, Transparent electrodes for efficient optoelectronics, *Adv. Electron. Mater.* 3 (2017), 1600529.
- [432] Fan Fu, Thomas Feurer, Timo Jäger, Low-temperature-processed efficient semi-transparent planar perovskite solar cells for bifacial and tandem applications, *Nat. Commun.* 6 (2015) 8932.
- [433] Yan-Gang Bi, Yue Feng Liu, Xu-Lin Zhang, Ultrathin metal films as the transparent electrode in ITO-free organic optoelectronic devices, *Adv. Opt. Mater.* 7 (2019), 1800778.
- [434] Yang (Michael) Yang, Qi Che, Yao-Tsung Hsieh, Multilayer transparent top electrode for solution processed perovskite/Cu(In,Ga)(Se,S)₂ four terminal tandem solar cells, *ACS Nano* 9 (2015) 7714–7721.
- [435] Fei Guo, Hamed Azimi, Yi Hou, High-performance semitransparent perovskite solar cells with solution-processed silver nanowires as top electrodes, *Nanoscale* 7 (2015) 1642–1649.
- [436] Jihoon Ahn, Hyewon Hwang, Sunho Jeong, Metal-nanowire-electrode-based perovskite solar cells: challenging issues and new opportunities, *Adv. Energy Mater.* 7 (2017), 1602751.
- [437] F. Behrouznejad, S. Shahbazi, N. Taghavinia, A study on utilizing different metals as the back contact of CH₃NH₃PbI₃ perovskite solar cells, *J. Mater. Chem. A* 4 (2016) 13488–13498.
- [438] You Peng, Zhike Liu, Qidong Tai, Efficient semitransparent perovskite solar cells with graphene electrodes, *Adv. Mater.* 27 (2015) 3632, 8.
- [439] Felix Lang, Marc A. Gluba, Steve Albrecht, In situ graphene doping as a route toward efficient perovskite tandem solar cells, *Phys. Status Solidi A* 213 (2016) 1989–1996.
- [440] Miha Filipič, Philipp Löper, Bjoern Niesen, CH₃NH₃PbI₃ perovskite / silicon tandem solar cells: characterization based optical simulations, *Opt. Express* 23 (2015) 263–278.
- [441] Cristina Momblona, Lidón Gil-Escrí, Enrico Bandiello, Efficient vacuum deposited p-i-n and n-i-p perovskite solar cells employing doped charge transport layers, *Energy Environ. Sci.* 9 (2016) 3456–3463.
- [442] Rebecca A. Belisle, Pratham Jain, Rohit Prasanna, Minimal effect of the hole-transport material ionization potential on the open-circuit voltage of perovskite solar cells, *ACS Energy Lett.* 1 (2016) 556–560.
- [443] Jae Woong Jung, Chu-Chen Chueh, Alex K.Y. Jen, High-performance semitransparent perovskite solar cells with 10% power conversion efficiency and 25% average visible transmittance based on transparent CuSCN as the hole-transporting material, *Adv. Energy Mater.* 5 (2015) 486.
- [444] Jiewei Liu, Sandeep K. Pathak, Nobuya Sakai, Copper thiocyanate: an efficient and affordable hole transporting material, toward thermally stable perovskite solar cells, *Adv. Mater. Interfaces* 3 (2016) 1600571.
- [445] Weijun Ke, Dewei Zhao, Corey R. Grice, Efficient planar perovskite solar cells using room-temperature vacuum-processed C₆₀ electron selective layers, *J. Mater. Chem. A* 3 (2015) 17971–17976.
- [446] Daniel J. Slotcavage, Hemamala I. Karunadasa, Michael D. McGehee, Light-induced phase segregation in halide-perovskite absorbers, *ACS Energy Lett.* 1 (2016) 1199–1205.
- [447] Michael Saliba, Taisuke Matsui, Konrad Domanski, Incorporation of rubidium cations into perovskite solar cells improves photovoltaic performance, *Science* 354 (2016) 206–209.
- [448] Michael Saliba, Taisuke Matsui, Ji-Youn Seo, Cesium-containing triple cation perovskite solar cells: improved stability, reproducibility and high efficiency, *Energy Environ. Sci.* 9 (2016) 1989–1997.
- [449] Kevin A. Bush, Kyle Frohma, Rohit Prasanna, Compositional engineering for efficient wide band gap perovskites with improved stability to photoinduced phase segregation, *ACS Energy Lett.* 3 (2018) 428–435.
- [450] E.L. Unger, L. Kegelmann, K. Suchan, Roadmap and roadblocks for the band gap tunability of metal halide perovskites, *J. Mater. Chem. A* 5 (2017) 11401–11409.
- [451] Yuze Lin, Bo Chen, Fuwen Zhao, Matching charge extraction contact for wide-bandgap perovskite solar cells, *Adv. Mater.* 29 (2017) 1700607.
- [452] Yue Yu, Changlei Wang, Corey R. Grice, Synergistic effects of lead thiocyanate additive and solvent annealing on the performance of wide-bandgap perovskite solar cells, *ACS Energy Lett.* 2 (2017) 1177–1182.
- [453] Yang Zhou, Feng Wang, Yu Cao, Benzylamine-treated wide-bandgap perovskite with high thermal-photostability and photovoltaic performance, *Adv. Energy Mater.* 7 (2017), 1701048.

- [454] Zhiping Wang, Qianqian Lin, Francis P. Chmiel, Efficient ambient-air-stable solar cells with 2D–3D heterostructured butylammonium-caesium-formamidinium lead halide perovskites, *Nat. Energy* 2 (2017) 17135.
- [455] Junghwan Kim, Maksud I. Saidaminov, Hairen Tan, Amide-catalyzed phase-selective crystallization reduces defect density in wide-bandgap perovskites, *Adv. Mater.* 30 (2018), 1706275.
- [456] Mojtaba Abdi-Jalebi, Zahra Andaji-Garmaroudi, Stefania Cacovich, Maximizing and stabilizing luminescence from halide perovskites with potassium passivation, *Nature* 555 (2018) 497–501.
- [457] Saba Gharibzadeh, Bahram Abdollahi Nejand, Marius Jakoby, Perovskite solar cells: record open-circuit voltage wide-bandgap perovskite solar cells utilizing 2D/3D perovskite heterostructure, *Adv. Energy Mater.* 9 (2019), 1970079.
- [458] Qianqian Lin, Ardalan Armin, Ravi Chandra Raju Nagiri, Electro-optics of perovskite solar cells, *Nat. Photonics* 9 (2015) 106–112.
- [459] Arman Mahboubi Soufiani, Zhuo Yang, Trevor Young, Impact of microstructure on the electron-hole interaction in lead halide perovskites, *Energy Environ. Sci.* 10 (2017) 1358–1366.
- [460] Zhaoning Song, Jérémie Werner, Suneth C. Watthage, Imaging the spatial evolution of degradation in perovskite/Si tandem solar cells after exposure to humid air, *IEEE J. Photovolt.* 7 (2017) 1563–1568.
- [461] Rudi Santbergen, Ryota Mishima, Tomomi Meguro, Minimizing optical losses in monolithic perovskite/c-Si tandem solar cells with a flat top cell, *Opt. Express* 24 (2016) 1288–1299.
- [462] Dai Shi, Yang Zeng, Wenzhong Shen, Perovskite/c-Si tandem solar cell with inverted nanopyramids: realizing high efficiency by controllable light trapping, *Sci. Rep.* 5 (2015) 16504.
- [463] Manoj Jaysankar, Miha Filipić, Bartosz Zielinski, Perovskite–silicon tandem solar modules with optimised light harvesting, *Energy Environ. Sci.* 11 (2018) 1489–1498.
- [464] Christoph Messmer, Baljeet S. Goraya, Sebastian Nold, The race for the best silicon bottom cell: Efficiency and cost evaluation of perovskite–silicon tandem solar cells, *Prog. Photovolt.* (2020) 1–16.



Jiakai Zhou is currently a Ph.D. student in Institute of Photoelectronic Thin Film Devices and Technology of Nankai University under the supervision of Prof. Guofu Hou. He received his B.S. degree in electronic information engineering from Xidian University in 2017, and M.S. degree in integrated circuit engineering from Hebei University of Technology in 2020. His main research focuses on the TOPCon solar cells.



Qian Huang is an associate professor in Institute of Photoelectronic Thin Film Devices and Technology of Nankai University. She received her Ph.D. from Nankai University in 2009. Her research mainly focuses on thin film photovoltaic materials/devices and the design of key materials for integrated circuits.



Yi Ding is an associate professor in Institute of Photoelectronic Thin Film Devices and Technology of Nankai University. He received his Ph.D. from Saitama University in 2010 and Lanzhou University in 2011, and started his postdocs at National Institute for Material Science and Tokyo Institute of Technology. His research mainly focuses on the on perovskite solar cells and organic/inorganic hybrid solar cells based on silicon quantum dots.



Guofu Hou is a full professor in Institute of Photoelectronic Thin Film Devices and Technology of Nankai University. He received his Ph.D. from Nankai University in 2005, and started his postdoc at the University of Toledo in 2009. His research mainly focuses on the performance improvement and industrialization of high-efficiency crystalline silicon heterojunction solar cells (SHJ, TOPCon, POLO, DASH) and PbX (X=S, Se) colloidal quantum dot solar cells, as well as the application of novel two-dimensional photoelectric materials and devices.



Ying Zhao received his PhD from Nankai University in 1995. He is a full professor and the dean of the College of Electronic Information and Optical Engineering in Nankai University. He is the vice-chair of the PVSEC International Advisory Committee. He is also the vice-president of China Renewable Energy Society and the director of PV Committee. He has been engaged in the research of photovoltaic materials and devices.